

University of Windsor

Scholarship at UWindor

Electronic Theses and Dissertations

Theses, Dissertations, and Major Papers

2014

Effect of grain refiners on squeeze casting of magnesium alloy AM60

Yanda Zou
University of Windsor

Follow this and additional works at: <https://scholar.uwindsor.ca/etd>

Recommended Citation

Zou, Yanda, "Effect of grain refiners on squeeze casting of magnesium alloy AM60" (2014). *Electronic Theses and Dissertations*. 5153.

<https://scholar.uwindsor.ca/etd/5153>

This online database contains the full-text of PhD dissertations and Masters' theses of University of Windsor students from 1954 forward. These documents are made available for personal study and research purposes only, in accordance with the Canadian Copyright Act and the Creative Commons license—CC BY-NC-ND (Attribution, Non-Commercial, No Derivative Works). Under this license, works must always be attributed to the copyright holder (original author), cannot be used for any commercial purposes, and may not be altered. Any other use would require the permission of the copyright holder. Students may inquire about withdrawing their dissertation and/or thesis from this database. For additional inquiries, please contact the repository administrator via email (scholarship@uwindsor.ca) or by telephone at 519-253-3000ext. 3208.

**EFFECT OF GRAIN REFINERS ON SQUEEZE CASTING
OF MAGNESIUM ALLOY AM60**

By

Yanda Zou

A Thesis
Submitted to the Faculty of Graduate Studies
through the Department of Mechanical, Automotive and Materials Engineering
in Partial Fulfillment of the Requirements for
the Degree of Master of Applied Science
at the University of Windsor

Windsor, Ontario, Canada

2014

© 2014 Yanda Zou

**EFFECT OF GRAIN REFINERS ON SQUEEZE CASTING
OF MAGNESIUM ALLOY AM60**

by

Yanda Zou

APPROVED BY:

X. Chen

Department Electrical and Computer Engineering

X. Nie

Department of Mechanical, Automotive and Materials Engineering

H. Hu, Advisor

Department of Mechanical, Automotive and Materials Engineering

May 13, 2014

DECLARATION OF ORIGINALITY

I hereby certify that I am the sole author of this thesis and that no part of this thesis has been published or submitted for publication.

I certify that, to the best of my knowledge, my thesis does not infringe upon anyone's copyright nor violate any proprietary rights and that any ideas, techniques, quotations, or any other material from the work of other people included in my thesis, published or otherwise, are fully acknowledged in accordance with the standard referencing practices. Furthermore, to the extent that I have included copyrighted material that surpasses the bounds of fair dealing within the meaning of the Canada Copyright Act, I certify that I have obtained a written permission from the copyright owner(s) to include such material(s) in my thesis and have included copies of such copyright clearances to my appendix.

I declare that this is a true copy of my thesis, including any final revisions, as approved by my thesis committee and the Graduate Studies office, and that this thesis has not been submitted for a higher degree to any other University or Institution.

ABSTRACT

The effect of hexachloroethane (C_2Cl_6) and calcium carbide (CaC_2) as grain refiners added into the squeeze casting AM60 magnesium alloys was investigated in this study. The results of thermal analysis and microstructural analysis indicate the occurrence of heterogeneous nucleation of primary magnesium during solidification. The microstructural analysis suggests that the nucleation behaviors of C_2Cl_6/CaC_2 -treated AM60 alloys may be attributed to the increase in nuclei and nucleation rate during the solidification of the magnesium alloy. Grain size measurements indicated that both C_2Cl_6 and CaC_2 have the capability to unify the average grain sizes of squeeze cast magnesium alloy AM60 among different section thicknesses. The tensile testing indicate the improved tensile properties especially in the thick sections. The corrosion tests showed an increase in corrosion resistance as the grain refiners were added into the squeeze cast alloy AM60.

DEDICATION

I dedicate this thesis to my parents and my girlfriend. Their love and support during my study in University of Windsor has given me strength and motivated me through difficult times during the research period.

ACKNOWLEDGEMENTS

First of all, I would like to thank my supervisor Dr. Henry Hu for giving me the opportunity to join the casting group in University of Windsor, for his excellent supervision of this research work.

Great thanks to the program reader, Dr. Xueyuan Nie, and the outside program reader, Dr. Xiang Chen for taking the time to review my thesis and giving me the suggestions for this study.

Many thanks to the department technicians including Mr. Andy Jenner and Mr. Matthew St. Louis for the sample preparation and the tensile test, Mr. Gang Li's advises on microstructure analysis, and Ms. Sharon Lackie's help for the SEM training, and also to the classmates in the casting group including Xuzhi Zhang, Meng Wang and Bojun Xiong, for their great help on the experiment of this research.

Finally, I would like to express my sincerest gratitude to my family for their love, support and encouragement.

TABLE OF CONTENTS

DECLARATION OF ORIGINALITY	iii
ABSTRACT.....	iv
DEDICATION.....	v
ACKNOWLEDGEMENTS	vi
LIST OF TABLES	ix
LIST OF FIGURES	x
CHAPTER 1: INTRODUCTION.....	1
1.1 Research Background.....	1
1.2 Objectives of this research	2
1.3 Thesis Layout	3
CHAPTER 2: LITERATURE REVIEW	4
2.1 Metallurgical Aspects of Magnesium Alloys.....	4
2.2 Die Casting Process.....	6
2.2.1 Die Casting	6
2.2.2 Advantages of Die Casting	8
2.2.3 Disadvantages of Die Casting.....	9
2.3 Squeeze Casting Process	9
2.3.1 Squeeze Casting Concept	9
2.3.2 Squeeze Casting Process	10
2.3.3 Squeeze Casting vs Die Casting	13
2.3.4 Effect of section Thickness on Tensile Properties of Magnesium Alloys.....	17
2.4 Grain Refinement of Magnesium Alloys	20
2.4.1 Aluminum Free and Aluminum Containing Magnesium Alloys	20
2.4.2 Grain Refinement of Aluminum-Free Magnesium Alloys.....	21

2.4.3 Grain Refinement of Aluminum Contain Magnesium Alloys.....	22
2.5 Summary	38
CHAPTER 3: EXPERIMENTAL PROCEDURES	40
3.1 Materials and Processing.....	40
3.2 Thermal Analysis	41
3.3 Microstructure Analysis	43
3.4 Tensile Testing	44
3.5 Potentiodynamic Polarization Testing	46
CHAPTER 4: RESULTS AND DISCUSSION	48
4.1 Appearance of Squeeze casting Products.....	48
4.2 Solidification of magnesium alloy AM60.....	49
4.2.1 Cooling Curve Analysis.....	49
4.2.2 DSC Analysis	54
4.3 Tensile Behaviour	55
4.3.1 Tensile Behaviour of cylindrical coupon.....	55
4.3.2 Tensile behaviour of 5-step casting	59
4.4 Microstructure Analysis	67
4.4.1 Magnesium alloy AM60.....	67
4.4.2 Grain structure of alloy AM60 cast in cylindrical mould.....	69
4.4.3 Grain refining mechanisms.....	78
4.5 Fracture surface analysis	83
4.6 Inclusion analysis	87
4.7 Corrosion test	90
4.8 Summary	93
CHAPTER 5: CONCLUSIONS	94
CHAPTER 6: FUTURE WORK.....	96
REFERENCES.....	97
APPENDICES: ADDITIONAL FIGURES.....	108
VITA AUCTORIS	129

LIST OF TABLES

Table 2-1 Grain refining method for casting magnesium alloys	39
Table 3-1 Chemical composition of cast alloy AM60	40
Table 3-2 Chemical properties of C_2Cl_6 and CaC_2	41
Table 4-1 DSC analysis results of AM60 and C_2Cl_6 / CaC_2 -treated AM60 alloy	55
Table 4-2 Tensile properties of AM60 C_2Cl_6 -treated and CaC_2 -treated specimens	56
Table 4-3 Best fit parameters of power law equation	59
Table 4-4 Tensile properties of squeeze casting alloy AM60 in different thicknesses	61
Table 4-5 Tensile properties of grain refined squeeze casting AM60 in different thicknesses	64
Table 4-6 Grain size measurements of the untreated and treated squeeze cast Mg alloy AM60	78
Table 4-7 Characteristic values for the polarization curves in Figure 4-37	93

LIST OF FIGURES

Figure 2- 1. Comparison of basic structural properties of magnesium with aluminum and iron [6].	6
Figure 2- 2. Schematic diagram of hot chamber die cast machine [16].	7
Figure 2- 3. Schematic diagram of cold chamber die cast machine [16].....	7
Figure 2- 4. Schematic diagram of the squeeze casting process [2].	11
Figure 2- 5. Schematic diagram of (a) direct, and (b) indirect squeeze casting process [22].....	12
Figure 2- 6. Mechanical properties of cast AZ91, (a) ultimate and yield strengths, and (b) elongation [27].....	15
Figure 2- 7. Optical micrographs showing (a) porosity in die cast AM50 alloy and (b) almost porosity-free squeeze cast AM50 alloy [28].	16
Figure 2- 8. Porosity levels of squeeze cast and die cast AM50 alloy [28].....	17
Figure 2- 9. Cooling rates vs. Section thickness of squeeze cast AM60 alloy [33].....	18
Figure 2- 10. Optical microstructure showing grain size of specimen with (a) 6 mm, (b) 10 mm, and (c) 20 mm of section thickness [33].....	19
Figure 2- 11. Tensile properties vs section thickness of squeeze cast AM60 alloy [33]...20	
Figure 2- 12. Schematic showing the accumulative roll bonding process [51].	24
Figure 2- 13. Effect of accumulative roll bonding on the microstructure of AZ31 alloy (a) first rolling, (b) second rolling, (c) third rolling, and (d) forth rolling [51].....	25
Figure 2- 14. Effect of source magnesium purity on the grain size of Mg-Al alloy [52].	26

Figure 2- 15. Result of EPMA analysis of AZ31 alloy [55].	29
Figure 2- 16. Optical microstructure of sand casting AZ31 alloy (a) no C ₂ Cl ₆ and (b) 0.6wt% C ₂ Cl ₆ addition [55].	29
Figure 2- 17. Optical microstructure of AZ91E alloy produced by adding C ₂ Cl ₆ and carbon powder [58].	30
Figure 2- 18. EPMA line analysis of Mg, Al, C and O elements on the line AB across the particle in AZ91E alloy [58].	32
Figure 2- 19. X-ray diffraction patterns of the AM60 containing different amount of Ca [62].	34
Figure 2- 20. Optical microstructure of AM60 alloy containing different amount of Ca in as-cast and annealing conditions [62].	35
Figure 2- 21. Grain refinement effect on AZ91 alloy [3].	37
Figure 2- 22. Effect of holding time on AM50 alloy [3].	38
Figure 3- 1. (a) Electric furnace with SF ₆ /CO ₂ gas protection, and (b) vertical hydraulic press.	41
Figure 3- 2. DSC-TGA Q600 analyzer.	42
Figure 3- 3. (a) Buehler optical image analyzer model 2012, and (b) Scanning electron microscopy (FEI Quanta 200 FEG).	44
Figure 3- 4. Schematic illustration of tensile specimen.	45
Figure 3- 5. Instron tensile testing machine (Model 8562).	45
Figure 3- 6. (a) Potentiodynamic polarization test set-up, and (b) EC-LAB SP 150 electrochemical apparatus for corrosion test.	46
Figure 4- 1. Squeeze cast cylindrical coupon.	48

Figure 4- 2. 5-step squeeze casting with a round-shape gating system.	49
Figure 4- 3. (a) Typical cooling curve, and (b) enlarge liquidus temperature region of AM60.	51
Figure 4- 4. (a) Typical cooling curve, and (b) enlarge liquidus region of C ₂ Cl ₆ -treated AM60.	52
Figure 4- 5. (a) Typical cooling curve, and (b) enlarge liquidus region of CaC ₂ -treated AM60.	53
Figure 4- 6. DSC trace of squeeze cast AM60 and C ₂ Cl ₆ /CaC ₂ -treated AM60 alloys.	54
Figure 4- 7. Engineering stress-strain curves of AM60 and C ₂ Cl ₆ /CaC ₂ -refined specimens.	56
Figure 4- 8. True stress-strain curves of AM60 and C ₂ Cl ₆ /CaC ₂ -refined specimens.	58
Figure 4- 9. Strain-hardening rate versus true strain for plastic deformation of AM60 and grain-refined specimens.	59
Figure 4- 10. Engineering stress-strain curves of squeeze cast alloy AM60 with 6 mm, 10 mm and 20 mm section thicknesses.	60
Figure 4- 11. Ultimate tensile strength (UTS), Yield strength (YS) and Elongation vs section thicknesses of alloy AM60.	61
Figure 4- 12. Ultimate tensile strength (UTS), Yield strength (YS) and Elongation vs section thicknesses of C ₂ Cl ₆ treated alloy AM60.	63
Figure 4- 13. Ultimate tensile strength (UTS), Yield strength (YS) and Elongation vs section thicknesses of CaC ₂ treated alloy AM60.	63
Figure 4- 14. Ultimate tensile strength (UTS), Yield strength (YS) and Elongation vs section thicknesses of C ₂ Cl ₆ treated alloy AM60.	64

Figure 4- 15. Ultimate tensile strength (UTS), Yield strength (YS) and Elongation vs section thicknesses of CaC ₂ treated alloy AM60.....	65
Figure 4- 16. Strain-hardening rate versus true strain for plastic deformation of (a) 6 mm sections,(b) 10 mm sections, and (c) 20 mm sections.....	66
Figure 4- 17. (a) Optical micrograph, and (b) SEM micrograph in SE mode of as-cast AM60.....	67
Figure 4- 18. EDS analysis of alloy AM60, (a) primary α -Mg, (b) β -Mg ₁₇ Al ₁₂ , and (c) Al-Mn phase.....	69
Figure 4- 19. Optical micrograph showing grain structure of squeeze cast AM60 in a cylindrical coupon in T4 condition.....	70
Figure 4- 20. Optical micrograph showing grain structure of C ₂ Cl ₆ -treated AM60 in a cylindrical coupon in T4 condition.....	71
Figure 4- 21. Optical micrograph showing grain structure of CaC ₂ -treated AM60 in a cylindrical coupon in T4 condition.....	71
Figure 4- 22. Grain size measurement of grain refined AM60 and untreated AM60.....	72
Figure 4- 23. Optical micrograph showing the grain sizes of squeeze cast AM60 with (a) 6 mm, (b) 10 mm, and (c) 20 mm of section thicknesses.....	74
Figure 4- 24. Optical micrograph showing the grain sizes of C ₂ Cl ₆ -treated AM60 with (a) 6 mm, (b) 10 mm, and (c) 20 mm of section thicknesses.....	76
Figure 4- 25. Optical micrograph showing the grain sizes of CaC ₂ -treated AM60 with (a) 6 mm,(b) 10 mm, and (c) 20 mm of section thicknesses.....	77
Figure 4- 26. Grain sizes vs. section thicknesses of AM60 specimens.....	78

Figure 4- 27. SEM micrograph in BSE mode showing Al_4C_3 as the heterogeneous nucleation site for C_2Cl_6 refined squeeze cast alloy AM60.	79
Figure 4- 28. EDS line analysis of (a) Mg, (b) C and (c) Al elements on line AB across the particle.	81
Figure 4- 29. High magnification SEM micrograph in SE mode showing the CaC_2 refined AM60 containing both $Mg_{17}Al_{12}$ and lamellar Al_2Ca phases.	82
Figure 4- 30. SEM fractographs in SE mode of the untreated squeeze cast AM60, (a) low and (b) high magnification.	84
Figure 4- 31. SEM fractographs in SE mode of C_2Cl_6 -treated squeeze cast AM60, (a) low and (b) high magnification.	85
Figure 4- 32. SEM fractographs in SE mode of CaC_2 -treated squeeze cast AM60, (a) low and (b) high magnification.	86
Figure 4- 33. Oxidation inclusion found in CaC_2 treated AM60 specimen.	88
Figure 4- 34. SEM micrograph in BSE mode of inclusion area of CaC_2 treated AM60 specimen.	88
Figure 4- 35. EDS analysis of (a) un-contaminated alloy, and (b) oxidation inclusions. ...	89
Figure 4- 36. SEM micrographs in SE mode showing the microstructures of (a) C_2Cl_6 refined specimen, (b) CaC_2 refined specimen, and (c) untreated AM60.	91
Figure 4- 37. The β -barrier concept showing the microstructure of (a) before and (b) after corrosion attack.	92
Figure 4- 38. Polarization curves for squeeze cast AM60 specimens in 3.5 wt% NaCl solution.	92

Figure Ap- 1. SEM fractographs in SE mode of the untreated squeeze cast AM60, (a) low and (b) high magnification from cylindrical coupon.	109
Figure Ap- 2. SEM fractographs in SE mode of the C ₂ Cl ₆ -refined squeeze cast AM60, (a) low and (b) high magnification from cylindrical coupon.	110
Figure Ap- 3. SEM fractographs in SE mode of the CaC ₂ -refined squeeze cast AM60, (a) low and (b) high magnification from cylindrical coupon.	111
Figure Ap- 4. SEM fractographs in SE mode of the untreated squeeze cast AM60, (a) low and (b) high magnification form 6 mm section thickness.....	112
Figure Ap- 5. SEM fractographs in SE mode of the C ₂ Cl ₆ -refined squeeze cast AM60, (a) low and (b) high magnification from 6 mm section thickness.....	113
Figure Ap- 6. SEM fractographs in SE mode of the CaC ₂ -refined squeeze cast AM60, (a) low and (b) high magnification from 6 mm section thickness.....	114
Figure Ap- 7. SEM fractographs in SE mode of the untreated squeeze cast AM60, (a) low and (b) high magnification form 20 mm section thickness.....	115
Figure Ap- 8. SEM fractographs in SE mode of the C ₂ Cl ₆ -refined squeeze cast AM60, (a) low and (b) high magnification from 20 mm section thickness.....	116
Figure Ap- 9. SEM fractographs in SE mode of the CaC ₂ -refined squeeze cast AM60, (a) low and (b) high magnification from 20 mm section thickness.....	117
Figure Ap- 10. Engineering Stress-strain curves for AM60 from cylindrical coupon. ..	118
Figure Ap- 11. Engineering Stress-strain curves for C ₂ Cl ₆ -refined AM60 from cylindrical coupon.....	119
Figure Ap- 12. Engineering Stress-strain curves for CaC ₂ -refined AM60 from cylindrical coupon.....	120

Figure Ap- 13. Engineering Stress-strain curves for squeeze cast AM60 in (a) 6 mm thickness, (b) 10 mm thickness, and (c) 20 mm thickness.....	122
Figure Ap- 14. Engineering Stress-strain curves for C_2Cl_6 -refined squeeze cast AM60 in (a) 6 mm thickness, (b) 10 mm thickness, and (c) 20 mm thickness.....	123
Figure Ap- 15. Engineering Stress-strain curves for CaC_2 -refined squeeze cast AM60 in (a) 6 mm thickness, (b) 10 mm thickness, and (c) 20 mm thickness.....	125
Figure Ap- 16. SEM micrograph in BSE mode showing Al_4C_3 as the heterogeneous nucleation site for C_2Cl_6 refined squeeze cast alloy AM60.....	125
Figure Ap- 17. (a) Typical cooling curve, and (b) enlarge liquidus temperature region of AM60.....	126
Figure Ap- 18. (a) Typical cooling curve, and (b) enlarge liquidus temperature region of C_2Cl_6 -refined AM60.....	127
Figure Ap- 19. (a) Typical cooling curve, and (b) enlarge liquidus temperature region of CaC_2 -refined AM60.....	128

CHAPTER 1: INTRODUCTION

1.1 Research Background

With an increasing emphasis on vehicle weight reduction, the demand for light weight automotive components continues to grow. Magnesium alloys are one of the lightest of all structural materials which makes them very attractive in the automotive industry. Aluminum and manganese are two alloying elements that are usually added in magnesium to improve the machinability and corrosion resistance behaviours of magnesium alloys [1]. Applications of casting magnesium alloys includes engine blocks, steering column components, steering knuckles, suspension links and various powertrain components.

Conventional die casting processes are well-developed for the manufacturing of a wide variety of aluminum and magnesium automotive parts. They possess many advantages such as low manufacturing cost, excellent dimensional accuracy and good repeatability. Casting defects, however, has been a major factor that limited the performance of die casting products. One of the most common die casting defects is the gas and shrinkage porosities, especially in areas with relatively thick cross sections. Squeeze casting, on the other hand, is an established process that build upon conventional die casting practices. High applied pressure in this process could keep entrapped gases in solution and squeeze molten metal from hot spots to incipient shrinkage pores. As a result, the porosity in squeeze casting components is almost eliminated. Consequently, superior mechanical properties of the casting resulting from the pore-free product can be achieved [2].

However, components made by squeeze casting usually contain heavy and thick cross sections, in which coarse grain structure tends to form. To minimize the microstructure inhomogeneity, grain structure in squeeze cast components need to be refined. The previous study by Wallace et al [3] showed hexachloroethane (C_2Cl_6) could effectively refined the grain structure of sand cast magnesium alloy AZ91. Calcium and its compounds (CaC_2) also have been proved to have the ability to stabilize the grain size of AZ91 alloys [4, 5]. However, there is almost no studies on solidification behaviour and grain structure development of squeeze casting magnesium alloy AM60 refined by C_2Cl_6 or CaC_2 .

1.2 Objectives of this research

The objectives of this study are:

1. To investigate the effect of two grain refiners i.e. C_2Cl_6 and CaC_2 on grain refinement of squeeze cast magnesium alloy AM60;
2. To study the effects of section thicknesses on solidification behaviours of refined squeeze cast alloy AM60;
3. To analyze the effects of grain refines on mechanical properties of refined squeeze cast alloy AM60;
4. To characterize microstructures of refined squeeze cast alloy AM60.
5. To understand the grain refining mechanisms of the tested grain refiner for squeeze cast alloy AM60; and

6. To evaluate the influence of the grain refiner on corrosion resistance behaviours of squeeze cast AM60 alloys.

1.3 Thesis Layout

The thesis contains six chapters. Chapter 1 provides a general introduction of squeeze casting AM60 alloy. Chapter 2 is the literature review on the current development of squeeze casting and the grain refinement processes of magnesium alloys. The detailed experimental procedures are described in Chapter 3. The experimental results and discussion of the thermal analysis, microstructures characterization, mechanical testing, corrosion behaviour and fractography are given in Chapter 4. In Chapter 5, the conclusions of the present work are summarized, recommendations for the future work are given in Chapter 6.

CHAPTER 2: LITERATURE REVIEW

2.1 Metallurgical Aspects of Magnesium Alloys

Today's interest in magnesium alloys for automotive applications is based on the combination of high strength and low density. Magnesium is the lightest of all engineering structural metals with a density of 1.74 g/cm^3 [1]. It is 35% lighter than aluminum and over four times lighter than steel [6]. For this reason, magnesium alloys are very attractive as structural material in all applications where weight savings are of great concern. Meanwhile, magnesium has the highest strength-to-weight ratio of any commonly used metals. Many other advantages including good castability, high die casting rates, dimensional accuracy and excellent machinability promote the utilization of this interesting lightweight metal in the automotive industry [7, 8]. Magnesium is barely used for engineering applications without being alloyed with other metals since pure magnesium has poor mechanical properties. The most common alloying elements with magnesium are aluminum, zinc, manganese and zirconium. The effects of these elements are briefly described as follows [9, 10].

Aluminum: Al has a maximum solubility of 12.7 wt% at eutectic temperature. It helps to increase the alloy strength and refine the grain size.

Zinc: Zn is a hardening agent which increase the strength of the alloy. It is commonly used up to 6.0 wt% with the addition of zirconium. It leads to a finer grain structure but also makes the alloy brittle even it is heat treatable.

Manganese: Improve the corrosion resistance of magnesium alloys by eliminating the iron elements. Up to 2.2 wt% is used with considerably less in conjunction with Al and Zn [11].

Zirconium: Excellent magnesium grain refiner, provide finer microstructure and as a result, increase the material strength.

The current magnesium components, including instrument panels, steering wheel armatures, steering column supports, seats, valve covers, and transfer cases, are mainly manufactured by high pressure die casting processes with conventional magnesium alloys: Mg-Al-Zn, AZ series and Mg-Al-Mn, AM series. Over 80% of the magnesium products are made of these two series [6, 12].

Specific strength and specific stiffness of materials are important for the design of weight saving components. The specific strength and stiffness of magnesium alloys are compared with both aluminum and iron in Figure 2-1. There is little difference in specific stiffness between Mg, Al and Fe. In the meantime, the specific strength of Mg is much higher than Al and Fe in the ratio of 14% and 67% [6].

The applications of magnesium alloys in the automotive industry are limited to the low temperature components simply due to the insufficient creep resistance of the alloys at temperatures above 130°C [13]. Softening the unstable phase causes the grain boundary sliding which has been observed to be the main creep mechanism in magnesium alloys at high temperatures. The idea of adding calcium and lithium into the alloys to eliminate the thermal unstable phases has been studied for decades. However, until today, very few practical methods have been developed [14].

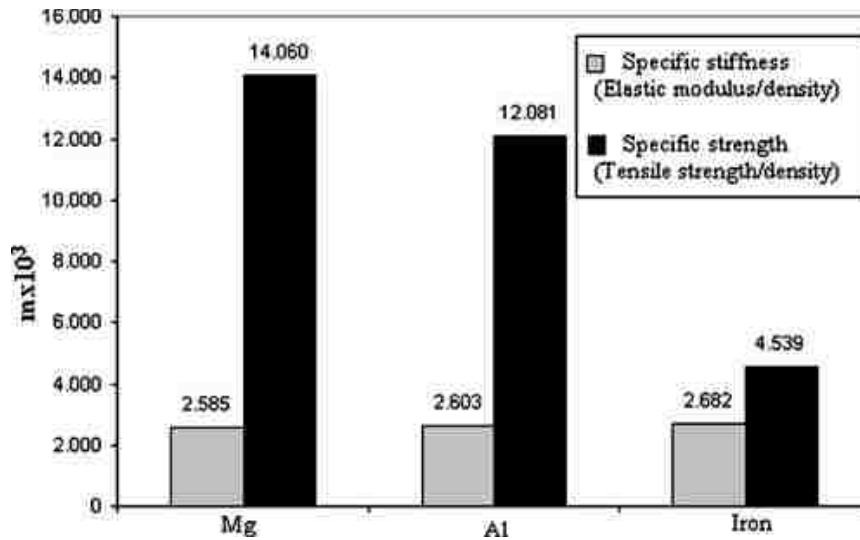


Figure 2- 1. Comparison of basic structural properties of magnesium with aluminum and iron [6].

2.2 Die Casting Process

2.2.1 Die Casting

Die casting is a metal casting process that is characterized by forcing molten metal under high pressure into a mold cavity. The mold cavity is usually created using two hardened tool steel dies, which have been machined into shape and work similarly to an injection mold during the process. The dies, can be designed to produce complex shapes with a high degree of accuracy and repeatability. Parts can be sharply defined, with smooth or textured surfaces, and are suitable for a wide variety of attractive and serviceable finishes [15]. Figures 2-2 and 2-3 schematically show the two types of commonly used die casting machines, hot chamber and cold chamber die casting [16].

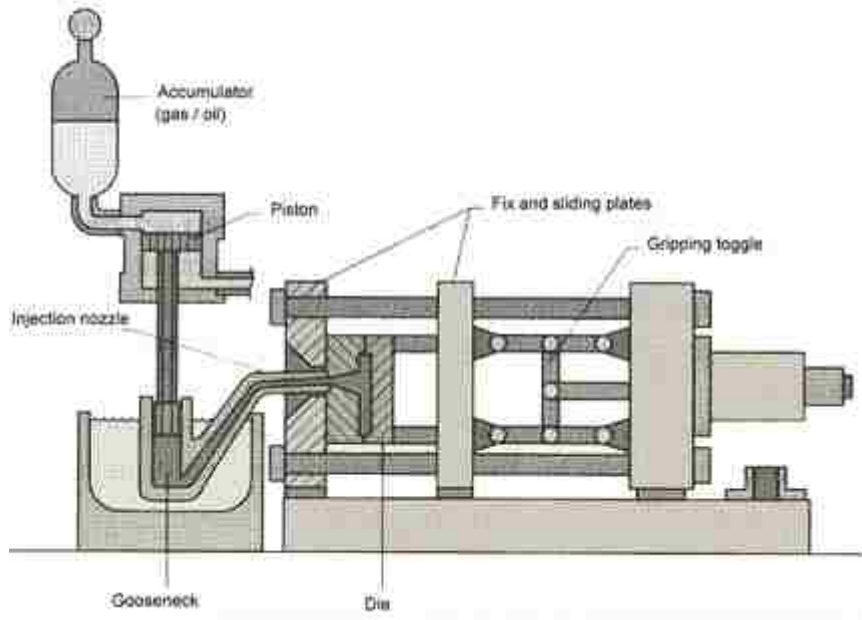


Figure 2- 2. Schematic diagram of hot chamber die cast machine [16].

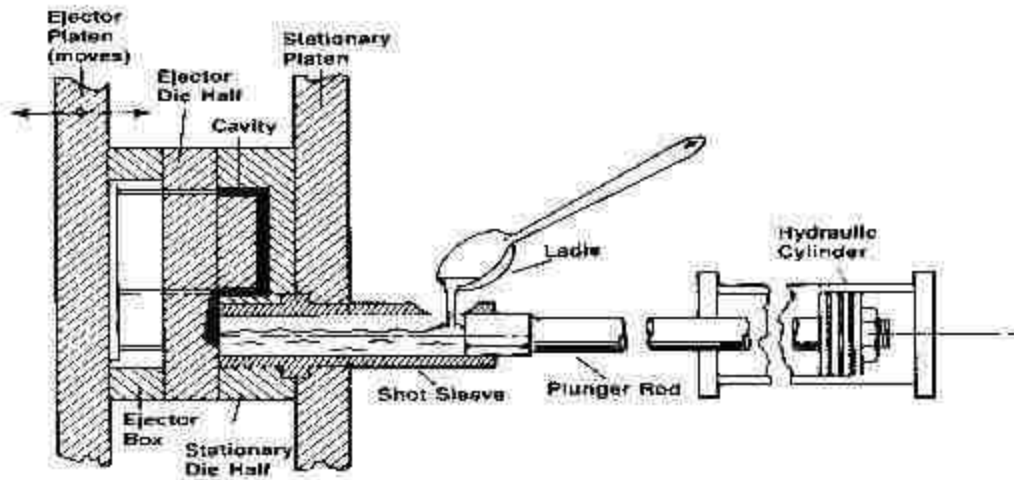


Figure 2- 3. Schematic diagram of cold chamber die cast machine [16].

2.2.1.1 Hot Chamber Die Casting

Hot chamber machines are used primarily for zinc, copper, magnesium and other low melting point alloys that do not readily attack and erode metal pots, cylinders and plungers. The injection mechanism of a hot chamber machine is immersed the molten metal bath of a metal holding furnace. The furnace is attached to the machine by a metal feed system called a gooseneck. As the injection cylinder plunger rises, a port in the injection cylinder opens, allowing molten metal to fill the cylinder. As the plunger moves downward it seals the port and force molten metal through the gooseneck and nozzle into the die cavity. After the metal has solidified in the die cavity, the plunger is withdrawn, and the die opens and the casting is ejected [17].

2.2.1.2 Cold Chamber Die Casting

Cold chamber machine are used for alloys such as aluminum and other alloys with high melting points. The molten metal is poured into a “cold chamber”, or cylindrical sleeve, manually by a hand ladle or by an automatic ladle. A hydraulically operated plunger seals the cold chamber port and forces metal into the locked die at high pressure. After the solidification process of the metal, a product is ejected by pins and the plunger returns to the original position [17].

2.2.2 Advantages of Die Casting

Die casting is an efficient and economical alternative to the other processes. When used to its maximum potential it can replace assemblies of a variety of parts

produced by various manufacturing processes at significant saving in cost and labor. The advantages of die casting are as follows:

1. The die casting can provide excellent dimensional accuracy and stability;
2. Secondary machining operations are reduced or eliminated because of the smooth surfaces of die casting products;
3. Die casting provides complex shapes with high levels of tolerance;
4. The die casting has the ability to accomplish high-speed production; and
5. Die cast parts are stronger than plastic injection moldings with the same dimensions. Thin wall castings are stronger and lighter than other casting methods [19, 20].

2.2.3 Disadvantages of Die Casting

There are three major disadvantages of die casting which includes:

1. The cost of dies and other equipment is very high;
2. It is not economical for a small quantity of casting production; and
3. Porosity problem such as shrinkage porosity, hydrogen dissolve porosity, lubricant vaporization porosity and trapped air porosity [19, 20].

2.3 Squeeze Casting Process

2.3.1 Squeeze Casting Concept

Squeeze casting is a process which involves the solidification of a molten metal in a closed die under an imposed high pressure. It is also known as liquid metal forging,

extrusion casting and pressure crystallization [2]. The high applied pressure, which is several orders of magnitude greater than the melt pressure developed in normal casting processes, keeps entrapped gases in solution and squeeze molten metal from hot spots to incipient shrinkage pores. As a result, the porosity in a squeeze-cast component is almost eliminated. Furthermore, due to the elimination of the air gap at the liquid-mould interface by the applied high pressure, the heat transfer across die surfaces is enhanced, which increases solidification and cooling rates. Thus, superior mechanical properties of the casting resulting from the pore-free fine microstructure are achieved in squeeze-casting processes [2, 21].

2.3.2 Squeeze Casting Process

Generally, the squeeze casting-fabricated engineering components are fine grained with excellent surface finish and have almost no porosity [21]. The mechanical properties of these products are significantly improved over the conventional castings such as sand casting and gravity casting. The process of squeeze casting which is schematically in Figure 2-4 involves the following steps:

1. A pre-specified amount of molten metal is poured into a preheated die cavity, located on the bed of a hydraulic press;
2. The pressure is activated to close off the die cavity and to pressurize the liquid metal;
3. The pressure is applied on the metal shortly until the complete of solidification. The adding of pressure can not only increase the rate of heat flow but also eliminate the shrinkage porosity; and

4. The upper punch returns to the original position and the product is ejected [2].

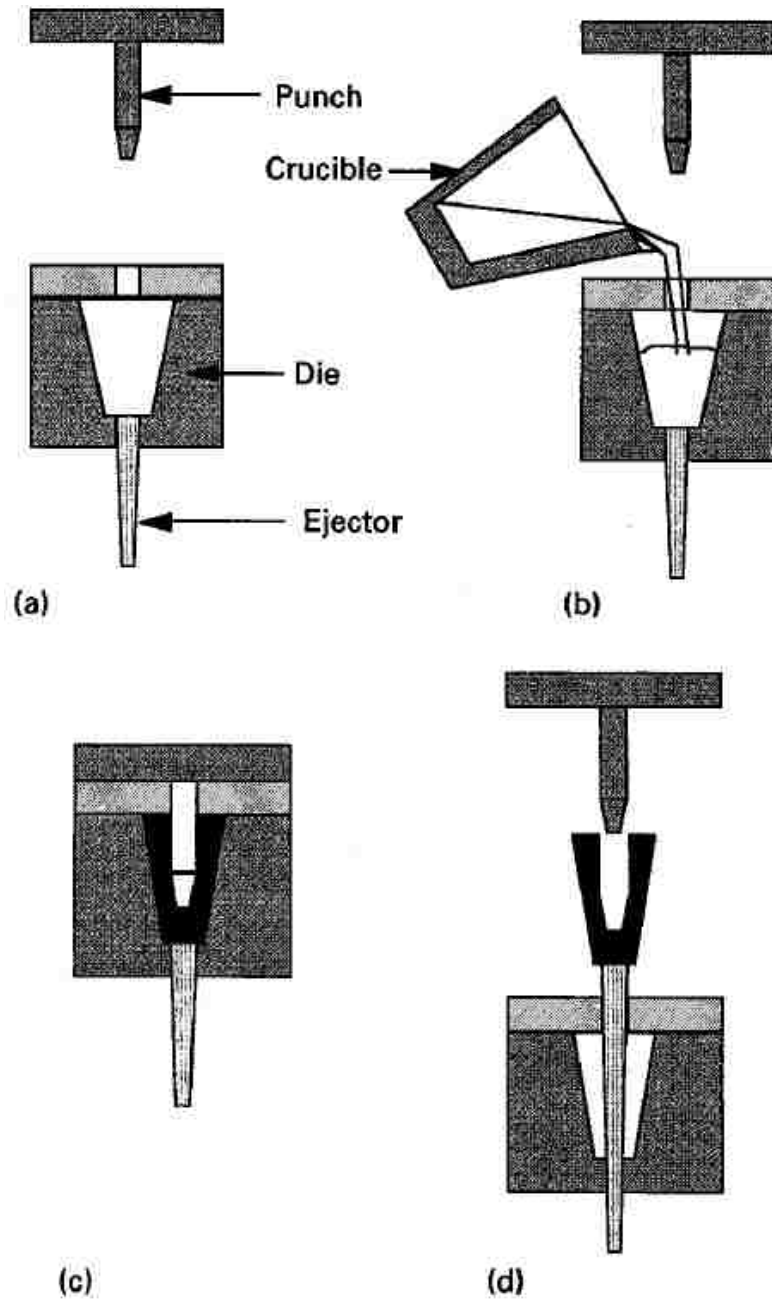


Figure 2- 4. Schematic diagram of the squeeze casting process [2].

Two basic forms of the process may be distinguished depending on whether the pressure is applied directly on to the solidifying casting product via an upper die or the applied pressure is exerted through an intermediate feeding system. The two different casting techniques are known as “direct” and “indirect” squeeze casting process. Schematically illustrates the two modes is showing in Figure 2-5 [22].

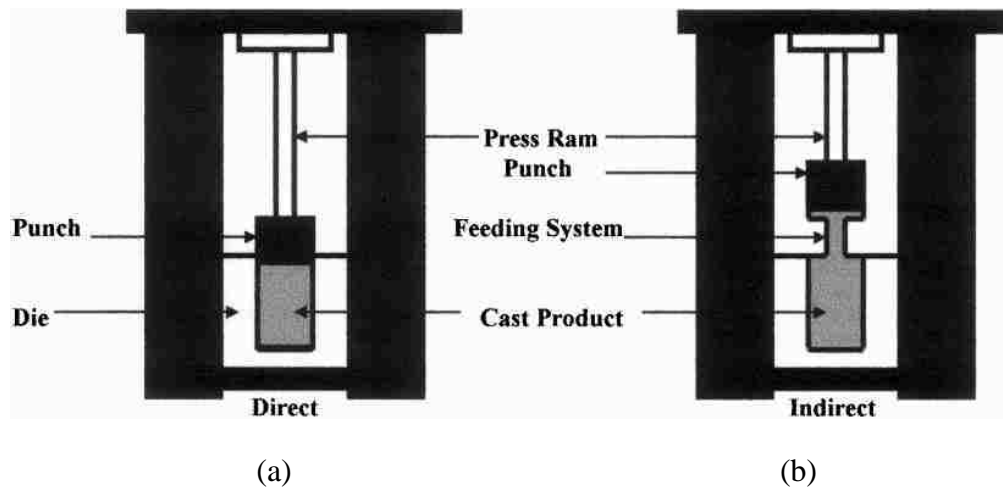


Figure 2- 5. Schematic diagram of (a) direct, and (b) indirect squeeze casting process [22].

The direct squeeze casting technique is characterized by direct pressure imposed on to the casting without any gating system, as shown in Figure 2-5. The heat transfer of the product is extremely fast and a fully densified components can be achieved. The reason for this is because the pressure is directly applied on to the entire surface of the molten metal during solidification. As a result, enhanced mechanical properties are attained. In the indirect technique, however, the pressure is exerted on a gate, which transmits the load to the component. Since the pressure is imposed at a distance from the component, it is difficult to maintain a high pressure on the component throughout its solidifying and cooling periods. This indicates that it is difficult to cast long freezing

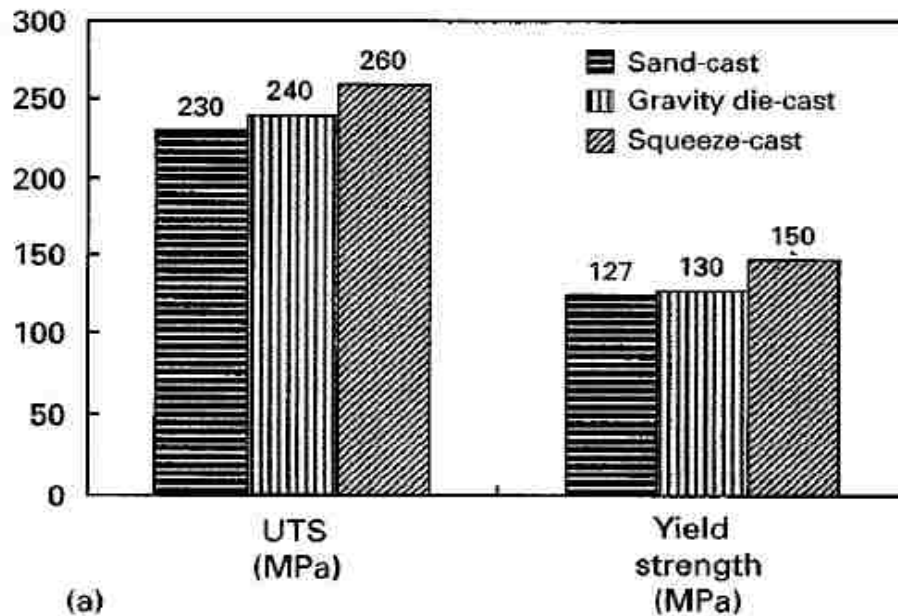
range alloys with the indirect technique. Also, metal yield is much lower than that achievable with direct squeeze casting, owing to the necessity of using a gating system. The advantage of the indirect technique is that, due to the presence of a gating system, a highly accurate external metering system is not necessary. Variation in metal volume are adjusted in the gate. Although it seems that the direct technique offers more opportunities for a wide range of alloys to be used for the production of high-strength, full-integrity metal casting and metal matrix composite components that is the philosophy of squeeze casting, more indirect than direct squeeze-casting machines are in operation at present. This is probably because the indirect process has successfully been commercialized [2].

2.3.3 Squeeze Casting vs Die Casting

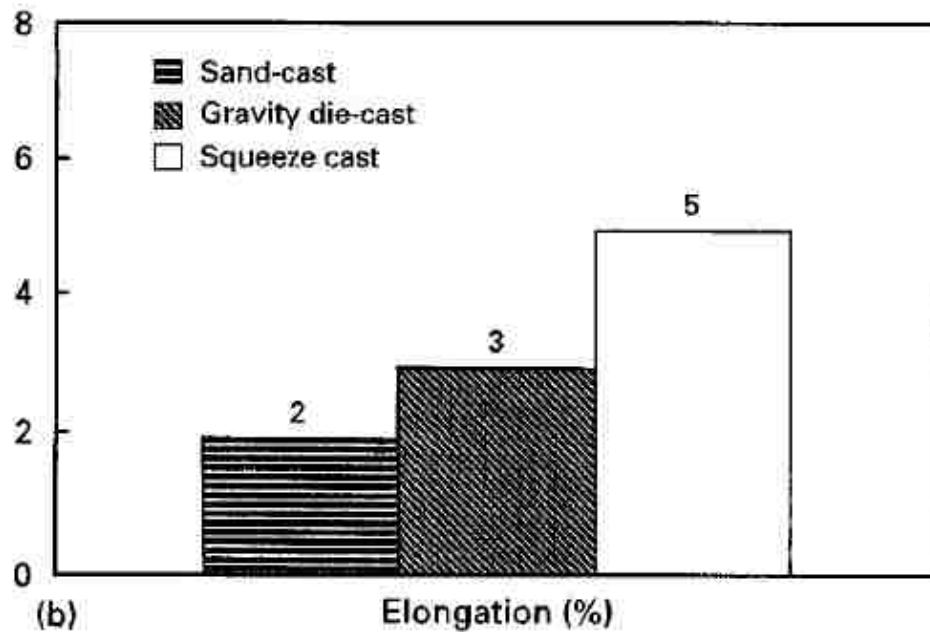
Since early 90s, applications of Mg alloys have received significant attention for vehicle weight reduction. Recently, the application of Mg alloys in cars has been mostly limited to die-cast parts, which are used at room temperature, such as steering-wheel cores, brake-pedal brackets, instrument panel and seat frames. The use of magnesium alloys in automotive power train has a great potential for further vehicles weight reduction of vehicles. The presence of $Mg_{17}Al_{12}$ phase is accepted to be responsible for the poor high-temperature performance of AM and AZ series magnesium alloys since it is metallurgically unstable at elevated temperatures ($T > 130^{\circ}C$) which leads to creep-induced precipitation causing grain boundary migration. Calcium addition is always a solution to this problem since $Mg_{17}Al_{12}$ can form some new phases with the Ca atoms and become the thermal stable Al_2Ca or sometimes $(Mg,Al)_2Ca$ phases. However, the calcium addition adversely affected the die-castability of magnesium alloys due to

extensive hot-cracking and die sticking. On the other hand, it has been pointed out that the die castings have relatively high gas porosity levels, particularly in an area with relatively thicker cross sections. The reason for this is probably due to the entrapment of air or gas in the melt during the high speed injection of turbulent molten metal into the cavity. And it is obvious that higher porosity levels leads to lower mechanical properties. Because of all the unsatisfied defect of die casting process, it is essential to develop alternative manufacturing process, such as squeeze casting, for magnesium alloys [23-26].

The comparison of squeeze casting over other casting processes of magnesium alloys such as sand casting, gravity casting and high pressure die casting in terms of tensile properties was studied by Chadwick and the results are shown in Figure 2-6. In all cases, the squeeze casting specimen exhibits the highest values of UTS, yield strength and elongations [27].



(a)



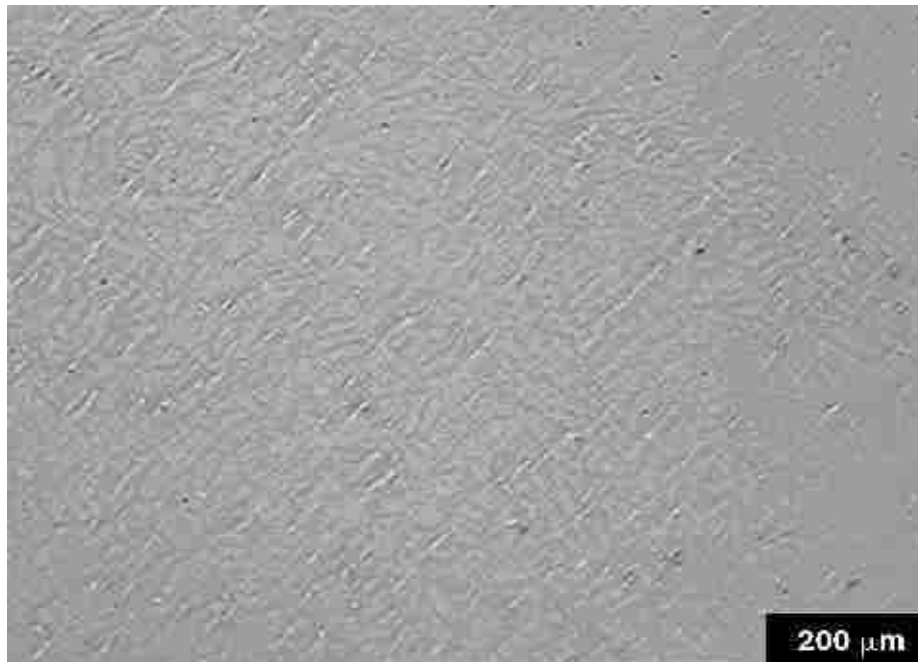
(b)

Figure 2- 6. Mechanical properties of cast AZ91, (a) ultimate and yield strengths, and (b) elongation [27].

The porosity elimination ability of squeeze castings over die casting processes of AM50 magnesium alloys was studied and the optical micrograph showing the porosity condition of both processes is present in Figure 2-7. It is observed that the squeeze cast AM50 alloy has virtually no porosity in the microstructure as shown in Figure 2-7(b). However, the typical pores can be easily spotted in the die cast specimen as indicated in Figure 7(a). The percentage of the porosity of both squeeze casting and die casting AM50 alloys based on the density measurements are quantitatively shown in Figure 8. In comparison with that (4.00%) of the die casting, the porosity level of squeeze casting is only 0.12%. With such a low porosity level, the better mechanical properties of magnesium alloys could be easily achieved [28, 29].



(a)



(b)

Figure 2- 7. Optical micrographs showing (a) porosity in die cast AM50 alloy and (b) almost porosity-free squeeze cast AM50 alloy [28].



Figure 2- 8. Porosity levels of squeeze cast and die cast AM50 alloy [28].

2.3.4 Effect of section Thickness on Tensile Properties of Magnesium Alloys

Since die casting is only suitable for producing thin-walled parts [8], when it comes to a relatively thicker part, the squeeze casting seems to be a more preferable choice by means of slow filling velocity, semi-solid processing and solidification under high pressure [30, 31, 32]. A recent study on the effect of section thicknesses on microstructure and tensile properties of squeeze casting magnesium alloys indicated that, a step mold was used and the squeeze cast AM60 alloy with three different section thickness (6 mm, 10 mm and 20 mm) was obtained [33]. It is obvious that thicker section leads to longer solidification time and lower cooling rate. The relationship between cooling rate and grain structure stated that the higher cooling rate, the finer the grain structure. Figures 2-9 and 2-10 show the cooling rate and the corresponding grain microstructure for each squeeze cast section. The cooling rate of 6 mm section is almost four times higher than those of 20 mm, as a result, the average grain size increases from

16 μm to 80 μm for each case. As a consequence, the 6 mm section shows better tensile properties than the 10 mm and 20 mm sections as shown in Figure 2-11 [33, 34].

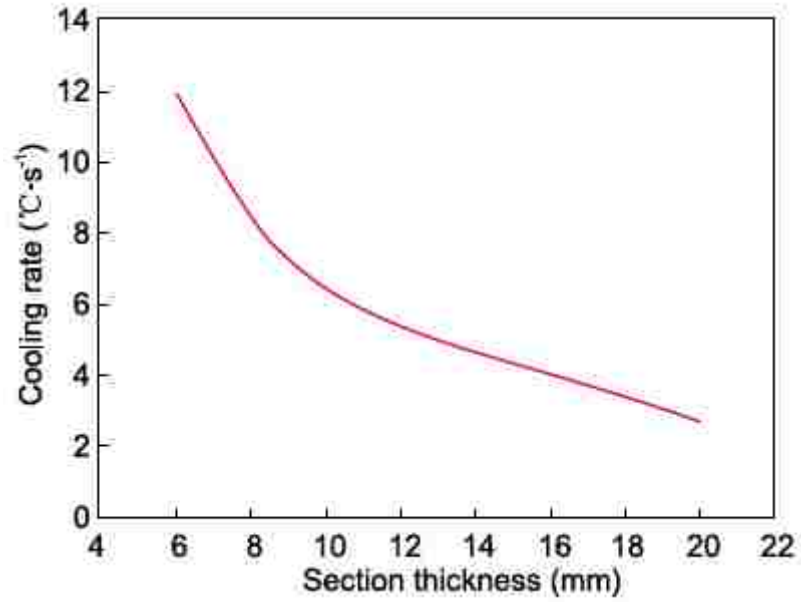
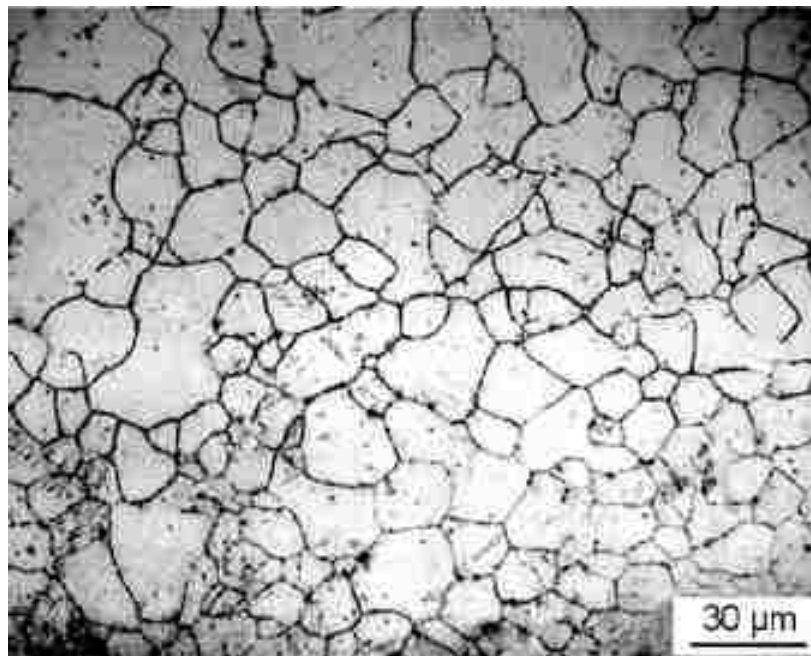
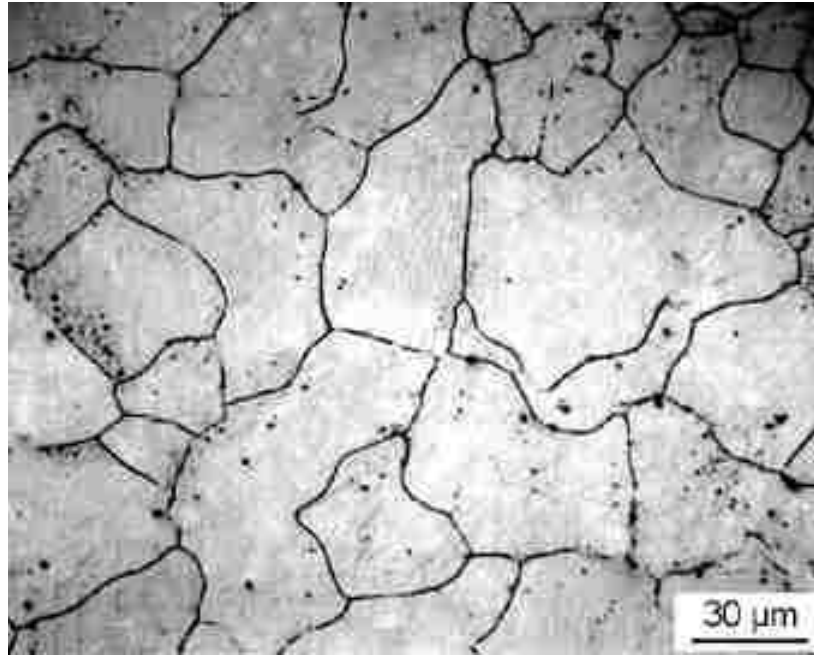


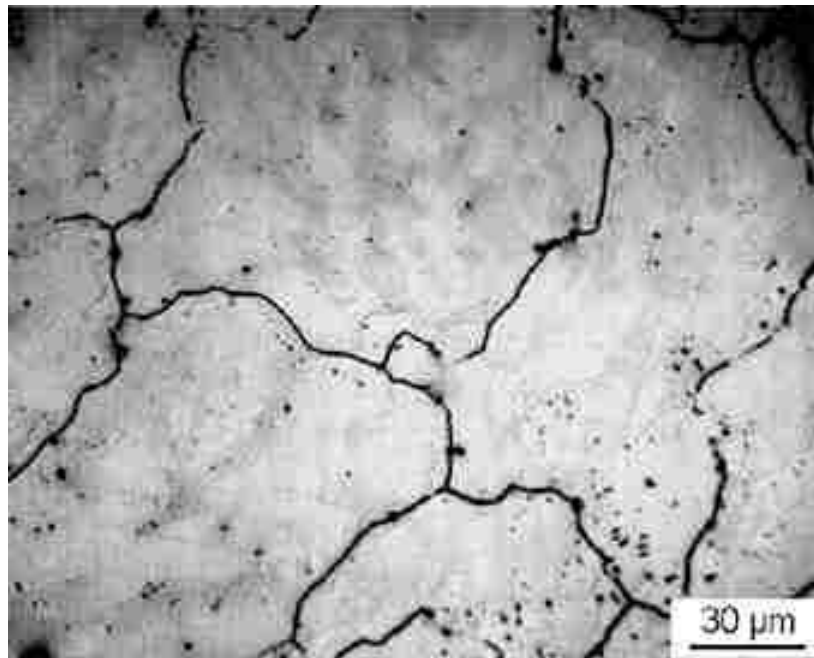
Figure 2- 9. Cooling rates vs. Section thickness of squeeze cast AM60 alloy [33].



(a)



(b)



(c)

Figure 2- 10. Optical microstructure showing grain size of specimen with (a) 6 mm, (b) 10 mm, and (c) 20 mm of section thickness [33].

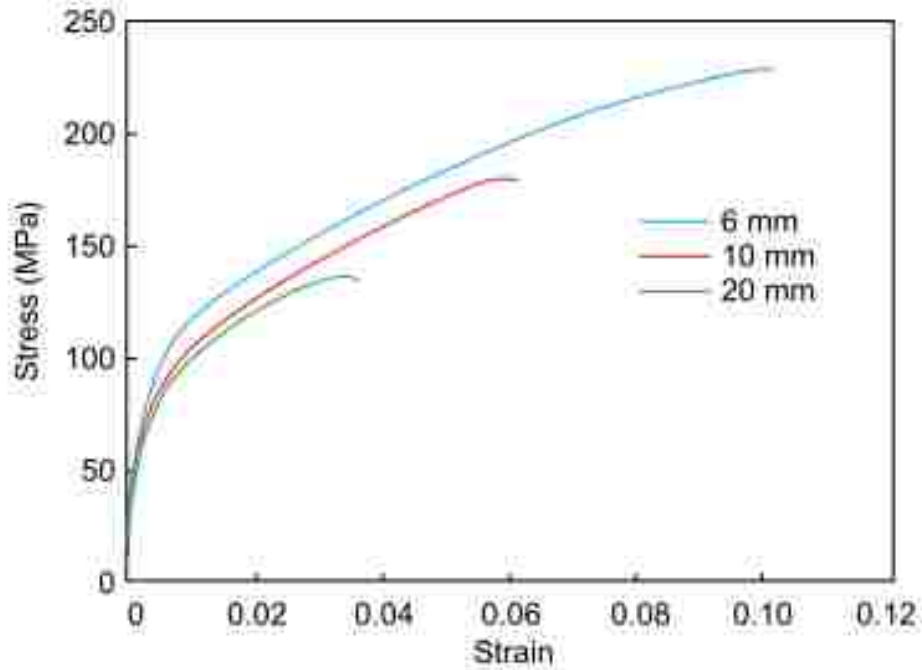


Figure 2- 11. Tensile properties vs section thickness of squeeze cast AM60 alloy [33].

2.4 Grain Refinement of Magnesium Alloys

2.4.1 Aluminum Free and Aluminum Containing Magnesium Alloys

The grain refinement of magnesium alloys is reviewed with regards to two broad groups of alloys: alloys that contain aluminum and alloys that do not contain aluminum. The alloys that are free of aluminum are generally very well refined by Zr master alloys. On the other hand, the understanding of grain refinement in aluminum containing alloys is poor and in many cases confusing probably due to the interaction between impurity elements and aluminum in affecting the potency of nucleant particles [35].

2.4.2 Grain Refinement of Aluminum-Free Magnesium Alloys

Recently, among all the aluminum free magnesium alloys, it has been widely accepted that Zr can significantly reduce the average grain size of Mg alloys to 50 μm comparing to a few millimetres at normal cooling rate. The addition of Zr in magnesium alloys also leads to the formation of near round grain, which further enhanced the structural uniformity of the final alloys [36, 37]. It has been reported that Zr can refine the grain size of Mg alloys in two ways by both soluble and insoluble contents. For the soluble Zr, it has been pointed out by Emley [38] that the grain refinement of magnesium alloys is based on the peritectic mechanism. It has been proposed that with the content of Zr at around 0.601%, the Zr can naturally form the basis for grain refinement of magnesium alloys. However, due to the low alloying efficiency of Zr, an excess of Zr has to be introduced to achieve the desired amount of Zr content for the optimum grain refinement. Normally, the Zr addition has to be 2.3% in order to ensure the 0.601% Zr content [39]. Recently, the solubility of Zr in magnesium alloys at peritectic temperature has been re-defined at 0.443% [40], which is almost 30% lower than the previous value at 0.601%. Further research has to be done to testify the new Zr content and if it can be established as a new basis of magnesium grain refinement with zirconium, it would largely reduce the cost of Zr refined magnesium alloys. Lee and his team recently show an even smaller Zr content at less than 0.32% [41]. In the past, the insoluble Zr such as undissolved Zr particles was believed to be irrelevant to grain refinement. Early work by Sauerwald [42] suggested that only the dissolved Zr at pouring temperature in magnesium alloys is effective for grain refinement. However, most recent research

proposed that undissolved Zr also plays an important role in the grain refinement process by settling at the grain boundaries and suppress the grain growth [43, 44].

2.4.3 Grain Refinement of Aluminum Contain Magnesium Alloys

Since the late 1930s, a number of approaches have been developed to obtain grain refinement in magnesium alloys that contain aluminum. These are briefly summarized as follows.

2.4.3.1 Superheating

The concept of superheating was first described in 1931 [45]. Unlike other alloys, magnesium alloys trend to benefit from high-temperature treatment since normally the elevated temperature leads to oxidation, gas absorption and grain coarsening. The process includes heating up the melting metal above the liquidus temperature of the alloy up to 180°C to 300°C for a short period of time, following by a rapid cooling and short holding time at pouring temperature. There are five major factors that influence the effect of the superheating treatment.

- 1) The aluminum content: Aluminum is a key element for successful grain refinement by superheating. The superheating does not have noticeable effect on magnesium alloys other than the Mg-Al alloys. Also, high aluminum content magnesium alloys (Al>8 wt%) are more rapid refined by superheating than low aluminum content alloys [36];
- 2) Fe and Mn also play an important role on superheating treatment of magnesium alloys. Generally, the superheating trends to have more effect on the high Fe and

Mn content magnesium alloys than the low content alloys [46];

- 3) The existence of silicon can also help to refine the grain size of magnesium alloys by superheating. However, that only happens on the magnesium alloys with low Fe content;
- 4) There is a specific temperature range for maximum grain refining efficiency by superheating, for instance, according to Tiner, the temperature range is 850°C to 900°C for Mg-9 % Al-2 %-Zn alloys [47]; and
- 5) Once sufficient treatment time is given, further increasing the holding time has no effect on the grain refinement. Repeating of the superheating treatment has also been considered to be no effect on grain refinement [46].

Even though the superheating treatment has great potential of refining the grain size of magnesium alloys. With the requirement of rapid cooling from the treatment temperature to the pouring temperature, grain refinement by superheating is less practical for a large pot of melt on a commercial scale [48, 49].

2.4.3.2 Accumulative Rolling Bonding

Among all the magnesium alloy grain refinement methods, rolling is the most probable technique to be scaled for fabricating large bulk sheet or plate samples. It is always combining with suitable superheating to further improve the grain size of the magnesium alloys [48]. According to Perez-Prado's research [51], the magnesium alloys (AZ31) were pre-heated to 400 °C and hold for 30 min. The original sheets were initially cut in 5 x 3 x 10 cm rectangular pieces, then the sheets were rolling using a single rolling pass of 80% reduction. Cut off the rolled sheets into five pieces, then stack of five pieces together so that the thickness of the stack was equal to the thickness of the original

sheets. Reheat the sheets and roll the stack again using the 80% reduction. Then repeat the process for the third and fourth time. The schematic diagram illustrate the whole process is showing in Figure 2-12.

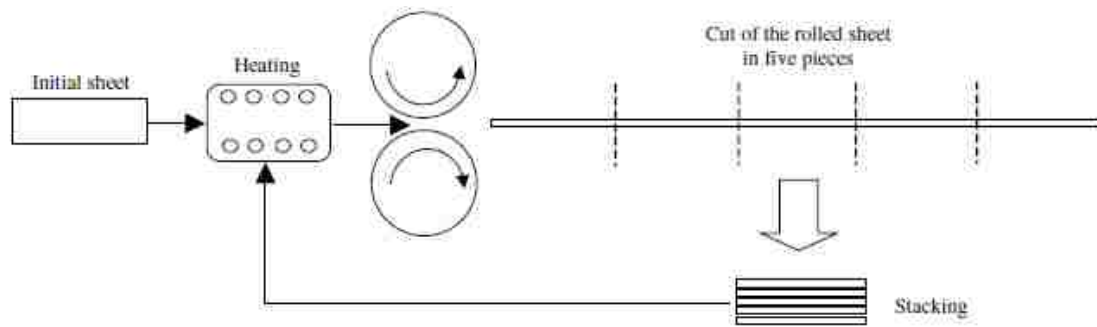


Figure 2- 12. Schematic showing the accumulative roll bonding process [51].

The microstructure of magnesium alloys processed by accumulative rolling is showing in Figure 2-13. After the four accumulative rolling stages, significant grain refinement was achieved. The average grain size of the AZ31 alloy after first pass was 4.2 μm . After subsequent passes, the grain size stabilized around 3 μm . This result implied that the grain refinement took place mainly during the first pass. In other words, when the minimum grain size was achieved, further rolling passes had limited noticeable refining effect.

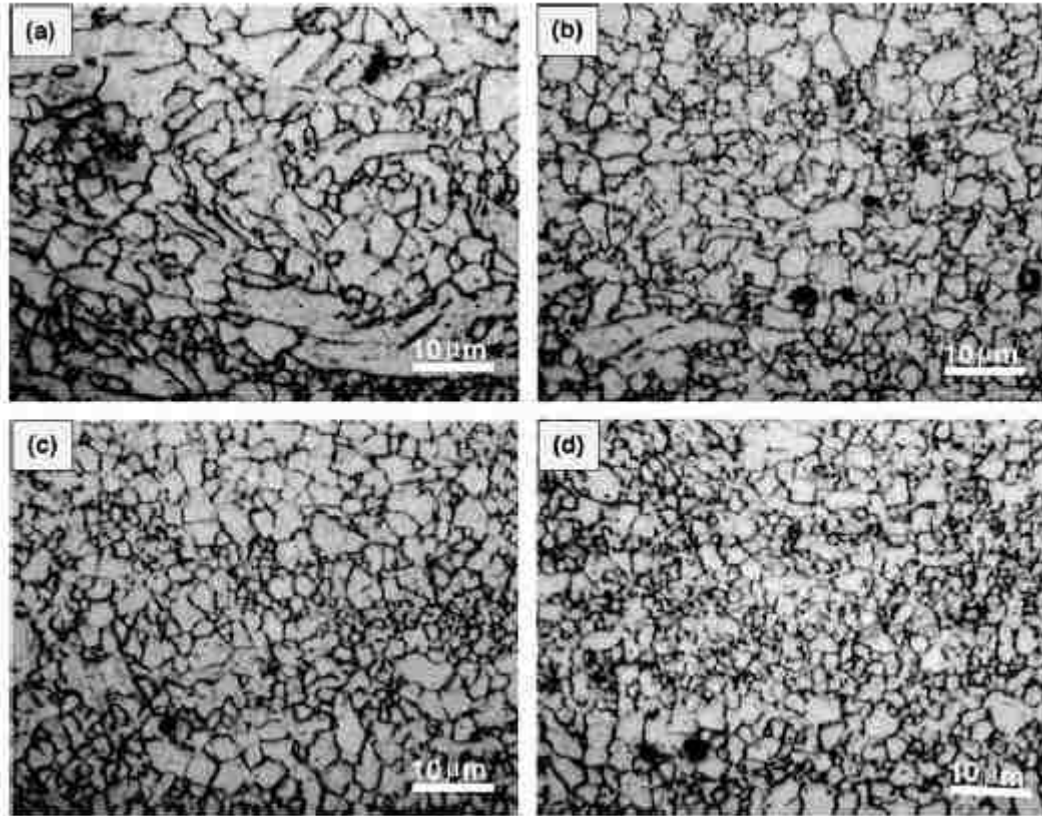


Figure 2- 13. Effect of accumulative roll bonding on the microstructure of AZ31 alloy (a) first rolling, (b) second rolling, (c) third rolling, and (d) fourth rolling [51].

2.4.3.3 Native Grain Refinement of Magnesium Alloys

High purity Mg-Al type alloys have a naturally fine grain size compared to commercial purity alloys with the same basic composition. It appears that the native grain refinement occurs only in magnesium alloys containing aluminum. This observation was first reported by Nelson and recent work by Cao further confirmed Nelson's result [52]. The grain size of a high purity magnesium alloy comparing with a commercial purity alloy with different Al contents is showing in Figure 2-14. In all scenarios, the high purity alloys consistently demonstrated a finer grain size than commercial alloys. The mechanisms of native grain refinement remain unclear. It was assumed that the nucleant

particles responsible for native grain refinement in Mg-Al alloys were Al_4C_3 particles. This hypothesis was built by Motegi et al [53] and they provided evidence showing the presence of particles that contained Al, C and O in the center of many magnesium grains. However, thermodynamically, the Al_2OC phase is less favourable than the formation of Al_4C_3 . In that case, the nucleant particle for high purity magnesium alloys was more likely to be Al_4C_3 .

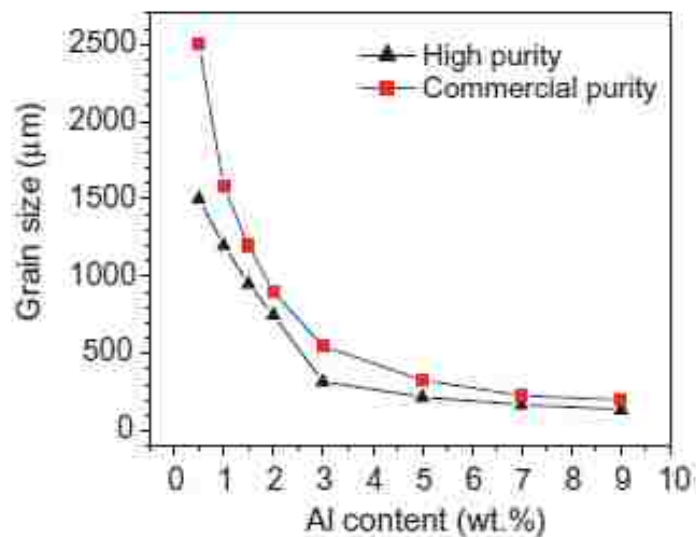


Figure 2- 14. Effect of source magnesium purity on the grain size of Mg-Al alloy [52].

2.4.3.4 Agitation Method

The agitation method simply involves stirring the molten metal with a high speed prior to pouring and is relatively successful when conducted at relatively high temperature. Even though the optimum process temperature for grain refinement has not been determined, Hultgren [54] observed that stirring at a low temperature ($<760^\circ\text{C}$) may not coarse the grain size instead of refinement. Tiner [47] found that stirring at the superheating temperature could improve the degree of grain refinement achieved by superheating method [55]. Due the lack of experimental data and publications about

agitation method, the mechanism of this process remains unclear, and further investigation is still needed.

2.4.3.5 Grain Refining Additions

The grain refiner addition method is the most widely used magnesium grain refinement process since it is relatively easier to operate. Besides, it requires lower operating temperature compared to that of superheating and agitation method provides some economic advantage [55].

Normally, the grain refiners of magnesium alloys containing aluminum can be classified into four groups which includes carbon containing grain refiners, calcium containing grain refiners, FeCl_3 grain refiners also called the Elfinal process and other rare earth elements grain refiners. The mechanisms of each grain refiners are described as follows.

2.4.3.5.1 Carbon containing grain refiners

The addition of carbon containing agents into the melt is a widely accepted grain refinement method of Mg-Al alloys in the industrial world. It offers many practical advantages because of the lower operating temperature and less fading. In carbon inoculation, various kinds of carbon agents, such as C_2Cl_6 , C_6H_6 , MgCO_3 and granular graphite have been proved to have successful grain refinement effect [56]. To explain the mechanism of this carbon addition method, a number of hypotheses have been proposed. So far, the most accepted hypotheses is that, Al_4C_3 , was the compound responsible for the refining effects. During the mixing process, the active carbon was liberated and then reformed as aluminum carbide. To trace the carbon element distribution in the Mg-Al

alloys, Jin [55] suggested using the Electron probe micro-analyzer (EPMA) area analysis method on as-cast AZ31 alloy and the results is shown in Figure 2-15. It appeared that the highest concentration of carbon was in the Al-Mn phase (red particles). This indicates that carbon can easily form a stable carbide phase with Al and Mn. However, the study by Yano et al [58] revealed that these particles had nothing to do with grain refinement or sometimes even deteriorate the refinement effect. Besides the irrelevant Al-Mn phase, the eutectic phase (yellow-green) had the highest carbon concentration as shown in Figure 2-15, followed by the edge of the dendritic arm (blue area) and the central dendritic arm (dark area). This observation indicates that segregation of carbon occurred during solidification and carbon had limited temperature-dependant solubility in magnesium. Therefore, during the solidification process, the carbon was ejected to the liquid-solid interface and greatly affected the constitutional undercooling at that region. Thus, the grain growth was restricted. Meanwhile, the liquid around the crystal was further under-cooled which allows other crystals to nucleate more easily in this region. The effect of 0.6 wt% C_2Cl_6 addition into the as-cast AZ31 alloys is shown in Figure 2-16. The as-cast AZ31 alloy shows a typical equiaxed dendritic structure. Due to the non-equilibrium solidification, many metastable eutectic particles (appeared as black dots) formed in the inter-dendritic region. It is clearly the grain size was significantly reduced from approximately 400 μm to less than 120 μm when C_2Cl_6 is added.

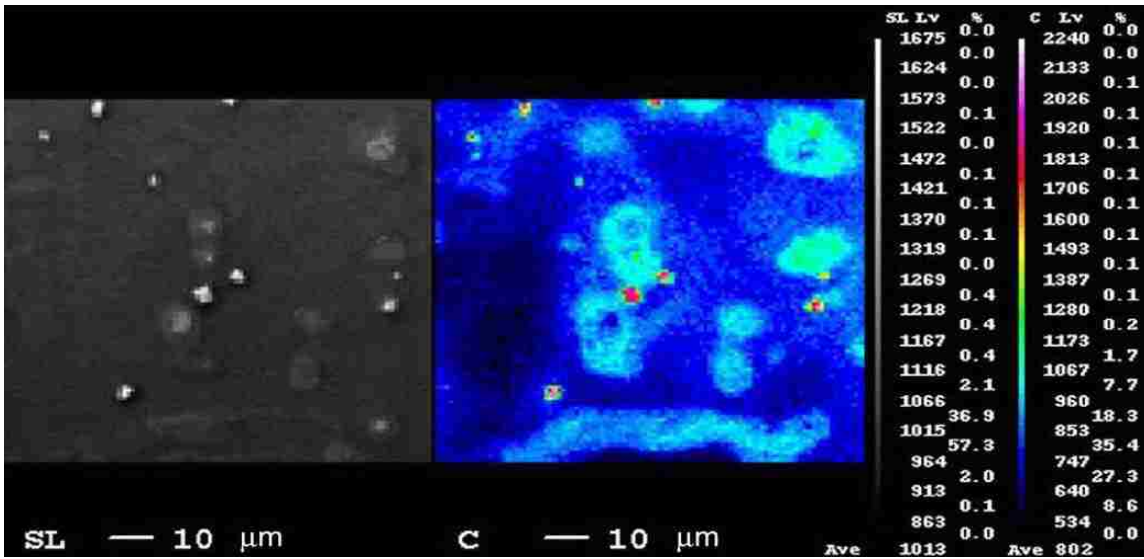


Figure 2- 15. Result of EPMA analysis of AZ31 alloy [55].

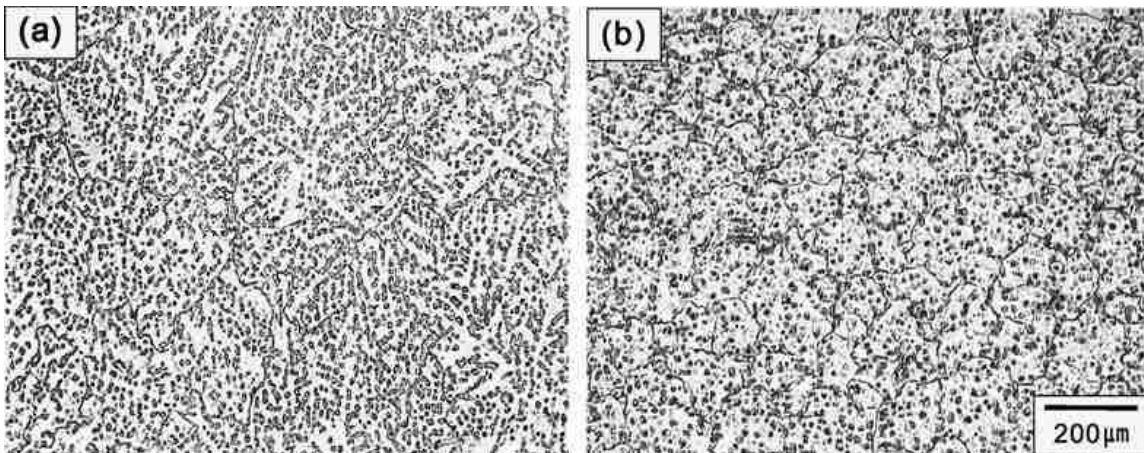


Figure 2- 16. Optical microstructure of sand casting AZ31 alloy (a) no C₂Cl₆ and (b) 0.6wt% C₂Cl₆ addition [55].

Recently, the most successful grain refiner of commercial use, C₂Cl₆, has been prohibited in the magnesium industry because it generates dioxins when introduced into the melt. Therefore, some other carbon containing grain refiners has to be developed to solve this problem. Chloride has almost nothing to do with the grain refinement process other than being released in the air and become toxic gas. Yano et al [58] proposed that,

instead of C_2Cl_6 , pure carbon powder can be used in the process to obtain a better grain size of magnesium alloys. It turns out the result was quit promising. With the help of the argon gas, the experiment was simply carried out by blowing the pure carbon powder into the melt before pouring.

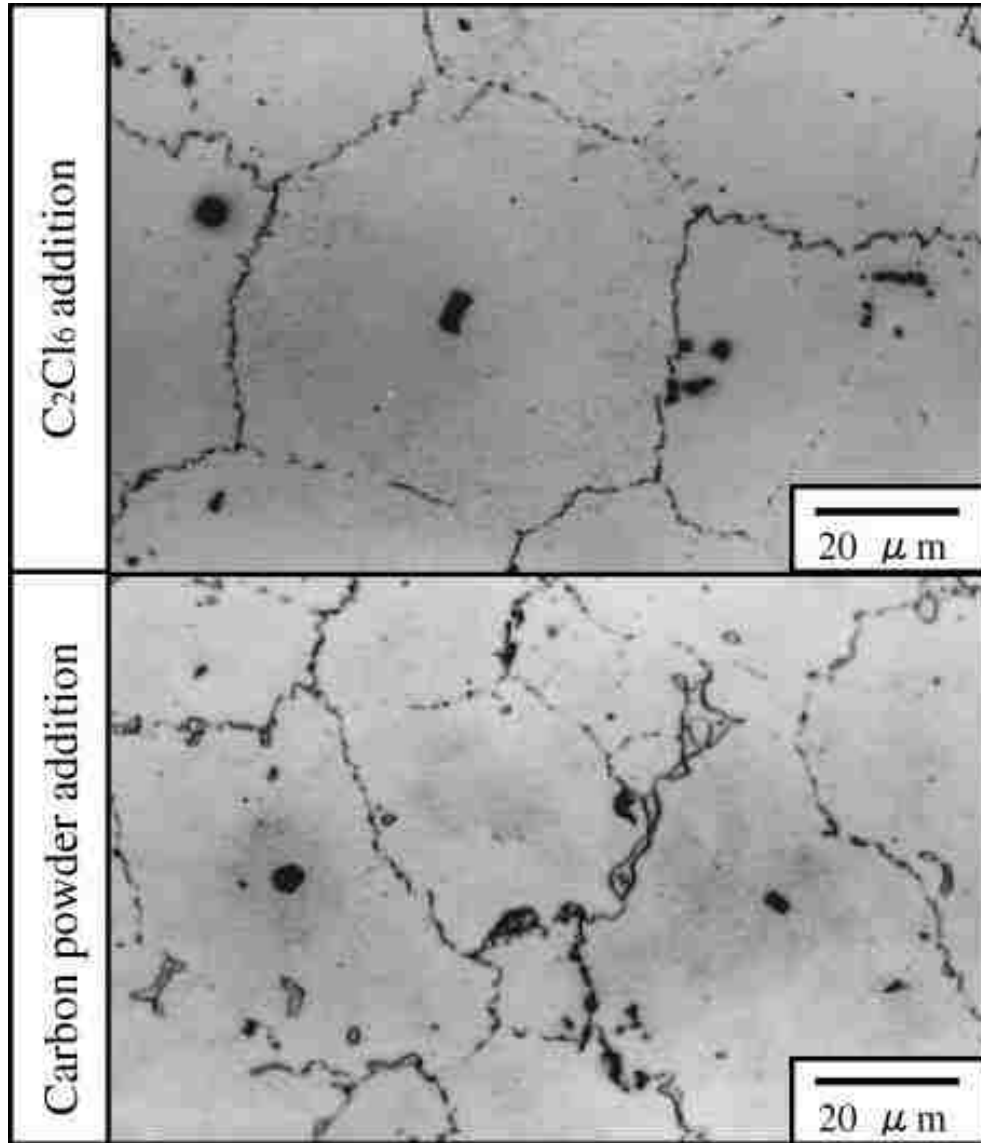


Figure 2- 17. Optical microstructure of AZ91E alloy produced by adding C_2Cl_6 and carbon powder [58].

Figure 2-17 shows the optical micrographs of AZ91 alloy by adding C_2Cl_6 and carbon powder. The same refinement effect can be found that the grain size reached approximately 70 μm in both cases. With the EPMA analysis, as shown in Figure 2-18, the concentration of Mg, Al, C and O elements were detected qualitatively by analysing A-B straight line across one particle. At the center of the particle (the black dot), the Al and C elements reached the maximum amount meanwhile Mg becomes the minimum. This observation further proved that Al_4C_3 acts as the nucleation site of magnesium alloys. Even though carbon powder could produce as fine grains as C_2Cl_6 did to the magnesium alloys, the process requires a relatively higher operating temperature at 750°C which makes it less attractive on the commercial point view.

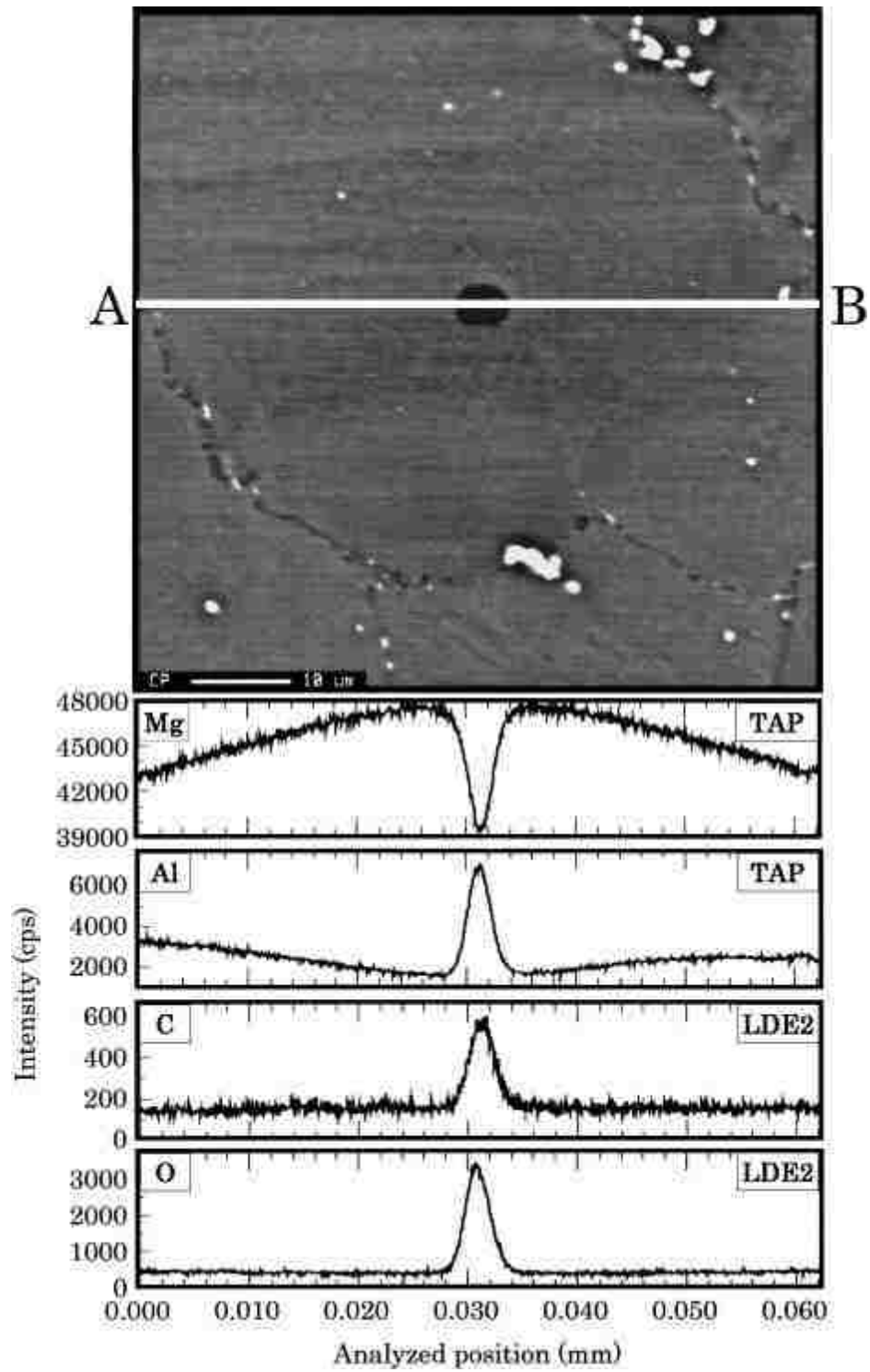


Figure 2- 18. EPMA line analysis of Mg, Al, C and O elements on the line AB across the particle in AZ91E alloy [58].

2.4.3.5.2 Calcium containing grain refiners:

Calcium is another important grain refiner for magnesium alloys. Numerous publications have proved that calcium is just as capable as carbon regarding to the grain refinement process of magnesium alloys [59-60]. Meanwhile, calcium is also a solution to further develop the Mg-Al alloys for high temperature applications. In the 1960s, the calcium was already added into the magnesium alloys in which both creep and oxidation resistance were significantly improved by having a chemical reaction with β -Mg₁₇Al₁₂ phase. Ninomiya et al [61] found out that depending on the mass ratio of Ca to Al, calcium atoms could reform to different phases. They proposed that for the Ca/Al ratios of less than 0.8, Al₂Ca is the only phase that would be formed. Higher value of Ca leads to the formation of both Mg₂Ca and Al₂Ca in the microstructure. As mentioned in the previous section, the key to improve the mechanical properties of magnesium alloys under high-temperature is the elimination of Mg₁₇Al₁₂ phase. To determine the reasonable amount of Ca addition into the magnesium alloys, Kondori and Mahmud [62] did a series of experiments and found out that, for AM60 alloys, the addition of 2.0 wt% of calcium could fully eliminate the Mg₁₇Al₁₂ phase. The X-ray diffraction analysis showing the presence of each phase is listed in Figure 2-19. When the calcium reached 2.0 wt%, the peak for Mg₁₇Al₁₂ phase vanished and Al₂Ca was the only phase detected in the XRD pattern. That means, the Mg₁₇Al₁₂ phase was fully suppressed by the calcium elements. Because of this β -phase suppressing process, the thermal stability of AM60 alloys was significantly improved. Figure 2-20 shows the optical micrographs of the improvement, in which, comparing to the AM60, significant grain reduction was found in the AM60 – 2.0Ca conditions.

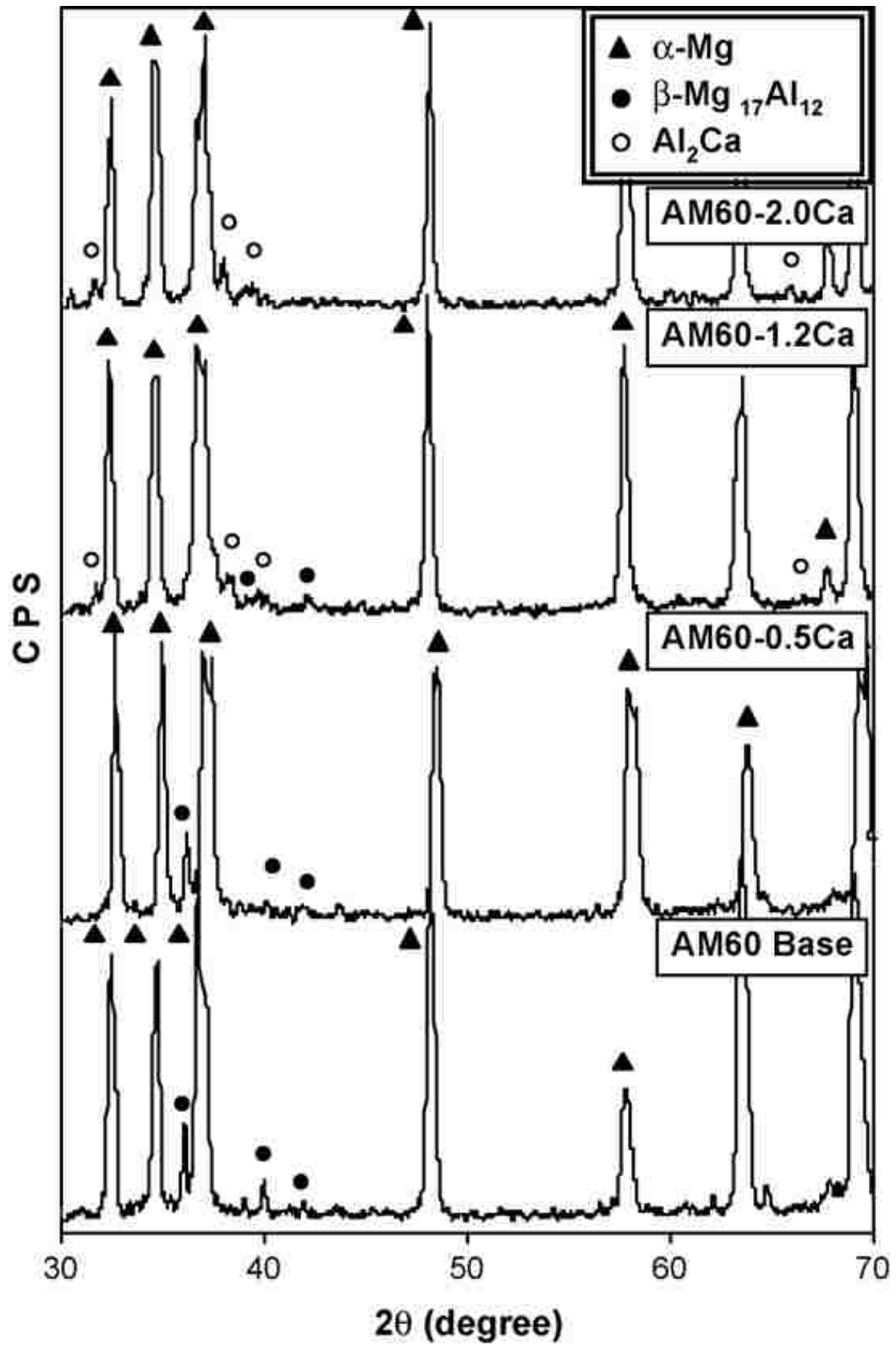


Figure 2- 19. X-ray diffraction patterns of the AM60 containing different amount of Ca [62].

In spite of all the advantages, the die-sticking and hot cracking were still the problem that limited the practical use of calcium grain refiners.

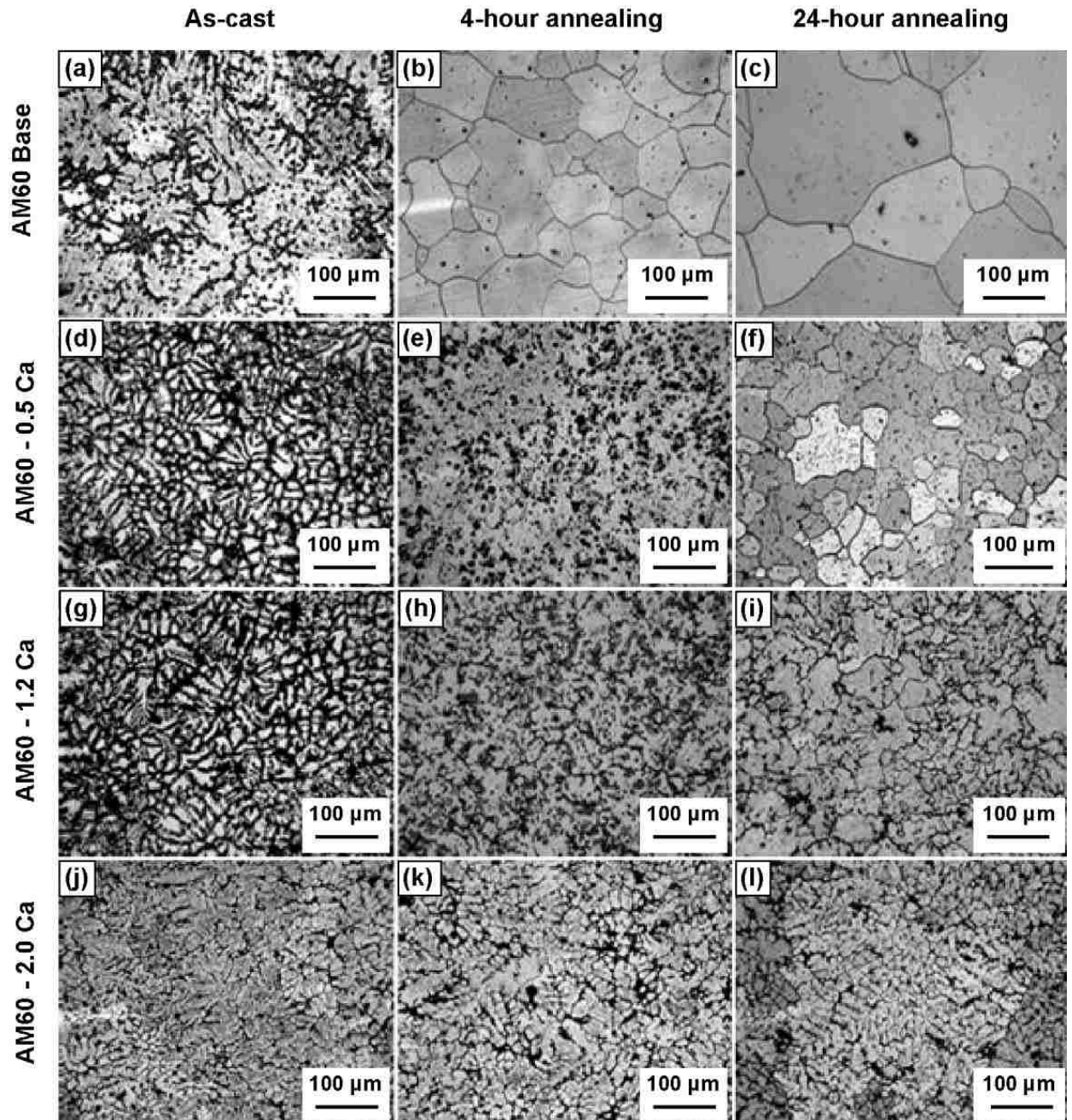


Figure 2- 20. Optical microstructure of AM60 alloy containing different amount of Ca in and annealing conditions [62].

2.4.3.5.3 $FeCl_3$ addition—the Elfinal process:

The Elfinal process involves the addition of anhydrous ferric chloride ($FeCl_3$) into the molten metal at the pouring temperature ($750^\circ C$). One of the advantages of this method is that it allows the melt to be held at pouring temperature for over an hour without any loss in grain refinement efficiency. It has been pointed out that this kind of grain refinement can only be achieved when Mn and at least 3 wt% of Al is present in the alloy. In this case, Emley [36] suggested that Fe-Mn-Al compounds should be the nucleation particle of Elfinal grain refinement process. However, since Fe is well known as detrimental to the corrosion resistance of magnesium alloys and this process releases a certain amount of Cl^- , this grain refinement approach still stays in the theoretical level.

2.4.3.5.5 Rare earth elements grain refiners:

Apart from the use of carbon, calcium and $FeCl_3$, many other additives have been tried. These includes Sr, RE, Th, B, AlN, TiB_2 and TiC. The comparisons of some popular grain refiners on sand casting AZ91E alloy have been carried out by Wallace et al [3]. It can be found out in Figure 2-21 that C_2Cl_6 has the best refinement effect followed by SiC and CaC_2 . Other refiners all take effect on the AZ91E alloy but apparently not very comparable with C_2Cl_6 [3].

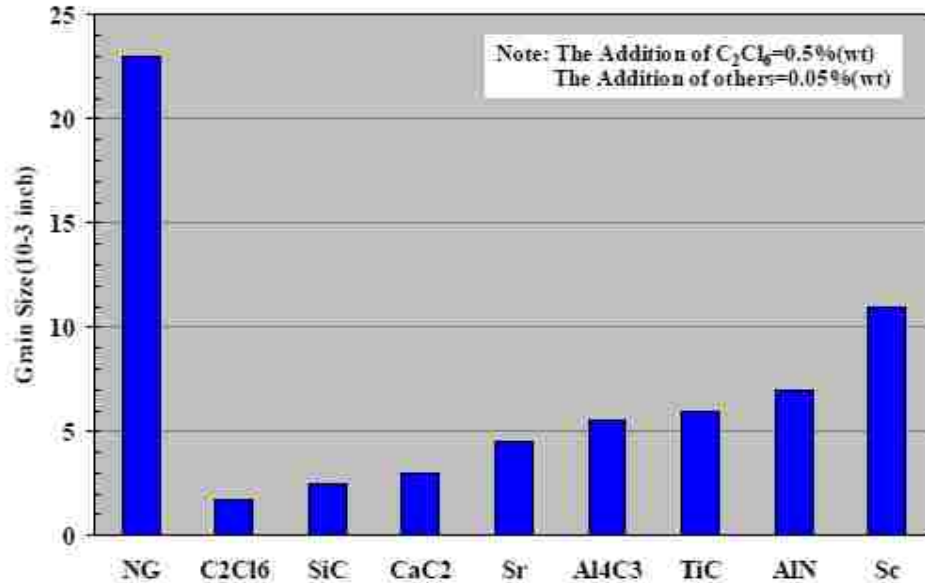


Figure 2- 21. Grain refinement effect on AZ91 alloy [3].

2.4.3.5.5 Holding Time

The holding time of the grain refiners in the melt before pouring is also a critical factor that affects the efficiency of the refinement process. The study of several grain refiners on AM50A alloy in term of the effect of holding time was carried out by Wallace et al [3]. It was pointed out that, at short holding times (in this case 45min), the grain diameter remains stable as shown in Figure 2-22. Karlsen et al [63] had the similar result when the holding time of wax-CaF₂ and C₂Cl₆ was studied on AZ91 alloys. With a longer holding time (more than 2 hours), the efficiency of the grain refiners could be reduced at a relatively lower operating temperature. However, the problem could be solved by simply increasing the temperature of the molten metal to at least 740°C. The grain size was approximately the same at all holding times in the temperature range 740 - 760°C [63].

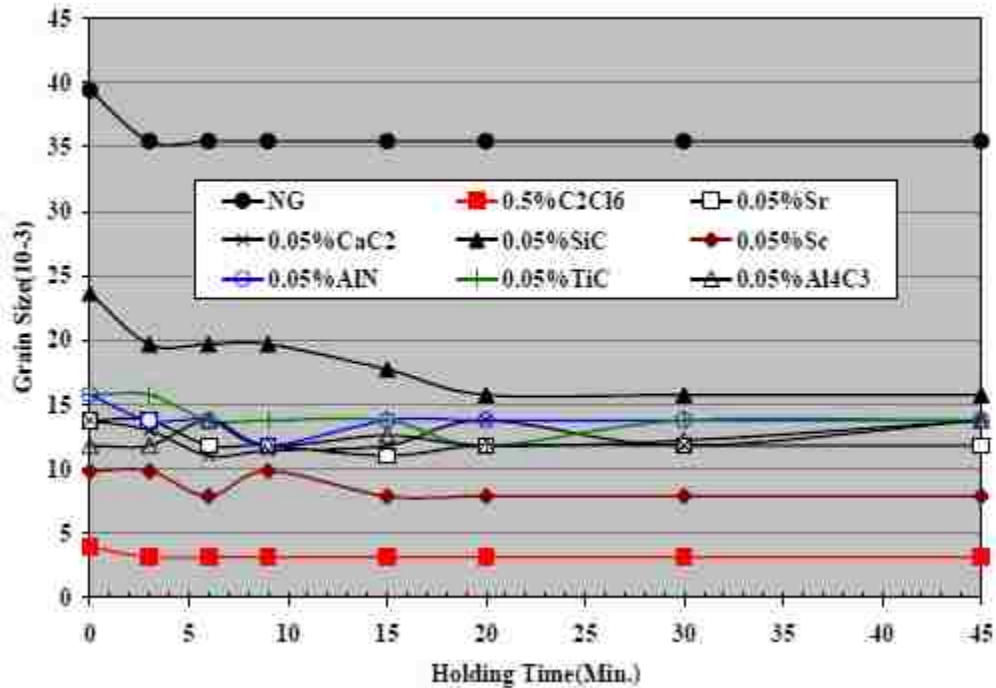


Figure 2- 22. Effect of holding time on AM50 alloy [3].

2.5 Summary

The literature on the grain refinement of magnesium alloys was reviewed according to whether the alloy contains aluminum. The aluminum free magnesium alloys are commonly refined by Zr and this kind of technique has been well established both scientifically and commercially. However, due to the high cost and lack of efficiency of the Zr addition, further development is still necessary. On the other hand, the understanding of grain refinement on aluminum containing magnesium alloys is still short of reliable data. Even though a number of grain fining method has been developed, they each suffer from different kinds of problems which makes them difficult to be used in the automotive industry. Meanwhile, the squeeze casting process has great advantages over die casting processes to produce thick casting, in which coarse microstructure is

present. To expand the application of the squeeze casting process to aluminum-containing magnesium alloys, it is essential to develop a scientific understanding of grain refinement mechanisms for squeeze cast magnesium alloys.

Table 2-1 Grain refining method for casting magnesium alloys

Al-containing Mg alloys	Grain Refiners			Superheating	Hot Rolling	References
	C ₂ Cl ₆	CaC ₂	FeCl ₃			
AZ31	Good	Good	NG	Good	Good	[50], [55], [64]
AZ91	Good	Good	Good	Good	NG	[3], [65], [66], [67]
AM50	Good	Good	NG	Good	NG	[3], [68]
AM60	Good	NG	NG	Good	Good	[69], [70]
Al-free Mg alloys	Zirconium			Superheating	Hot Rolling	
ZK40	Very Good			Good	NG	[71], [72]
WE54	Very Good			NG	NG	[73]
QE22	Very Good			NG	NG	[74]

CHAPTER 3: EXPERIMENTAL PROCEDURES

3.1 Materials and Processing

Commercially-available magnesium alloy AM60 was used as the base alloy for the study. The chemical composition of the alloy is given in Table 3-1. Two conventional grain refiners for aluminum-containing magnesium alloys, hexachloroethane (99% C_2Cl_6) and calcium carbide (80% CaC_2) powders produced by Sigma Aldrich® were selected as the grain refiners of the alloy. The chemical properties of each grain refiner are listed in Table 3-2. The amount of C_2Cl_6 and CaC_2 addition were both 0.5 wt% at first based on the previous studies. Then the amount of CaC_2 addition was cut into half (0.25 wt%) due to the high inclusion level cause by melt oxidation. Alloy specimens were prepared by using a mixing and casting process which was carried out by an electric furnace and a 75-ton vertical hydraulic press showing in Figure 3-1. Basically, the melt processing of C_2Cl_6/CaC_2 -refined magnesium alloy AM60 consisted of mixing the pre-heated C_2Cl_6/CaC_2 powders with the liquid alloy AM60, and melt stirring. In each batch, 0.5 kg of the C_2Cl_6/CaC_2 -treated melt was prepared in the electric resistance furnace using a steel crucible under the protection of SF_6/CO_2 gas blend. The melt was held at 700 °C for half an hour, stirred for 10 minutes, and cast at 700 °C. The un-refined AM60 was also cast at the same condition.

Table 3-1 Chemical composition of cast alloy AM60

AM60	Magnesium	Aluminum	Manganese	Zinc
Content (%)	93.2	6.0	0.38	0.2

Table 3-2 Chemical properties of C_2Cl_6 and CaC_2

	Assay (%)	Melting Point (°C)	Density (g/ml)
C_2Cl_6	99	185	2.091
CaC_2	80	2000	2.220



(a)



(b)

Figure 3- 1. (a) Electric furnace with SF_6/CO_2 gas protection, and (b) vertical hydraulic press.

3.2 Thermal Analysis

The DSC test was carried out using a DSC-TGA Q600 analyzer manufactured by TA Instrument at a heating rate of $10\text{ }^\circ\text{C}$ per minute over the temperature range of 50 to $800\text{ }^\circ\text{C}$. An argon flow rate of 100 ml/min was used to prevent sample contamination from the measurement beams and also the oxidation during and after DSC runs. The nitrogen-cooling was also used for all runs after heating. Before each test run, a baseline

run was required and the DSC trace was then corrected by subtracting the baseline. Figure 3-2 shows the DSC analyzer used in the experiment.



Figure 3- 2. DSC-TGA Q600 analyzer.

For the cooling analysis, about 0.2 kg of melt samples was taken from the well-stirred alloy melt at 700 °C into a steel crucible. A chromel-alumel (K-type) thermocouple protected by a thin steel sheath was positioned at a distance of 0.02 m from the bottom of the crucible center, and was connected to a computer-based data acquisition system to measure the temperature variation. In cooling analysis, the temperature of the solidifying AM60 alloy and grain-refined sample was recorded by the data acquisition system at a regular interval of 500 ms as they cooled (25 °C/min) from the completely liquid state, through the solidification range, to become fully solid. The melt samples were protected with SF₆/CO₂ gas blend during the entire measurement period. The melt temperature (T) vs. time (t) data was processed and cooling curves (T vs. t) were plotted

using the Microsoft Excel spreadsheet software. Several duplicate runs on each melt were conducted to ensure an uncertainty of $\pm 0.1\%$.

3.3 Microstructure Analysis

Specimens were sectioned, mounted and polished from the center of the squeeze cast disc and prepared following the standard metallographic procedures. To reveal the grain boundaries, a T4 heat treatment was subjected to the as-cast AM60 specimens to dissolve the β intermetallics ($Mg_{17}Al_{12}$). The heat treatment was conducted in an electric furnace. In order to prevent the sample oxidation when exposed to the hot air, all samples were placed in a steel cup and covered with sand. Before the microstructure analysis, the as-cast specimens were etched using a solution of acetic-picral (5 ml acetic acid, 6 g picric acid, 10 ml H_2O and 100 ml ethanol) for 5 seconds, and the T4 heat treated specimens were etched using a solution of acetic-glycol (20 ml acetic acid, 1 ml HNO_3 , 60 ml ethylene glycol and 20 ml H_2O) for 20 seconds. A Buehler optical image analyzer 2002 system was used to determine the primary characteristics of the specimens, as shown in Figure 3-3 (a). The detailed features of the microstructure were characterized at high magnification using a FEI Quanta 200 FEG scanning electron microscope (SEM) which is shown in Figure 3-3 (b).



(a)

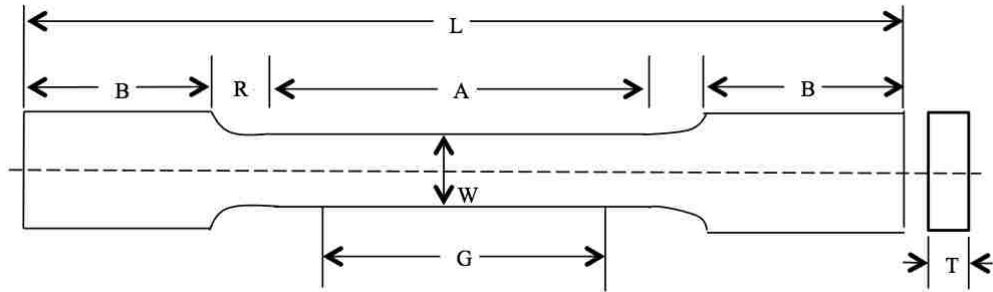


(b)

Figure 3- 3. (a) Buehler optical image analyzer model 2012, and (b) Scanning electron microscopy (FEI Quanta 200 FEG).

3.4 Tensile Testing

Tensile testing was carried out to evaluate the effect of grain refiners on the mechanical properties of the alloy. Each specimen was polished by grinding paper of grit 320 to avoid stress concentration and cross-section dimensions were measured for tensile testing. The tensile tests were performed at room temperature with a strain rate of 2.00 mm/min. The outputting data, including displacement measured by extensometer and tensile load, were then analyzed. The average 0.2% offset yield (YS) as well as highest observed ultimate tensile strength (UTS) and % elongation (E_f) was also determined for each heat treatment condition. Figures 3-4 and 3-5 show the dimensions of tensile specimens and the Instron tensile machine, respectively.



- G:** gage length 25 ± 0.1 mm **W:** width 6 ± 0.1 mm
- T:** thickness 3 ± 0.1 mm **R:** radius of fillet 6 mm
- L:** overall length 100 mm **A:** reduced section 32 mm
- B:** length of grip section 30 mm

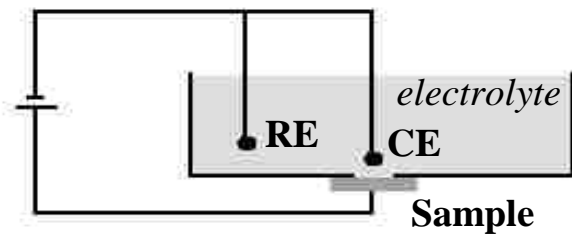
Figure 3- 4. Schematic illustration of tensile specimen.



Figure 3- 5. Instron tensile testing machine (Model 8562).

3.5 Potentiodynamic Polarization Testing

Potentiodynamic polarization testing was carried out by exposing 0.8 cm² of sample surface area to the electrolytic media. Each sample was tested using 3.5% wt NaCl solutions. Two electrodes were submerged in the electrolytic: a counter electrode, CE, near the sample surface, and a reference electrode, RE, elsewhere in the solution. The set-up shown in Figure 3-6 describes the system.



(a)



(b)

Figure 3- 6. (a) Potentiodynamic polarization test set-up, and (b) EC-LAB SP 150 electrochemical apparatus for corrosion test.

The potentiodynamic polarization testing curves were plotted by EC-Lab® software. The corrosion current density, i_{corr} , which is equal to corrosion rate, was approximated from the curve. Meanwhile, the anodic and cathodic slopes β_A and β_C were calculated. Equation 3-1 expresses the determination of the polarization resistance.

$$R = \frac{\beta_a \beta_c}{2.303 i_{corr} (\beta_a + \beta_c)} \quad (3-1)$$

CHAPTER 4: RESULTS AND DISCUSSION

4.1 Appearance of Squeeze casting Products

A squeeze cast cylindrical coupon with a diameter of 100 mm and a height of 25 mm was shown in Figure 4-1. For all three conditions (un-treated AM60 alloy, C_2Cl_6 -treated AM60 alloy and CaC_2 -treated AM60 alloy), tensile testing specimens were cut out from the bottom section of the respective coupon. The reason for this is that, the bottom section had a direct contact with the piston during the squeeze casting processes, which resulted in rapid cooling rate during solidification of the alloys under an applied pressure. As a consequence, high quality and enhanced mechanical properties in the bottom section were achieved.



Figure 4- 1. Squeeze cast cylindrical coupon.

The 5-step shape casting product designed for studying the effect of section thickness on microstructure of squeeze casting alloys AM60 is shown in Figure 4-2 in three views. The 5 steps, from top to bottom, have the respective dimensions of 100x30x3 mm, 100x30x4 mm, 100x30x6mm, 100x30x10 mm and 100x30x20 mm. In this study, the 6 mm, 10 mm and 20 mm sections were extracted from the step casting for tensile testing and microstructural analyses.

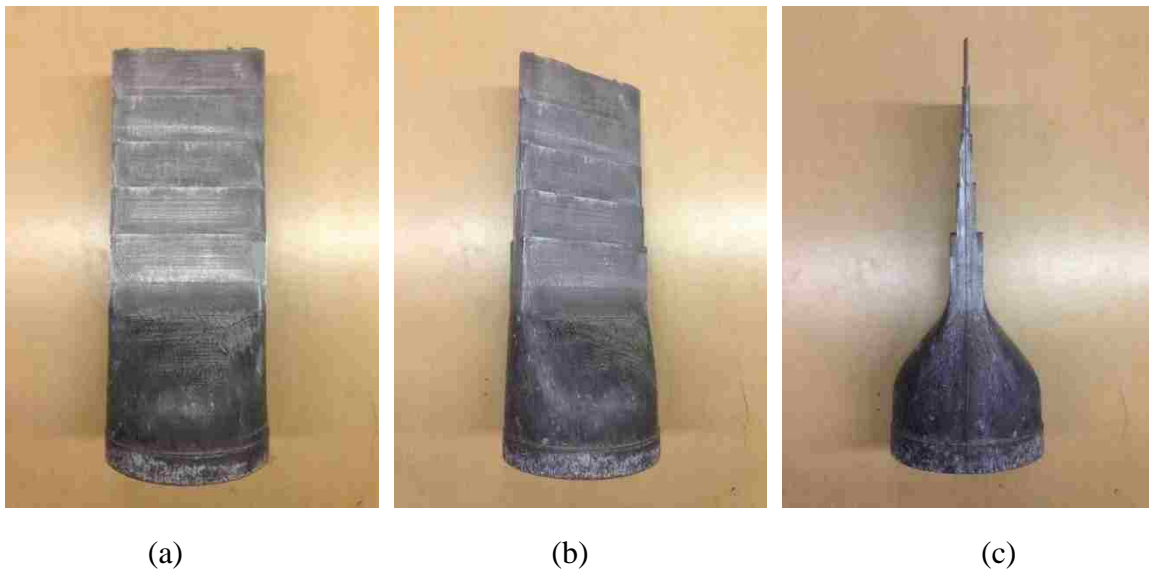


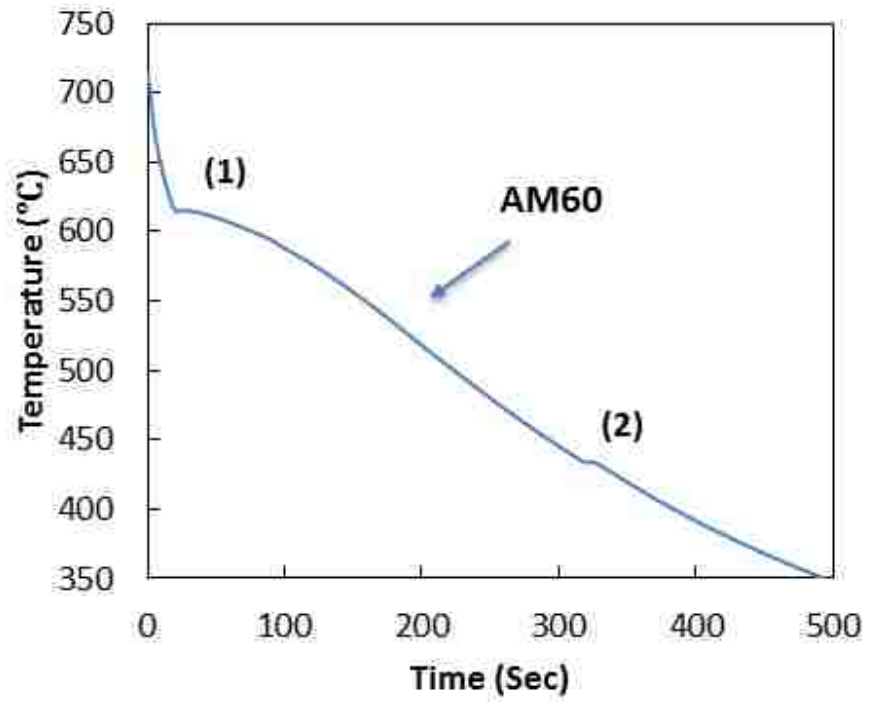
Figure 4- 2. 5-step squeeze casting with a round-shape gating system.

4.2 Solidification of magnesium alloy AM60

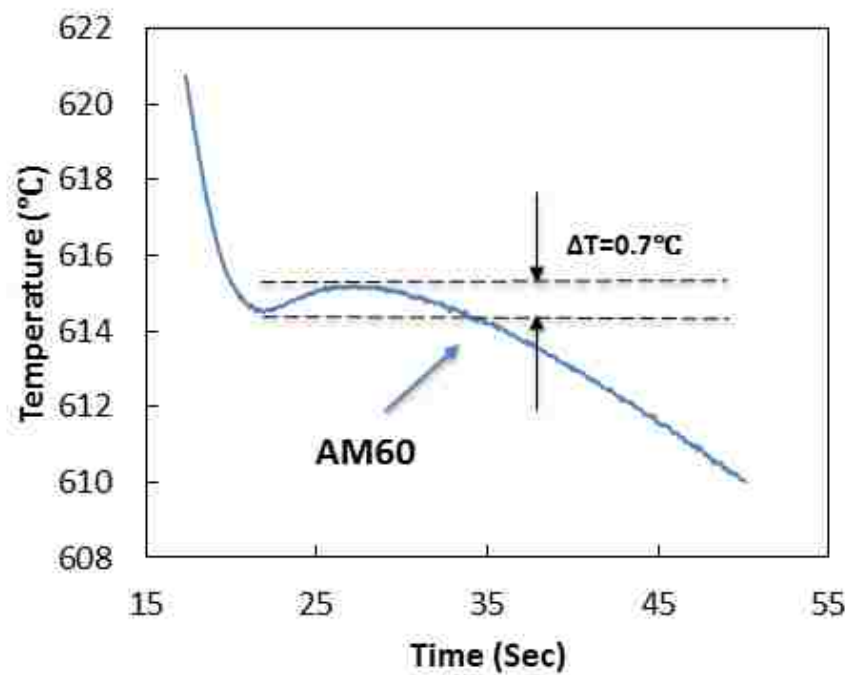
4.2.1 Cooling Curve Analysis

To understand the solidification processes of the grain refiner-treated AM60 alloys, the cooling curves of the materials were measured. Figure 4-3 (a) represents the typical result of thermal analysis for AM60 alloy. Two distinct stages during the solidification process are easily observed, stage (1), the nucleation of primary magnesium

phase at around 614.5 °C, and stage (2), the eutectic reaction, i.e., $L \rightarrow \alpha\text{-Mg} + \beta\text{-Mg}_{17}\text{Al}_{12}$ at around 435 °C. The enlarged stage (1) of the cooling curve given in Figure 4-3 (b) evidently shows a considerable difference in the degree of supercooling ($\Delta T = 0.7$ °C) at the liquidus temperature plateau. The cooling curves of C_2Cl_6 and CaC_2 -treated AM60 alloy are given in Figure 4-4 (a) and Figure 4-5 (a), respectively. Base on the cooling curves, no appreciable difference is presented in the liquidus and solidus temperatures between AM60 and the grain-refined AM60 alloys. For both C_2Cl_6 and CaC_2 -treated AM60, however, no apparent supercooling is observed in Figure 4-4 (b) and Figure 4-5 (b), which illustrated the enlarged stage (2) of the cooling curve. It was reported by Kurfman [75] that supercooling of magnesium and aluminum alloys can be correlated to their grain structure. A measurable supercooling is required for the solidification process to cause the nucleation reaction to begin. This supercooling, acting as the thermodynamic driving force while heterogeneous nuclei is absent, usually appears on the cooling curve as a drop in temperature below the equilibrium temperature for the nucleation reaction. Once the nucleation reaction commences, the temperature of the solidification fronts rises due to evolved latent heat, and the grain growth occurs at the temperature close to the normal equilibrium temperature. With the addition of the grain refiners, the number of nuclei and the nucleation rates likely increase. Consequently, small or no supercooling appear on the cooling curves as the fine grain structures are achieved. The difference in supercooling appearance can be directly attributed to the mechanism of the primary phase nucleation, and consequently, the extent of grain refinement.

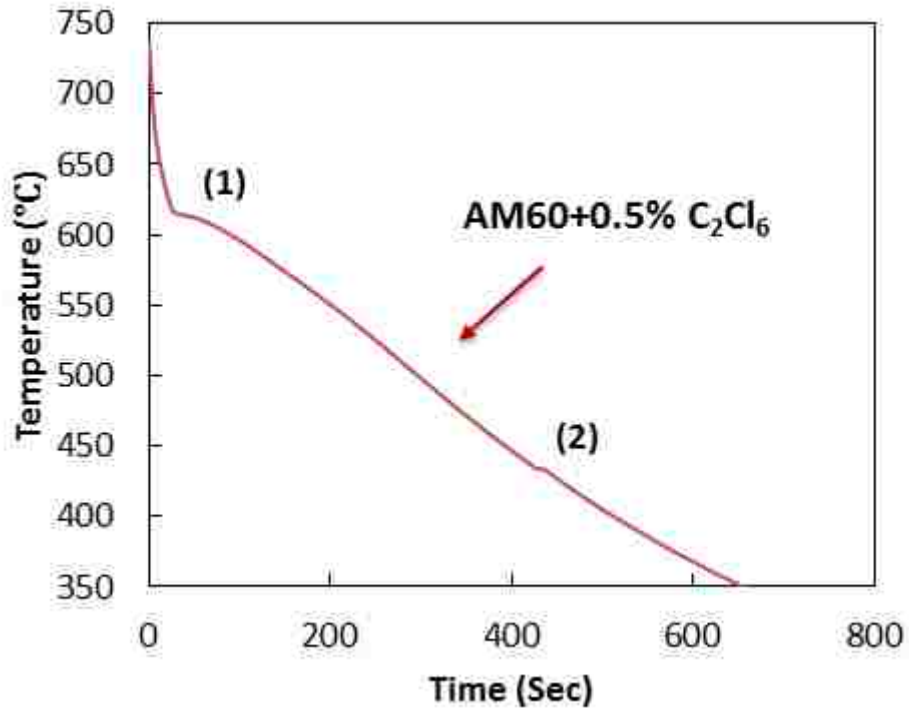


(a)

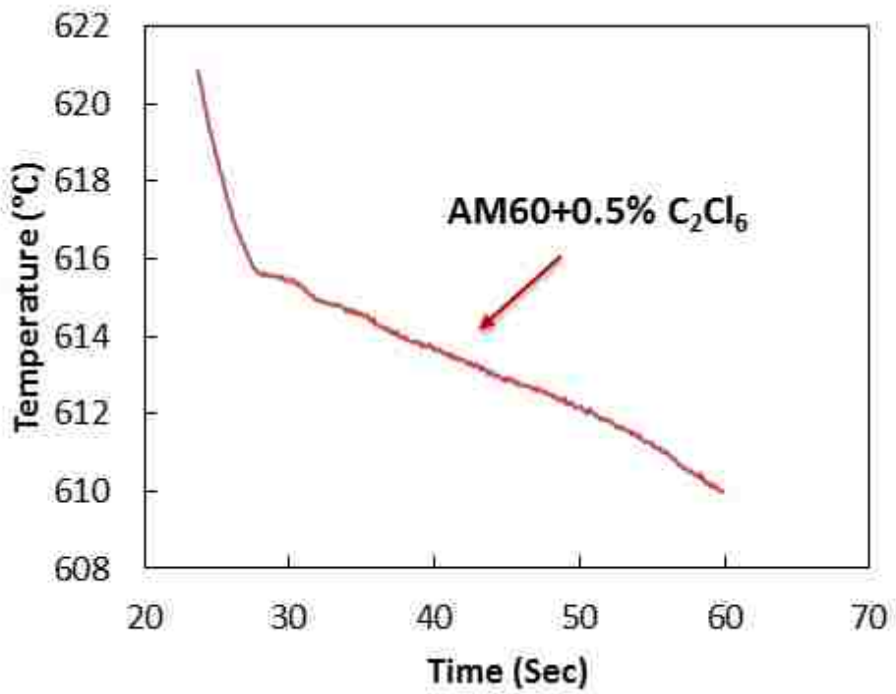


(b)

Figure 4- 3. (a) Typical cooling curve, and (b) enlarge liquidus temperature region of AM60.

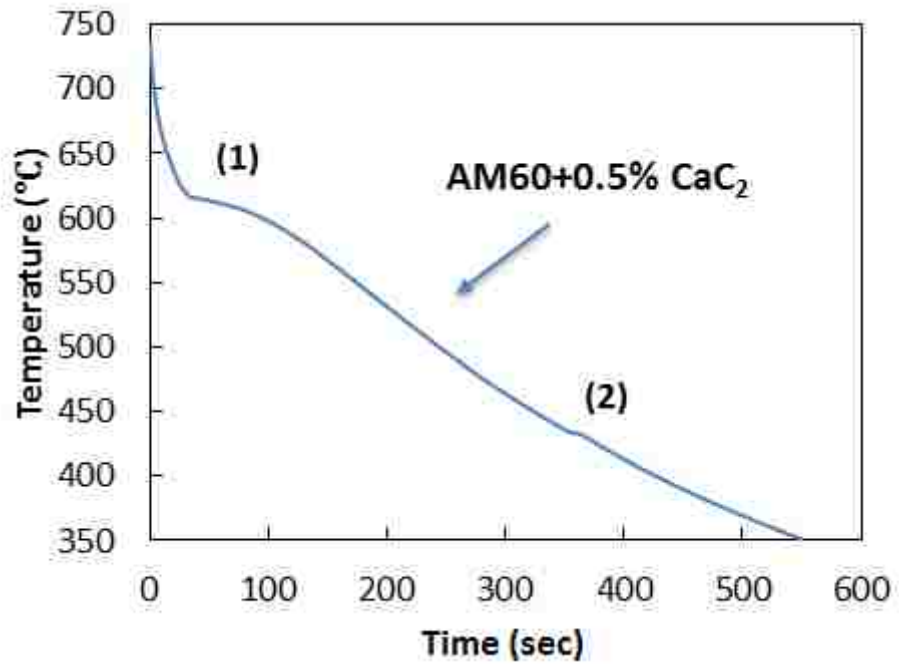


(a)

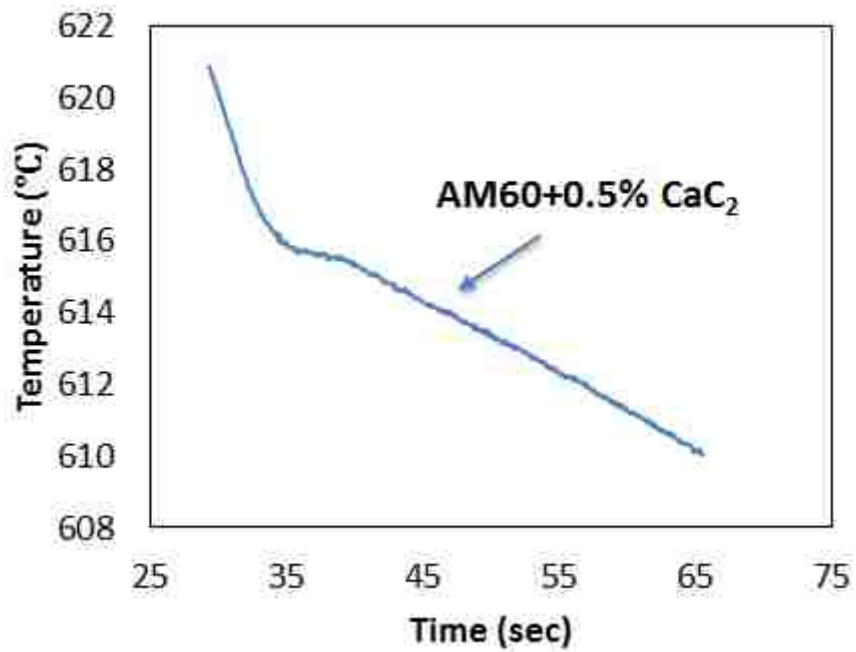


(b)

Figure 4- 4. (a) Typical cooling curve, and (b) enlarge liquidus region of C_2Cl_6 -treated AM60.



(a)



(b)

Figure 4- 5. (a) Typical cooling curve, and (b) enlarge liquidus region of CaC_2 -treated AM60.

4.2.2 DSC Analysis

Figure 4-6 presents the typical melting curves for AM60 and C_2Cl_6/CaC_2 -treated AM60. Upon heating the samples, two typical endothermic peaks at around 615 °C and 435 °C were observed. The former peak at 615 °C was induced by the melting of primary α -Mg phase. The latter one was present to melt the eutectic β -phase ($Mg_{17}Al_{12}$). It can be found out in Figure 4-6 and Table 4-1 that, with the addition of C_2Cl_6/CaC_2 in the AM60 alloy, the melting temperatures of primary α -Mg phase and eutectic phase were shifted to a lower value. This observation should be attribute to the addition of grain refiner C_2Cl_6 and CaC_2 .

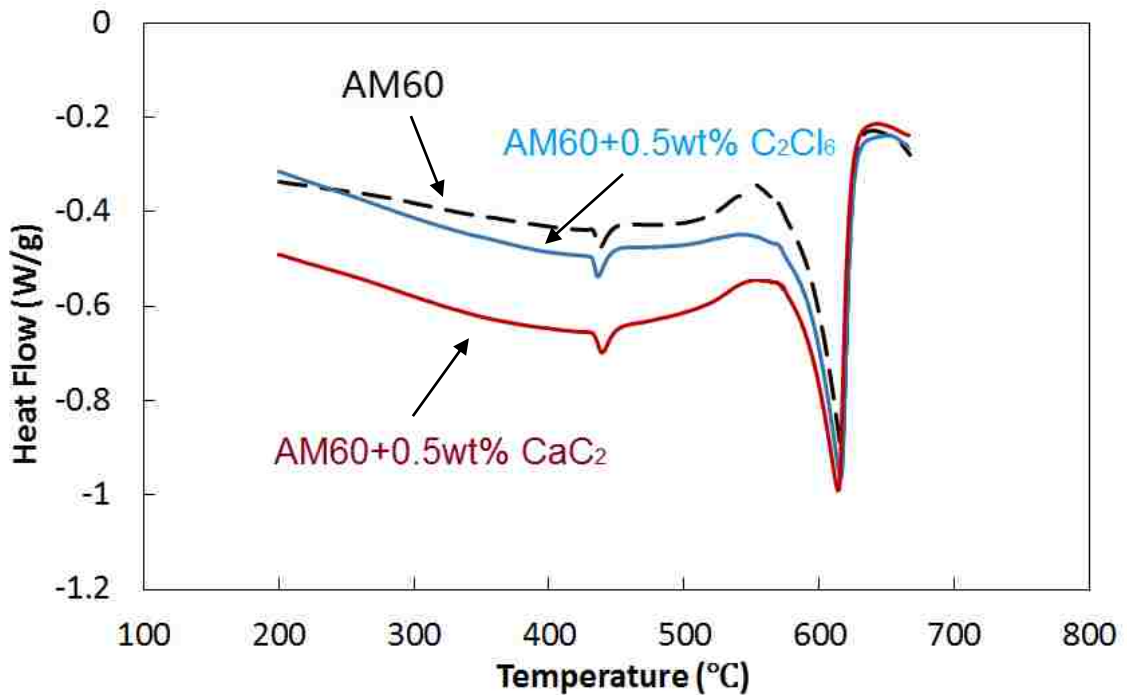


Figure 4- 6. DSC trace of squeeze cast AM60 and C_2Cl_6/CaC_2 -treated AM60 alloys.

Table 4-1 DSC analysis results of AM60 and C₂Cl₆/CaC₂-treated AM60 alloy

	Liquidus Temperature (°C)	Eutectic Temperature (°C)
AM60	616.8	437.4
AM60+C ₂ Cl ₆	615.7	436.2
AM60+CaC ₂	613.9	436.5

4.3 Tensile Behaviour

4.3.1 Tensile Behaviour of cylindrical coupon

The typical engineering stress-strain curves for AM60 and two grain-refined AM60 alloys are shown in Figure 4-7. The corresponding tensile properties such as ultimate tensile strength (UTS), yield strength (YS) and elongation (E_f) are summarized in Table 4-2. It can be seen from Figure 4-7 and Table 4-2 that, the tensile properties of both C₂Cl₆ and CaC₂ treated AM60 alloys were raised to a higher level compare to the un-treated AM60 specimen. The yield strengths of both C₂Cl₆ and CaC₂ treated specimens rose to around 91 MPa on average, which represented an increase of over 14% compared to the un-treated AM60 alloy. It is well know that grain size is one of the major factors that effects the mechanical properties of metals and alloys. According to Hall-Patch equation [76]:

$$\sigma_y = \sigma_0 + Kd^{-1/2} \quad (4-1)$$

where σ_0 is the yield stress of a single crystal, K is the constant and d is the average grain size.

The mechanical properties, especially the yield strength of the material increase significantly with grain size reduction. In this case, the increase in yield strength of C₂Cl₆

and CaC_2 treated AM60 alloys should attribute to the smaller grain sizes cause by the addition of the grain refiners. Meanwhile, the comparable yield strength of the two treated alloys indicates that the two grain refiners, C_2Cl_6 and CaC_2 , are likely to have the similar grain refining capability on squeeze cast alloy AM60.

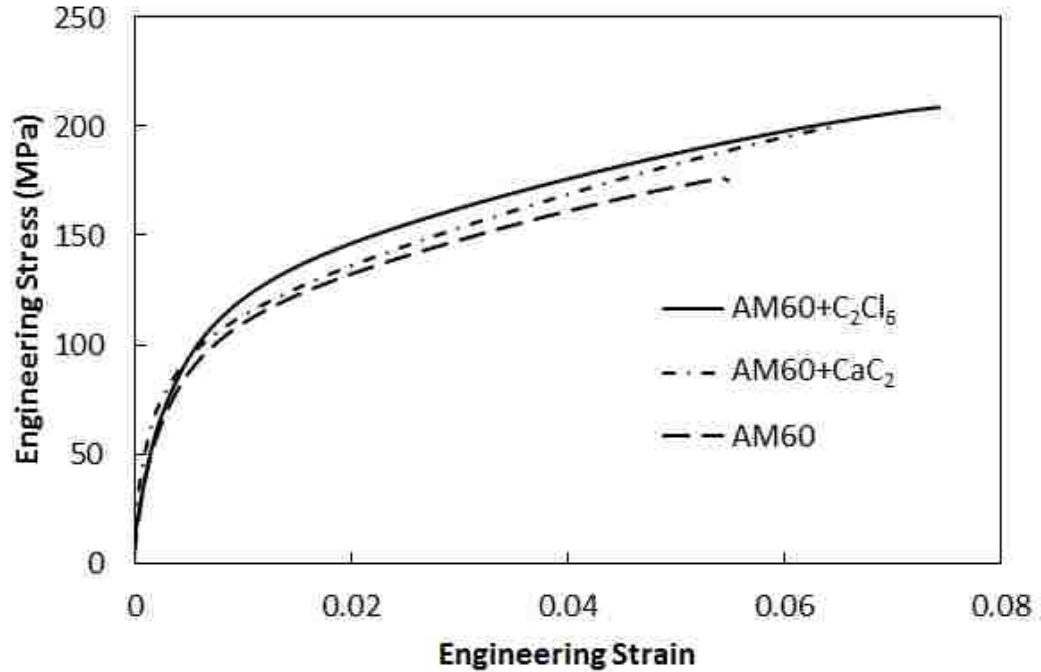


Figure 4- 7. Engineering stress-strain curves of AM60 and $\text{C}_2\text{Cl}_6/\text{CaC}_2$ -refined specimens.

Table 4-2 Tensile properties of AM60 C_2Cl_6 -treated and CaC_2 -treated specimens

	YS (MPa)	UTS (MPa)	E_f (%)
AM60	80.1 ± 4.33	174.9 ± 9.96	5.48 ± 1.59
AM60+ C_2Cl_6	92.5 ± 1.74	208.7 ± 3.85	7.42 ± 0.62
AM60+ CaC_2	90.3 ± 2.82	200.1 ± 5.91	6.45 ± 1.08

The ultimate tensile strength of AM60 alloy was also improved by the addition of C_2Cl_6 and CaC_2 powders. The UTS is 208.7 MPa for C_2Cl_6 -treated specimen and 200.1 MPa for the CaC_2 -treated alloy, which is an increase of 19.1% and 14.4% over the un-

treated alloy AM60 (174.9 MPa), respectively. The elongation of C_2Cl_6 -treated specimen is 7.42%, which was improved by 35% over the un-treated alloy AM60. However, the elongation of CaC_2 -treated specimen was 6.45%, which is an improvement of only 17%. The relatively low elongation level of CaC_2 -treated alloy should be resulting from the high inclusion level cause by the addition of CaC_2 powders.

The true stress-strain curves are given in Figure 4.8 which was generated from the engineering stress-strain curves using the following equation:

$$\sigma_t = \sigma_e (1 + \epsilon_e) \quad (4-2)$$

$$\epsilon_t = \ln (1 + \epsilon_e) \quad (4-3)$$

where σ_t is the true stress, σ_e is the engineering stress, ϵ_t is the true strain, and ϵ_e is the engineering strain.

The strain-hardening behaviours of AM60 and two grain-refined specimens can be seen in a plot of strain-hardening rate ($d\sigma/d\epsilon$) versus true plastic strain (ϵ_t) during the plastic deformation, as shown in Figure 4-9, which was derived from the true stress-strain curves from Figure 4.8. The stress-strain curve for metals is usually described by the power law relationship for plastic deformation as shown in the following equation:

$$\sigma = K \epsilon^n \quad (4-4)$$

where K is the strength index, ϵ is the plastic strain and n is the strain hardening exponent.

The strain hardening rate ($d\sigma/d\varepsilon$) can be obtained by the differentiation of Equation 4-4. The best fit parameters of power law equation for AM60 and grain-refined specimens are given in Table 4-3. All three materials shown the same trend that the strain-hardening rate decreased with the increase in true strain. It is clear that the strain-hardening rate during the plastic deformation of both C_2Cl_6 and CaC_2 treated alloy AM60 were constantly higher than un-treated specimens. The onset of plastic deformation of C_2Cl_6 and CaC_2 treated AM60 were 6205 MPa and 5970 MPa, respectively, which were both higher with respect to un-treated AM60 at 5495 MPa. The high strain-hardening rates implies that, the C_2Cl_6/CaC_2 -treated alloys are able to spontaneously strengthen themselves to a large extent, in response to extensive plastic deformation prior to fracture.

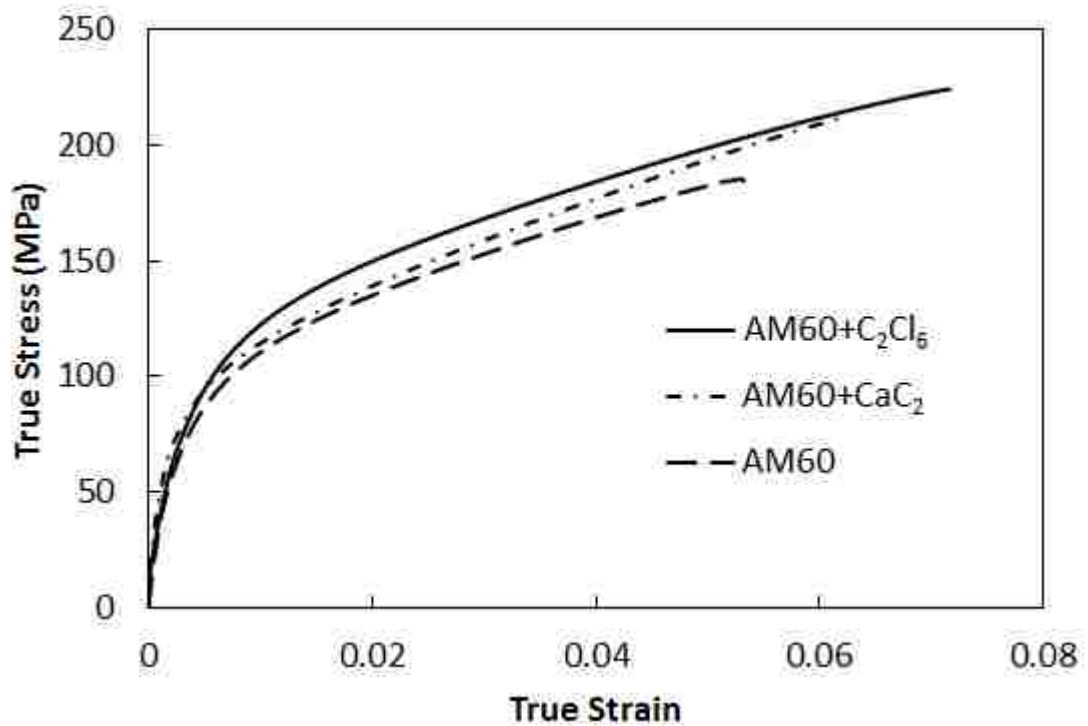


Figure 4- 8. True stress-strain curves of AM60 and C_2Cl_6/CaC_2 -refined specimens.

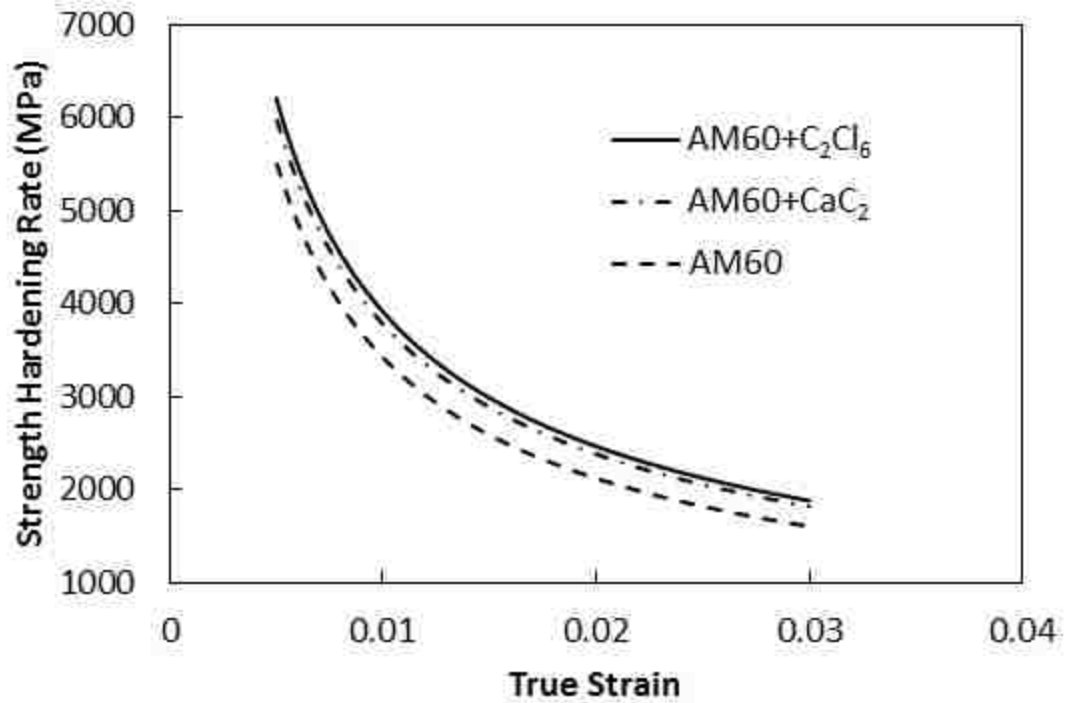


Figure 4- 9. Strain-hardening rate versus true strain for plastic deformation of AM60 and grain-refined specimens.

Table 4-3 Best fit parameters of power law equation

	K (MPa)	n	R ²
AM60	459.04	0.3109	0.9989
AM60+C ₂ Cl ₆	501.65	0.3086	0.9873
AM60+CaC ₂	527.32	0.3357	0.9831

4.3.2 Tensile behaviour of 5-step casting

4.3.2.1 Untreated AM60 alloy

Figure 4-10 shows the representative engineering stress-strain curves for the three thicknesses 6 mm, 10 mm and 20 mm for alloy AM60. Typical tensile behaviours can be observed from the curves. The curves show that under the tensile loads, the alloy

deformed elastically first. Once the yield point is reached, the alloy starts to deformation plastically.

The variation of tensile properties with section thicknesses of alloy AM60 are shown in Table 4-4 and Figure 4-11. It is obvious that the ultimate tensile strength, yield strength and elongation of the 6 mm thick samples are higher than the thicker 10 mm and 20 mm sections. It can be seen from Table 4-4 that, with the increase in thickness from 6 mm to 20 mm, the UTS, YS and E_f were reduced from 220.5 MPa, 96 MPa and 9.0% to 135.3 MPa, 67 MPa and 3.42%, which brings to a decrease of 38.6%, 30.2% and 62.0%, respectively. The decrease in tensile properties with the increased thicknesses should be attributed to the coarser grain structure.

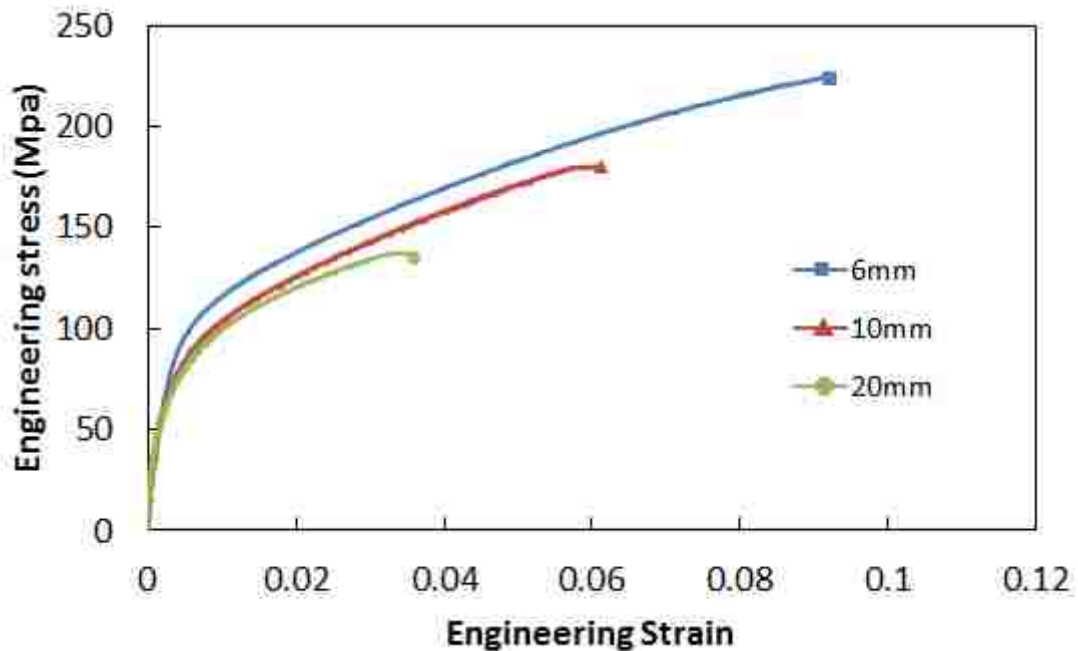


Figure 4- 10. Engineering stress-strain curves of squeeze cast alloy AM60 with 6 mm, 10 mm and 20 mm section thicknesses.

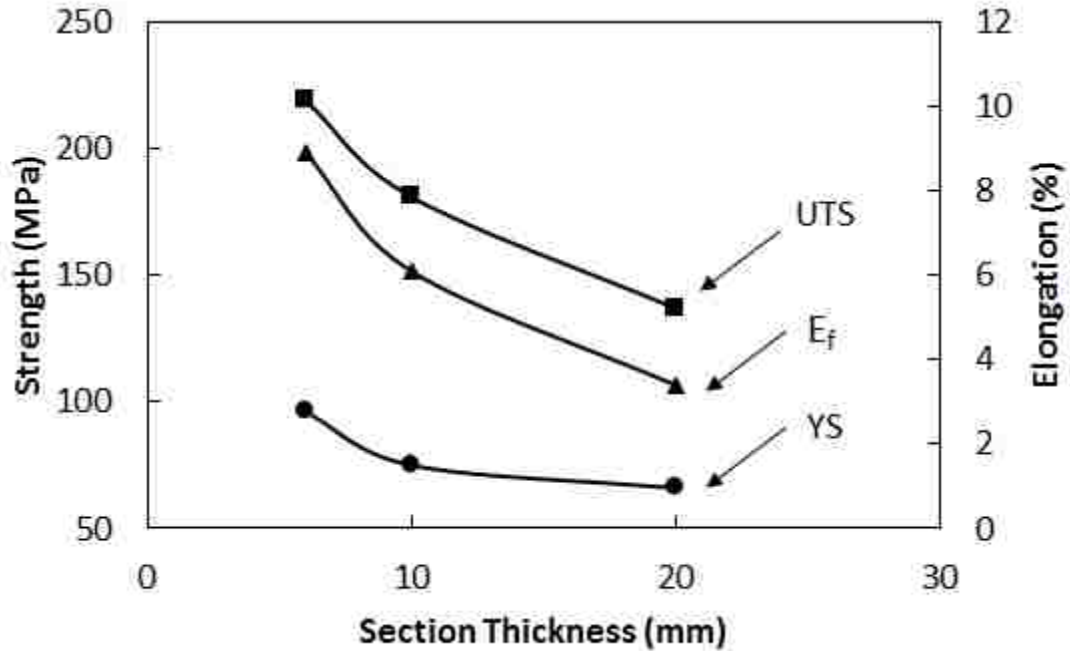


Figure 4- 11. Ultimate tensile strength (UTS), Yield strength (YS) and Elongation vs section thicknesses of alloy AM60.

Table 4-4 Tensile properties of squeeze casting alloy AM60 in different thicknesses

Thickness (mm)	YS (MPa)	UTS (MPa)	E _f (%)
6	96 ± 4.88	220.5 ± 6.28	9.01 ± 0.62
10	74 ± 7.91	180.3 ± 9.46	6.11 ± 1.35
20	67 ± 3.21	135.3 ± 5.56	3.42 ± 0.78

4.3.3.2 C₂Cl₆ and CaC₂ treated AM60 alloys

The engineering stress-strain curves of the grain refiner-treated AM60 alloys are shown in Figures 4-12 and 4-13, and the respective tensile testing results are given in Table 4-4. The tensile curves show similar trends when subjected to the external loads as described in the case of untreated AM60 alloy. The tensile properties of the 6 mm sections remain higher than those of the 10 mm and 20 mm sections as shown in Figures 4-14 and 4-15. It appears that the grain refiners were able to reduce the variation in the

tensile properties in different sections of alloy AM60. The decrease in UTS, YS and E_f of C_2Cl_6 -treated specimens from 6 mm to 20 mm were 1%, 7% and 37%, and in the case of CaC_2 -treated specimens, the decrease were 18%, 9% and 30%, respectively. Compared to the un-treated AM60 specimen, the variation in tensile properties of different section thicknesses were significantly reduced.

Meanwhile, it can be found out that, the grain refiners had a relatively higher effects on the mechanical properties of the thicker 20 mm sections than 10 mm and 6 mm sections. The UTS, YS and E_f of the 20 mm sections were 203.6 MPa, 101.1 MPa and 6.1% for C_2Cl_6 -treated specimens and 200.1 MPa 80.4 MPa and 6.8% for the CaC_2 -treated alloys. Which, resulting an increase of 50.5%, 50.9%, 78.4% and 47.9%, 20.1%, 98.8% for the respective tensile properties over the un-treated AM60 alloy. This founding was supported by the respective strain hardening rates of different section thicknesses listed in Figure 4-16. The improvements of strain hardening rates of the 20 mm sections were higher than 10 mm and 6 mm sections. Also, it seems that the grain refiners have a limited effect on the 6 mm section of alloy AM60. This is probably due to the high cooling rate of the thinner 6 mm section during the solidification. The high solidification rate might offset the effect of refiners on grain structure development. However, the squeeze casting technology is mainly used for relatively thick casting components in the industry. The improvement of tensile properties in thick sections is the goal of this work instead of refining microstructure in thin sections of castings.

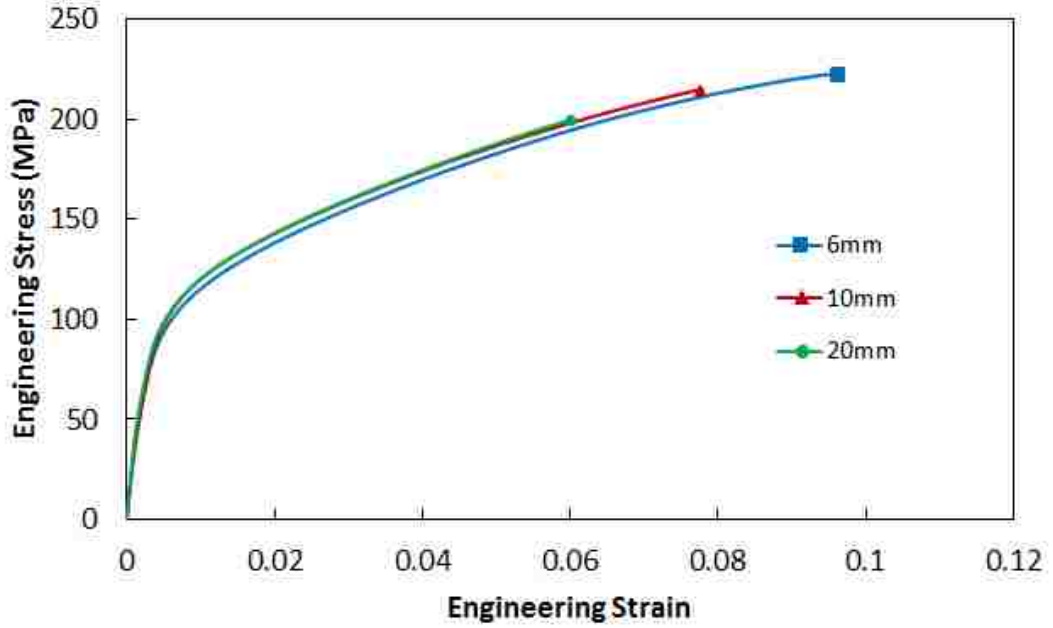


Figure 4- 12. Ultimate tensile strength (UTS), Yield strength (YS) and Elongation vs section thicknesses of C_2Cl_6 treated alloy AM60.

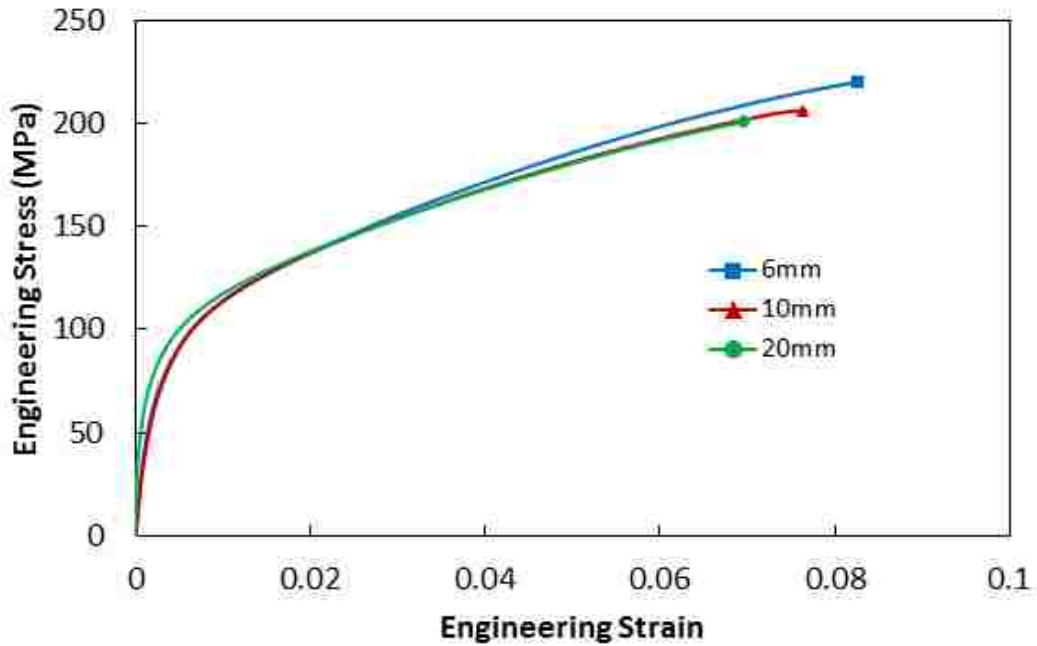


Figure 4- 13. Ultimate tensile strength (UTS), Yield strength (YS) and Elongation vs section thicknesses of CaC_2 treated alloy AM60.

Table 4-5 Tensile properties of grain refined squeeze casting AM60 in different thicknesses

Thickness (mm)	C ₂ Cl ₆ -treated AM60			CaC ₂ -treated AM60		
	YS (MPa)	UTS (MPa)	E _f (%)	YS (MPa)	UTS (MPa)	E _f (%)
6	102.5 ± 4.3	222.0 ± 6.1	10.3 ± 0.9	98.8 ± 6.6	220.2 ± 9.6	9.1 ± 1.1
10	100.6 ± 6.0	215.6 ± 8.6	8.2 ± 1.2	85.7 ± 4.8	206.8 ± 8.3	8.3 ± 0.8
20	101.1 ± 5.4	203.6 ± 8.3	6.3 ± 1.4	80.4 ± 2.2	200.1 ± 5.2	6.8 ± 0.3

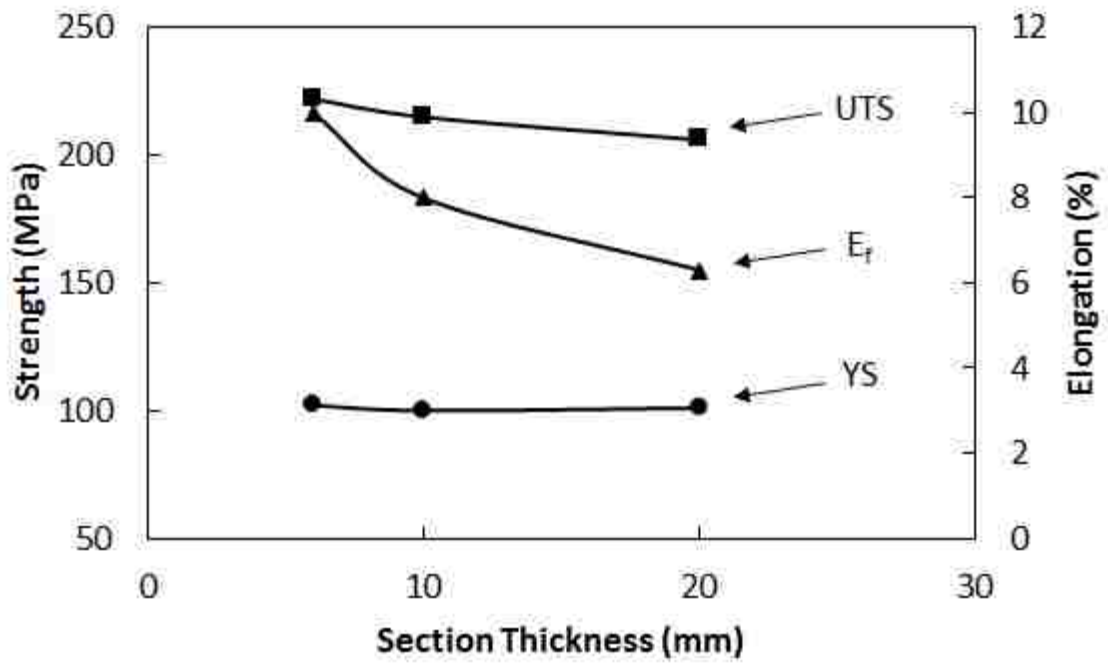


Figure 4- 14. Ultimate tensile strength (UTS), yYield strength (YS) and Elongation vs section thicknesses of C₂Cl₆ treated alloy AM60.

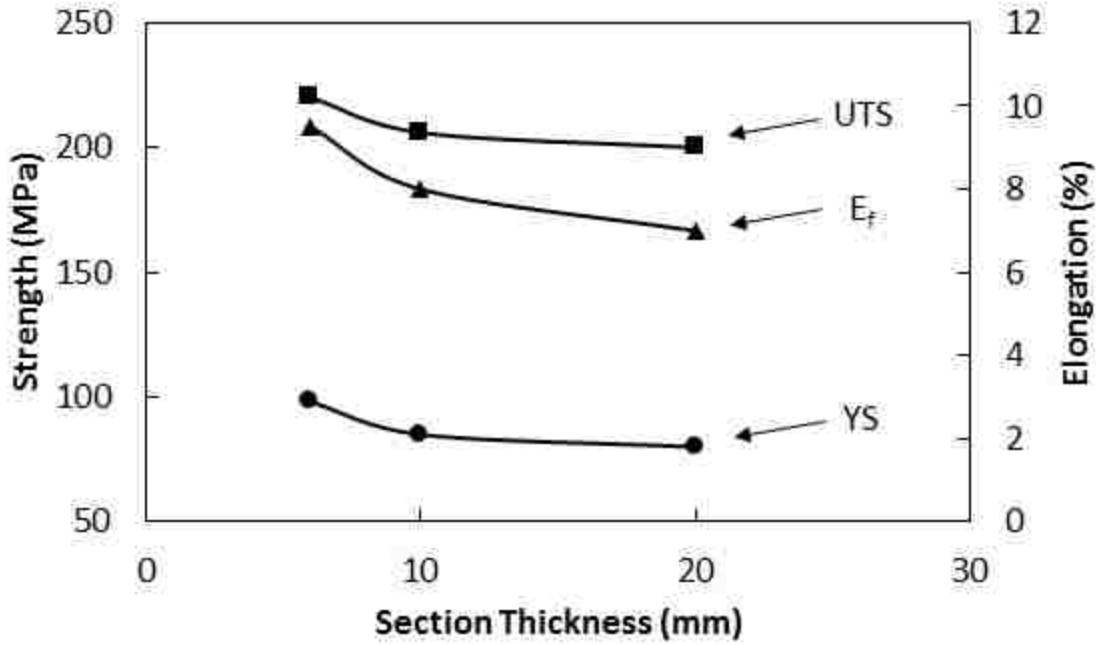
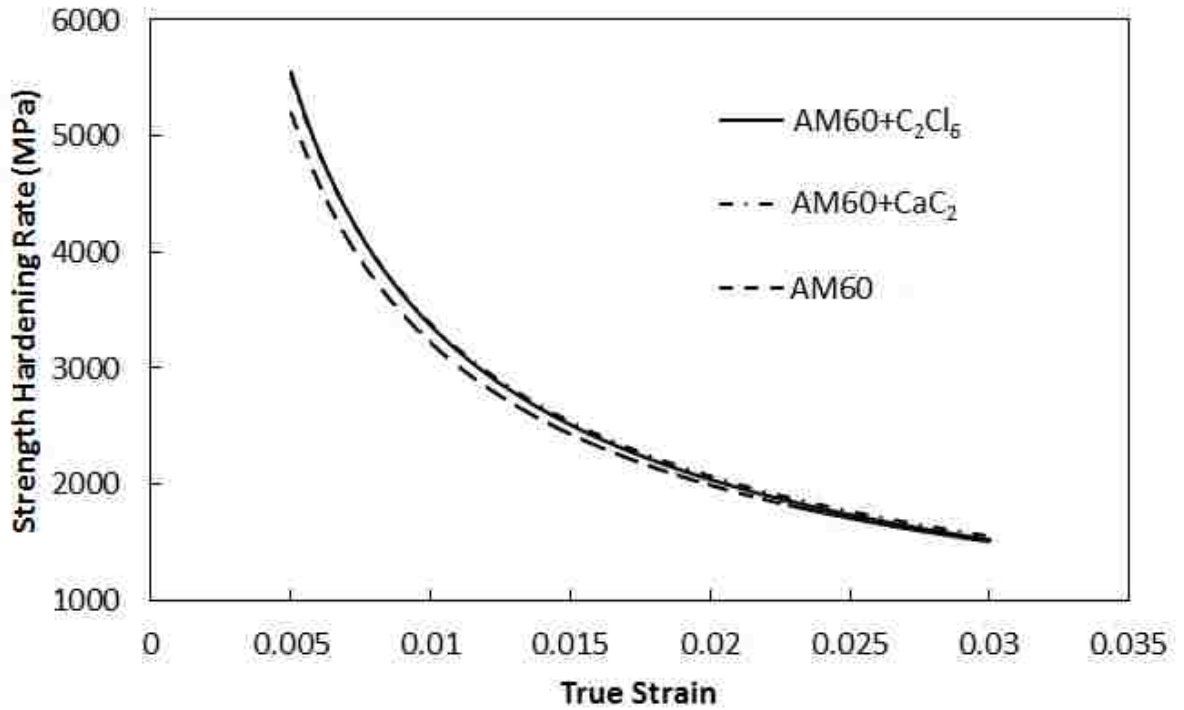
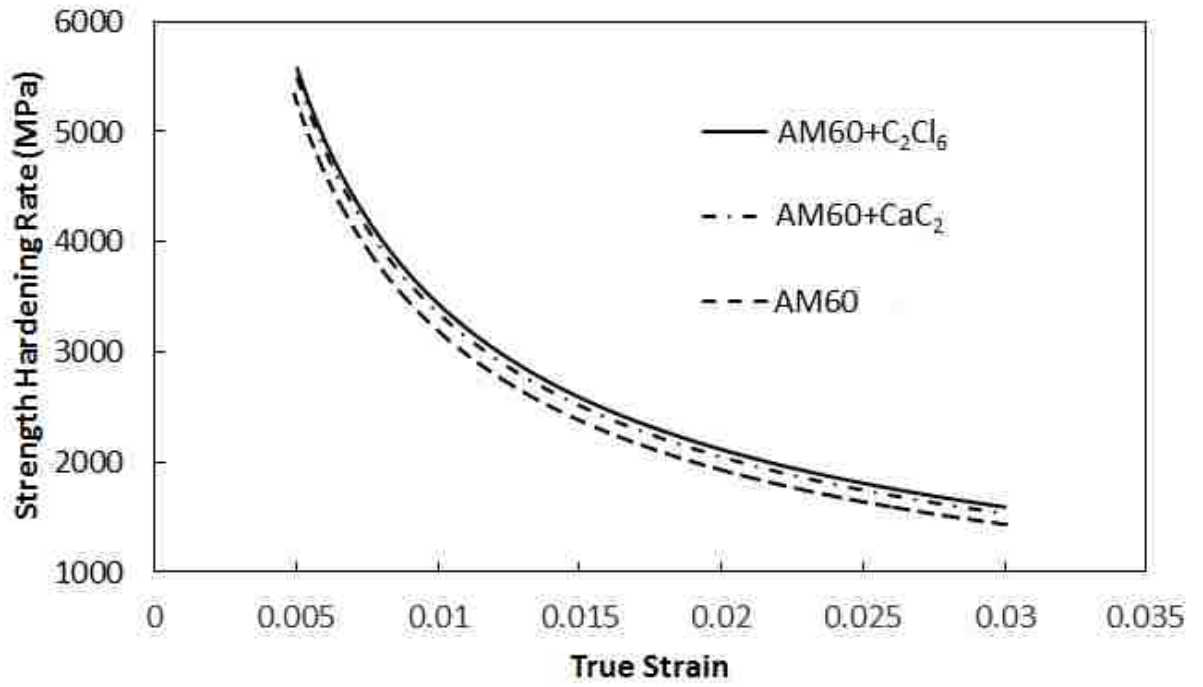


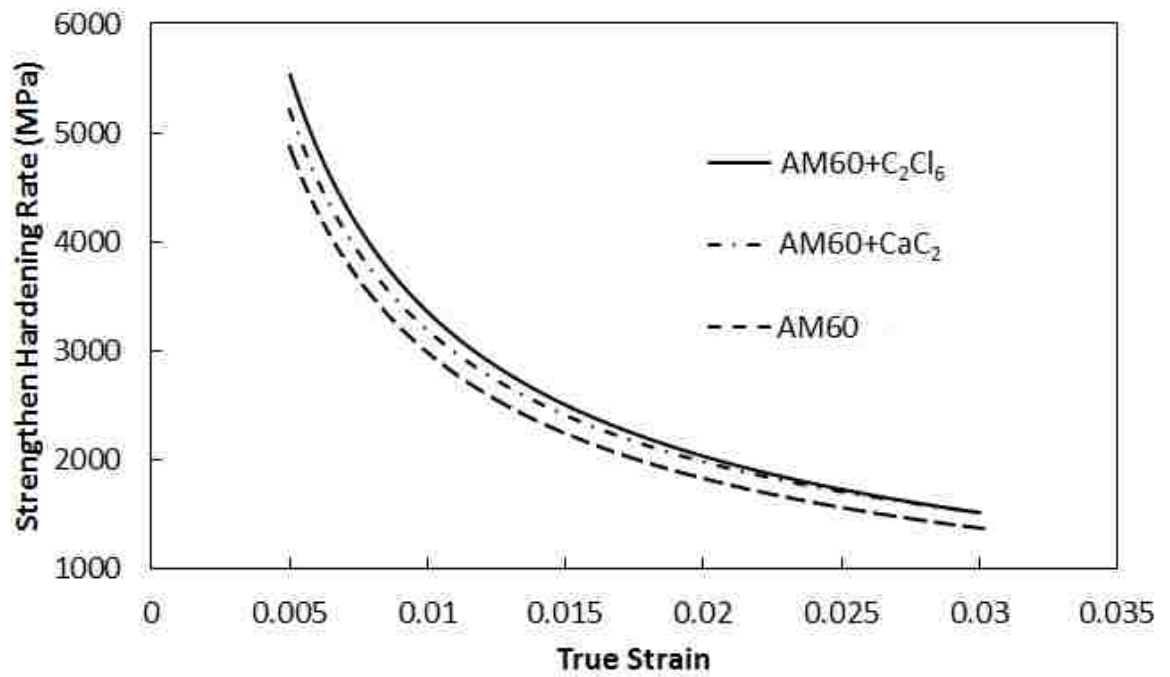
Figure 4- 15. Ultimate tensile strength (UTS), Yield strength (YS) and Elongation vs section thicknesses of CaC_2 treated alloy AM60.



(a)



(b)



(c)

Figure 4- 16. Strain-hardening rate versus true strain for plastic deformation of (a) 6 mm sections, (b) 10 mm sections, and (c) 20 mm sections.

4.4 Microstructure Analysis

4.4.1 Magnesium alloy AM60

The optical and SEM micrographs of as-cast AM60 alloy are revealed in Figure 4-17. There were no noticeable casting defects on the surface of the specimen as shown in Figure 4-17 (a). The grain boundaries are believed to be disguised by the β -intermetallics ($Mg_{17}Al_{12}$) as illustrated in Figure 4-17 (b), which made them invisible in the as-cast conditions. A closer examination by SEM and EDS showed three typical phases in alloy AM60, which are primary α -Mg phase (dark area labeled A), eutectic β - $Mg_{17}Al_{12}$ phase (light grey area labeled B) and Al-Mn intermetallic phase (bright are labeled C) as displayed in Figure 4-17 (b). The EDS results of the three phases in the alloy were listed in Figure 4-18.

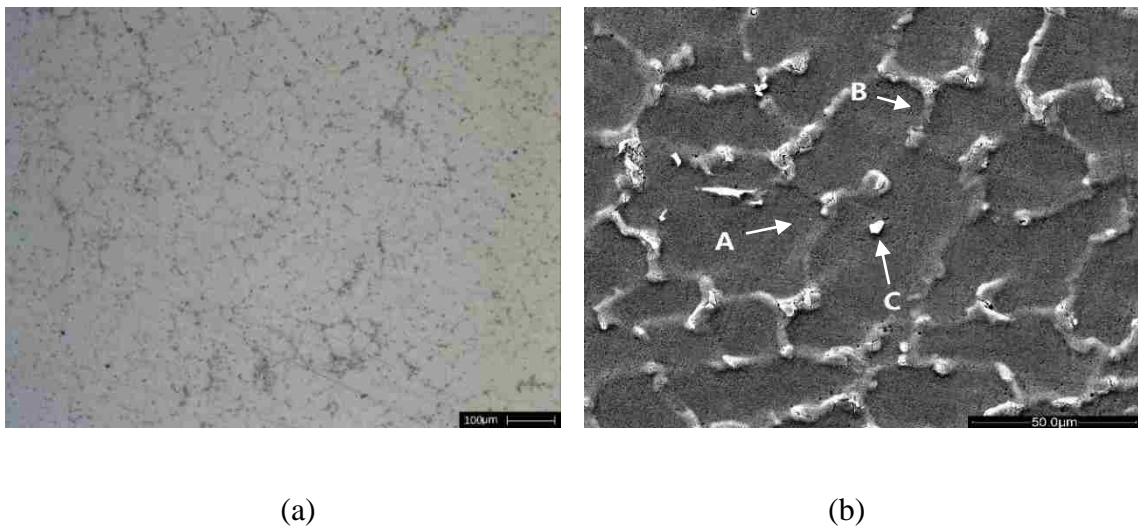
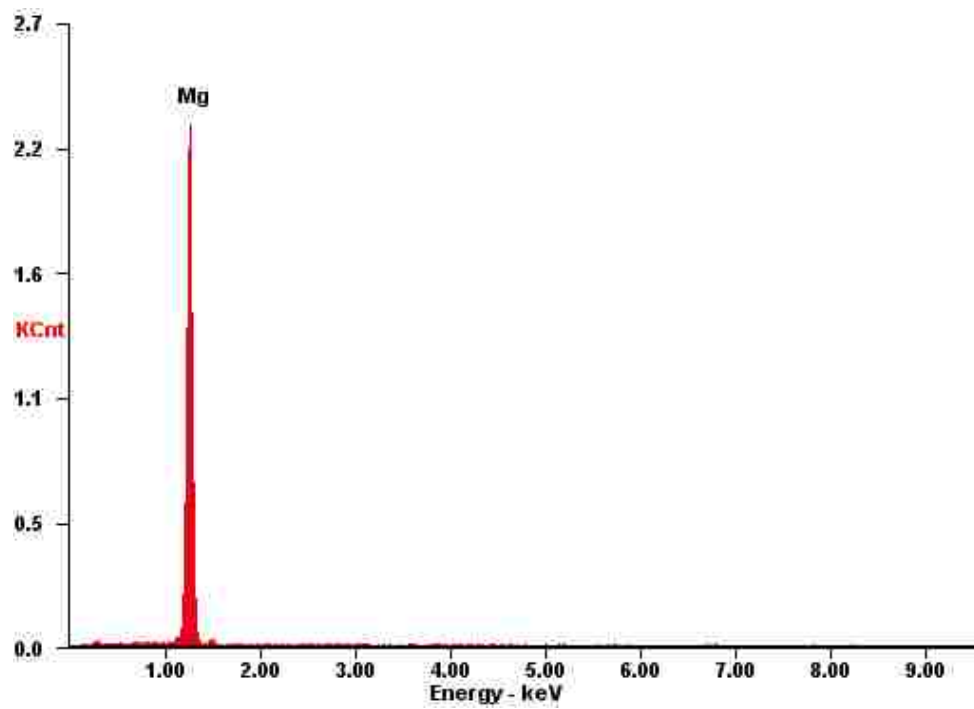
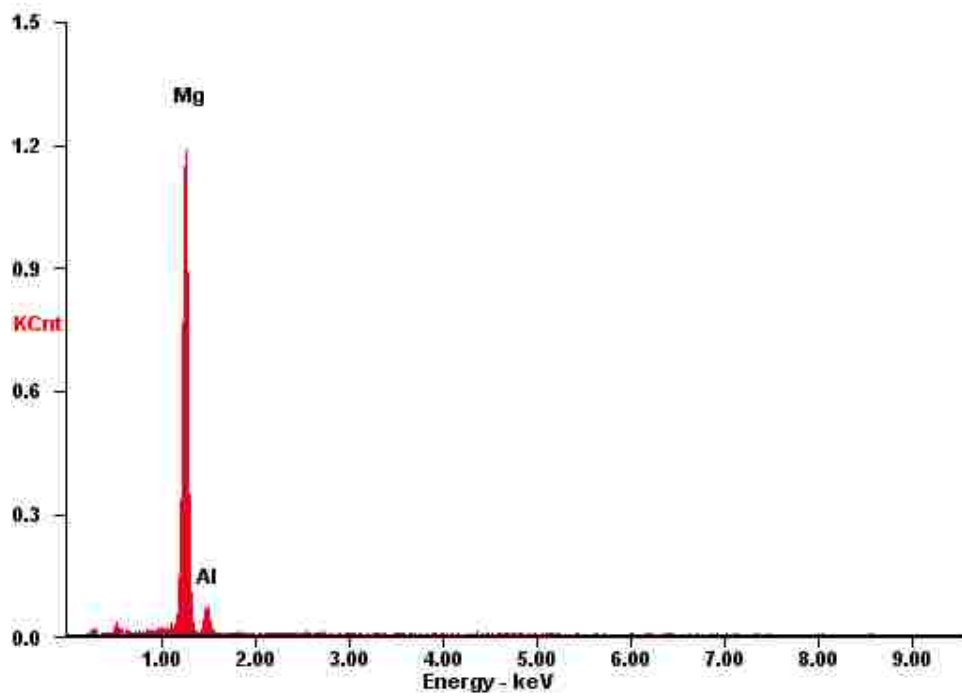


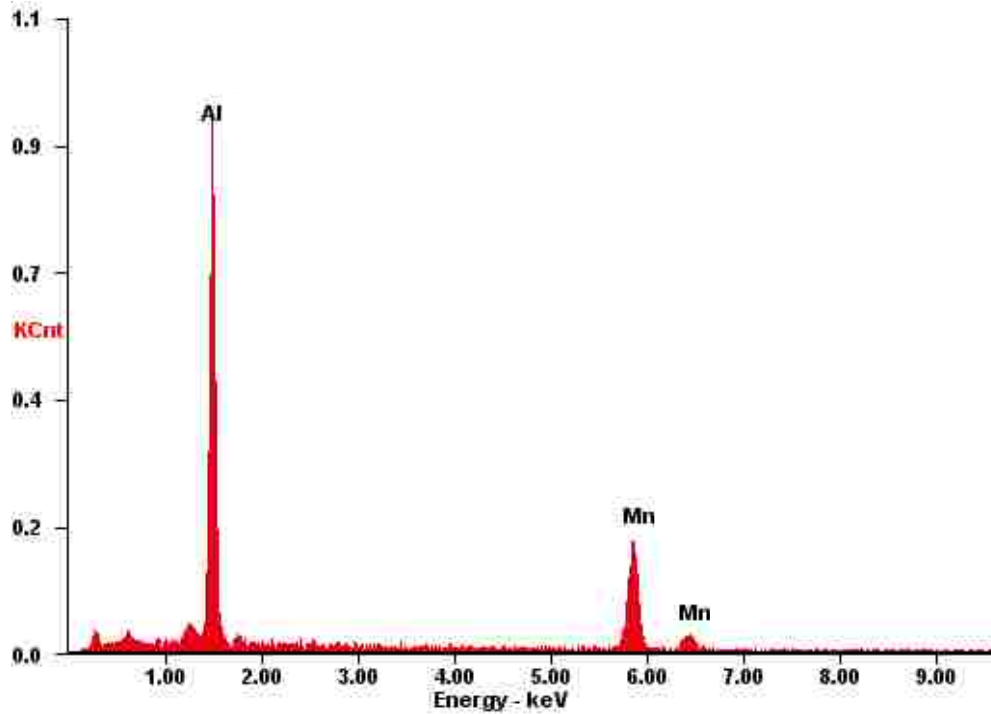
Figure 4- 17. (a) Optical micrograph, and (b) SEM micrograph in SE mode of as-cast AM60.



(a)



(b)



(c)

Figure 4- 18. EDS analysis of alloy AM60, (a) primary α -Mg, (b) β -Mg₁₇Al₁₂, and (c) Al phase.

4.4.2 Grain structure of alloy AM60 cast in cylindrical mould

Figures 4-19 to 4-21 illustrate the microstructure of AM60 alloy and C₂Cl₆/CaC₂-treated AM60 alloys in T4 condition. Grain boundaries were revealed after the T4 heat-treatment process by dissolving the β -Mg₁₇Al₁₂ intermetallics. As can be seen, the grains in the C₂Cl₆ and CaC₂ treated AM60 were evidently finer than those of AM60 alloy. Figure 4-22 presents the grain size measurements from the heat-treated specimen of AM60 alloy in comparison to that of the C₂Cl₆ and CaC₂ treated AM60. It is worth noting that the grain size of the AM60 alloy was reduced by almost two times in both C₂Cl₆ and CaC₂ treated specimens due to the grain refinement effect of the C₂Cl₆ and CaC₂ addition

to the alloys. The grain size of the AM60 alloys was reduced from 70 μm to 35 μm and 38 μm by the addition of C_2Cl_6 and CaC_2 powders.

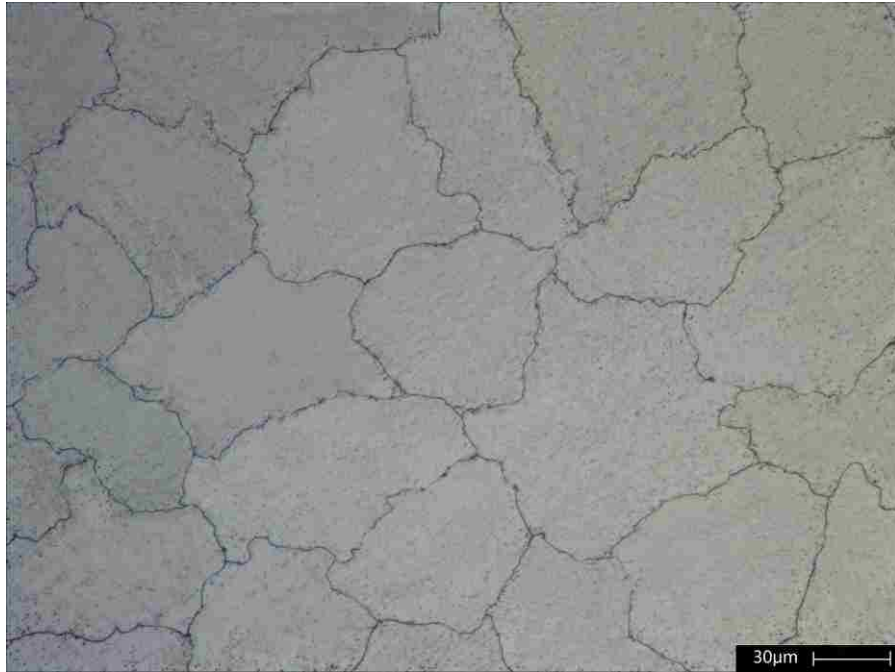


Figure 4- 19. Optical micrograph showing grain structure of squeeze cast AM60 in a cylindrical coupon in T4 condition.



Figure 4- 20. Optical micrograph showing grain structure of C_2Cl_6 -treated AM60 in a cylindrical coupon in T4 condition.



Figure 4- 21. Optical micrograph showing grain structure of CaC_2 -treated AM60 in a cylindrical coupon in T4 condition.

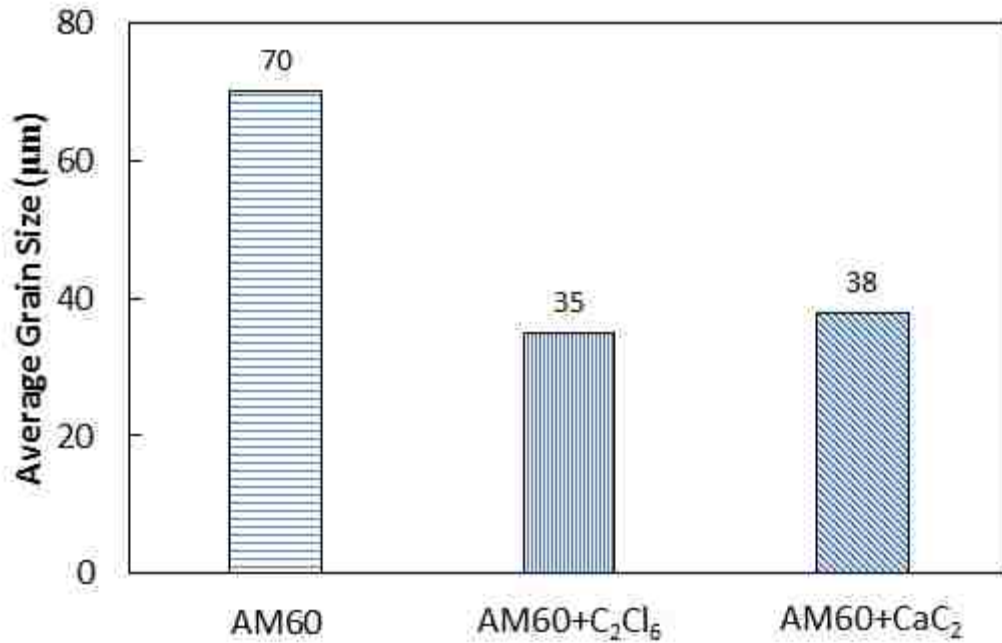
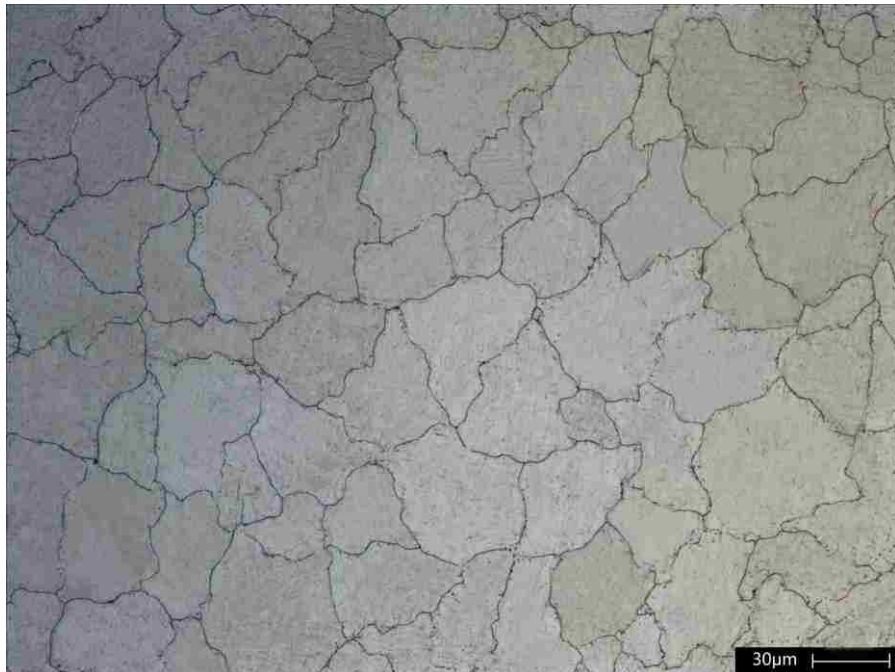


Figure 4- 22. Grain size measurement of grain refined AM60 and untreated AM60.

Figure 4-23 shows the optical microstructures of squeeze cast AM60 specimens with section thicknesses of 6, 10 and 20 mm, respectively. It can be seen that, the average grain size increased from 30 µm for 6 mm specimen to 88 µm for 20 mm specimen. The thicker sections contained greater total thermal energy which required more time for releasing during the solidification process since the thermal conductivity and the temperature of the mold were the same for all sections. As a result, longer cooling time was needed for the thicker section, which led to a slower cooling rate and results in a coarser microstructure.

However, with the addition of the grain refiners, the grain sizes were significantly refined especially in the 10 mm and 20 mm sections as shown in Figures 4-24 and 4-25. Table 4-6 lists the grain size measurements of the un-treated and treated squeeze cast magnesium alloy AM60. It can be seen from Figure 4-26 that, the difference in grain

sizes between different sections for the refined specimens were largely reduced. In the case of C_2Cl_6 -refined specimens, all three sections show the similar grain size at an average of $27\ \mu\text{m}$, which in this case, are even finer than the thinnest section of un-treated specimens. This observation indicates the excellent grain refining ability of C_2Cl_6 powders on squeeze casting magnesium alloy AM60. For the CaC_2 -refined specimens, the grain sizes were also refined to a noticeable level. The average grain size of 20 mm thickness for CaC_2 -refined specimen was $45\ \mu\text{m}$, almost cut into half size compared to the un-treated AM60 alloy at the same thickness.



(a)

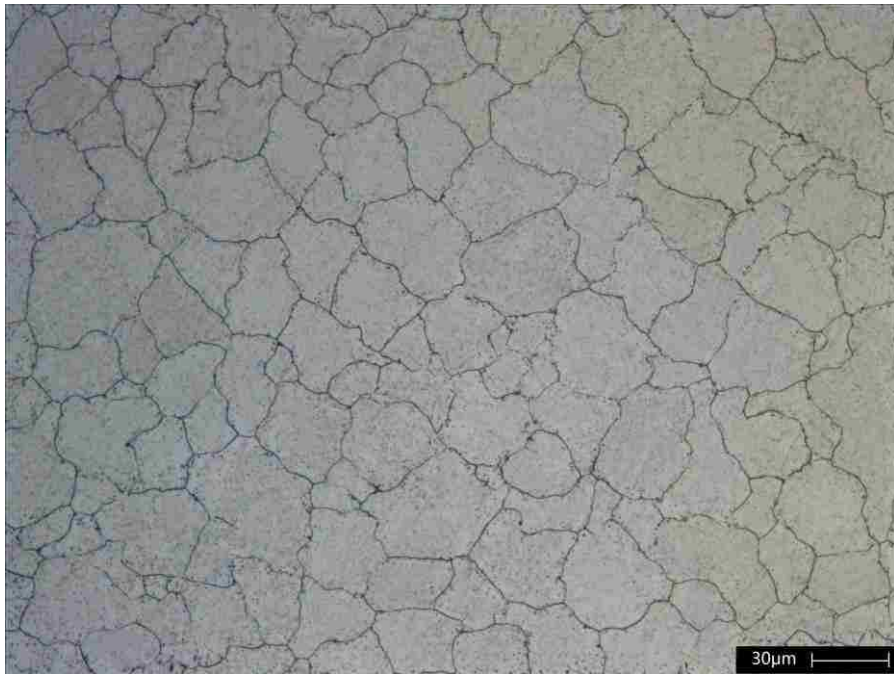


(b)

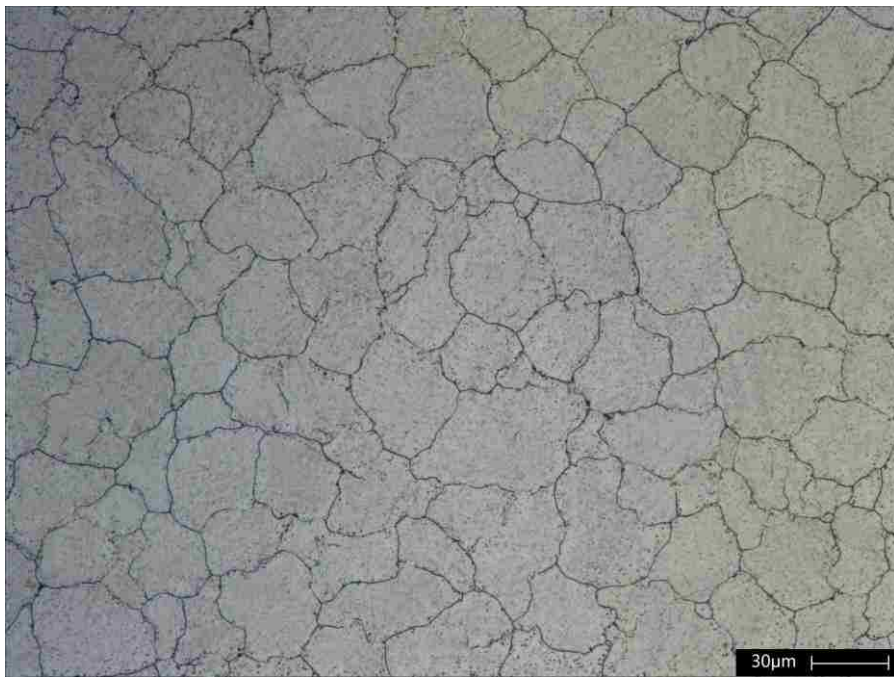


(c)

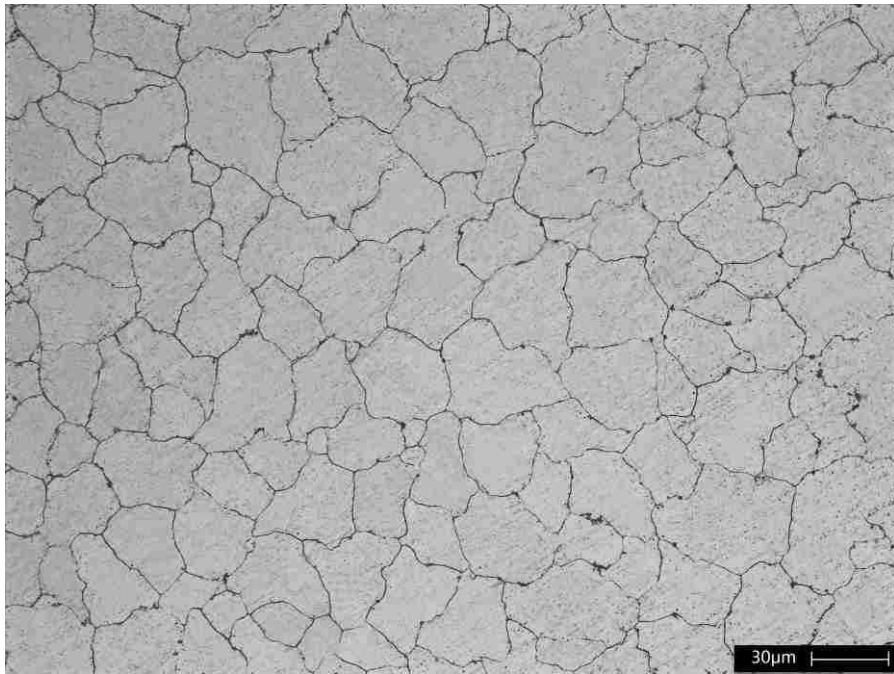
Figure 4- 23. Optical micrograph showing the grain sizes of squeeze cast AM60 with (a) 6 mm, (b) 10 mm, and (c) 20 mm of section thicknesses.



(a)

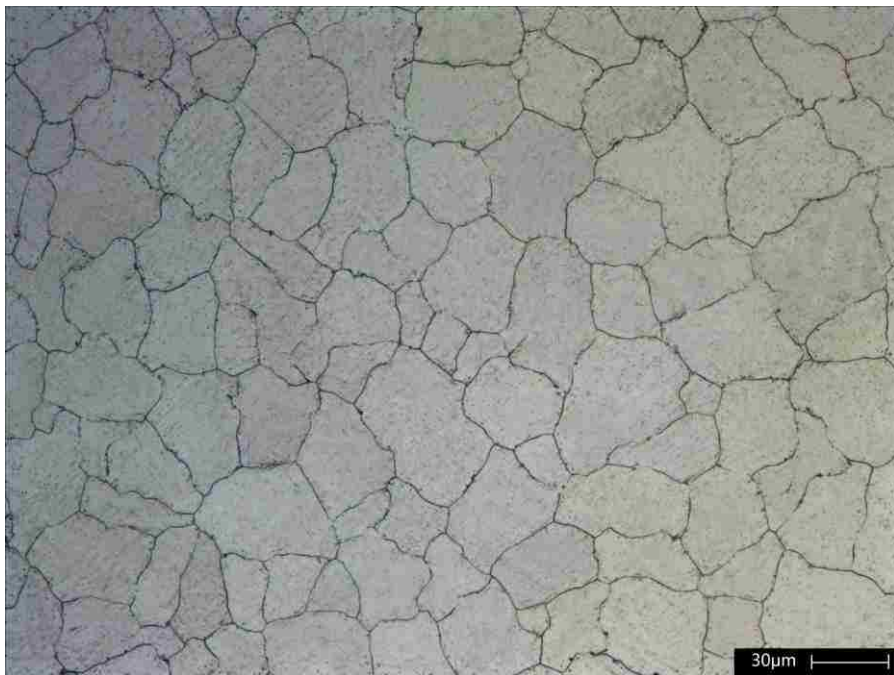


(b)



(c)

Figure 4- 24. Optical micrograph showing the grain sizes of C_2Cl_6 -treated AM60 with (a) 6 mm, (b) 10 mm, and (c) 20 mm of section thicknesses.



(a)



(b)



(c)

Figure 4- 25. Optical micrograph showing the grain sizes of CaC_2 -treated AM60 with (a) 6 mm, (b) 10 mm, and (c) 20 mm of section thicknesses.

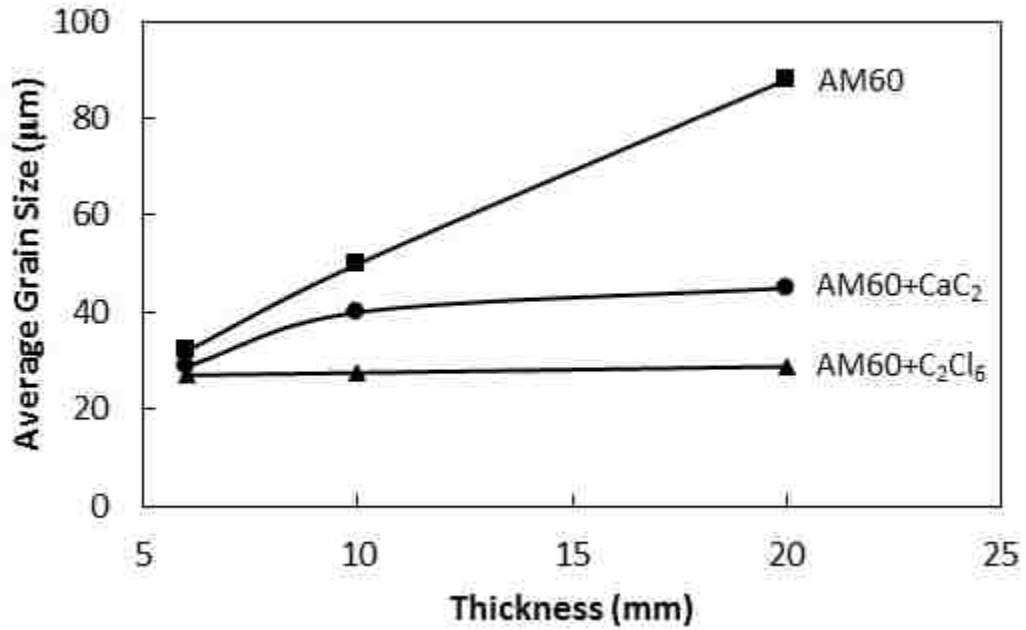


Figure 4- 26. Grain sizes vs. section thicknesses of AM60 specimens.

Table 4-6 Grain size measurements of the untreated and treated squeeze cast Mg alloy AM60

	AM60 (µm)	AM60+C ₂ Cl ₆ (µm)	AM60+CaC ₂ (µm)
6 mm	32	27	29
10 mm	50	28	40
20 mm	88	29	45

The optical microstructure analysis combining with the outcome tensile testing results further suggest that both C₂Cl₆ and CaC₂ have good grain refining capabilities on squeeze casting magnesium alloy AM60.

4.4.3 Grain refining mechanisms

It has been well accepted that aluminum carbide, Al₄C₃, was the compound responsible for the grain refining effects of Mg-Al alloys [77, 78]. The SEM micrograph

of Al_4C_3 acting as the heterogeneous nucleation site is shown in Figure 4-27. EDS line analysis was also used to qualitatively analyze the existing elements. The EDS analysis was done by drawing line A-B across the particle. Mg, Al and C were detected since they all reached the peak value at the particle as shown in Figure 2-28. It can be seen that, Al and C reached the maximum concentrations at the particle while the concentration of Mg dropped to the minimum level. This finding implied that the compound consisting of Al and C could provide heterogeneous nucleation site of squeeze cast magnesium alloy AM60. This observation is consistent with the nucleation mechanism proposed by [77, 78], in which Al_4C_3 was found to be the nucleation site.

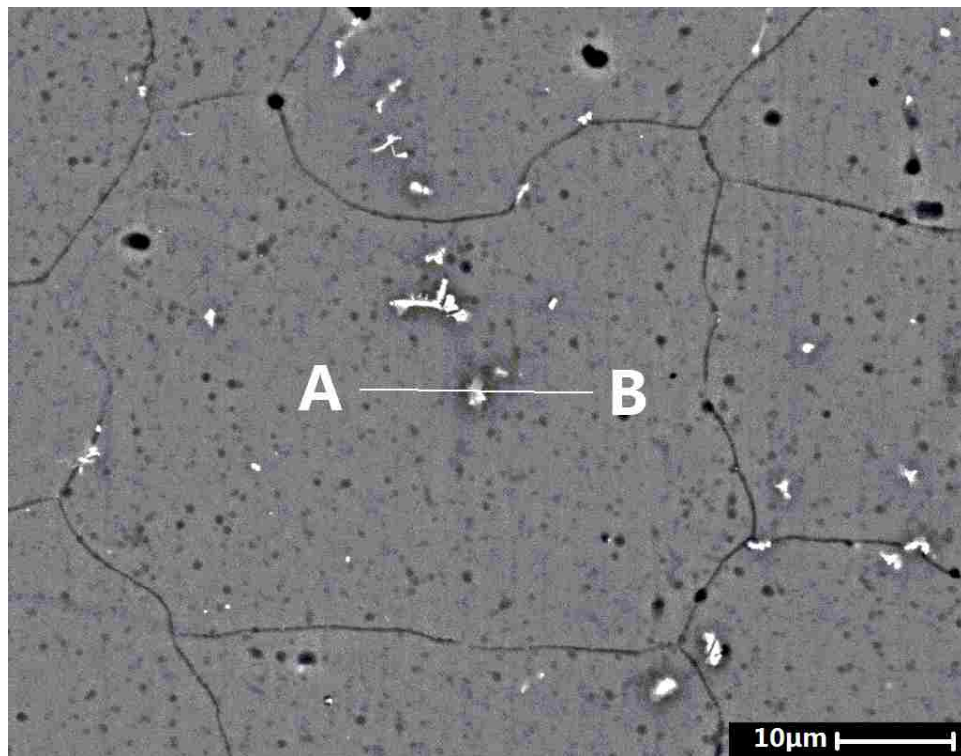
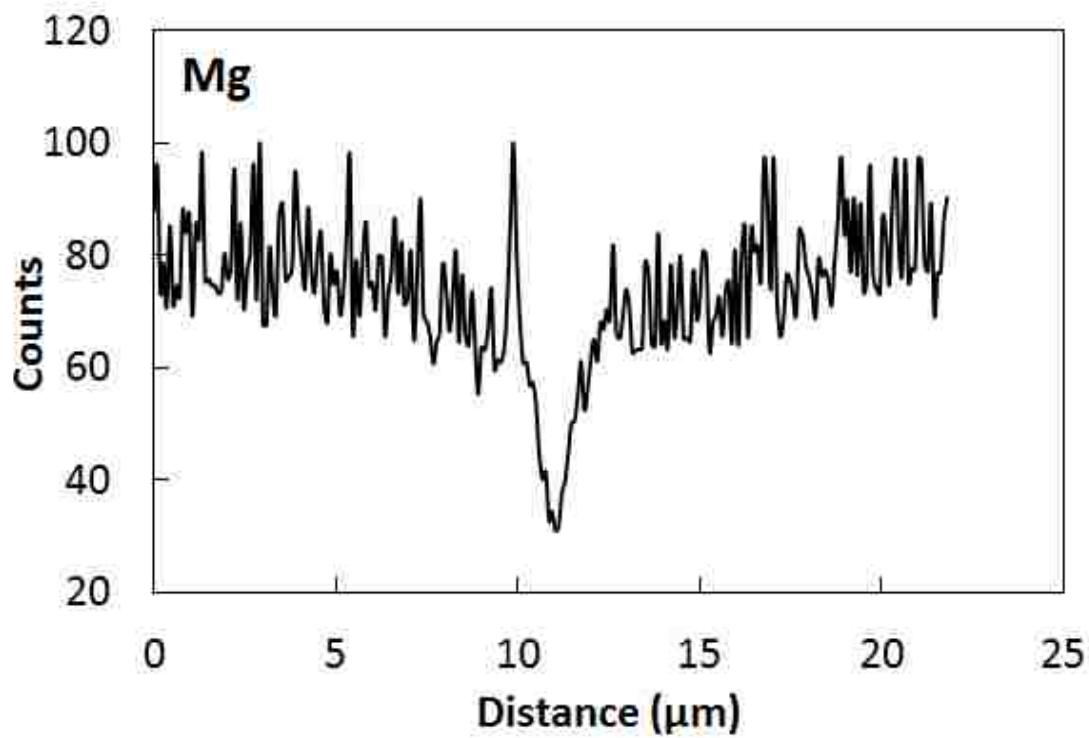
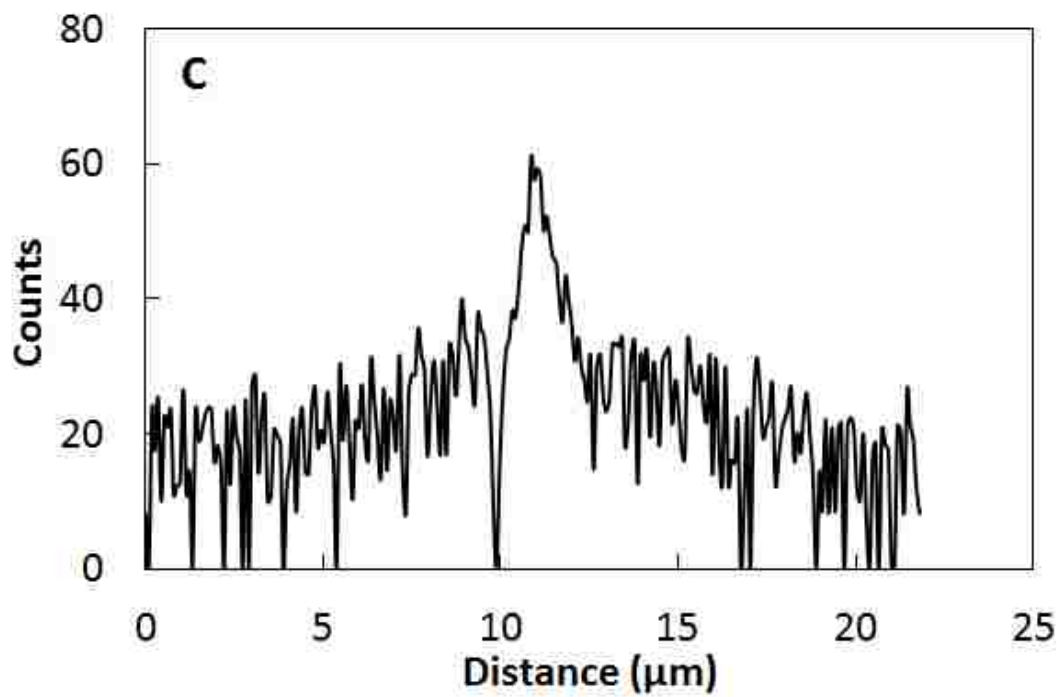


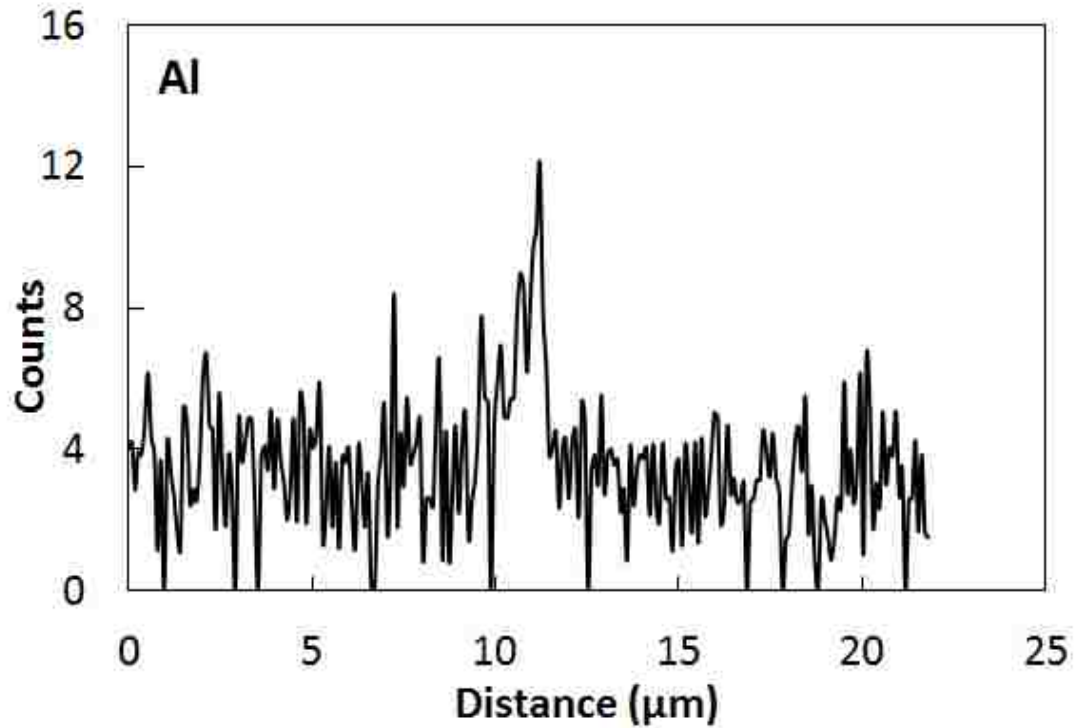
Figure 4- 27. SEM micrograph in BSE mode showing Al_4C_3 as the heterogeneous nucleation site for C_2Cl_6 refined squeeze cast alloy AM60.



(a)



(b)



(c)

Figure 4- 28. EDS line analysis of (a) Mg, (b) C and (c) Al elements on line AB across the particle.

It has been reported by Ninoomiya et al [61] and Han et al [79] that, depending on the mass ratio of Ca to Al in the Mg-Al alloys, the Ca can form new phases with the β -intermetallics ($Mg_{17}Al_{12}$). They claimed that, with the Ca/Al ratio less than 0.8, $(Al, Mg)_2Ca$ should be the only phase that would be formed. It was also pointed out by Kondori [62] and Han et al [79] that, with the addition of 2.0 wt% of Ca into AM60 alloys (Ca/Al = 0.4), the β -intermetallics could be fully suppressed. In this study, the addition of CaC_2 was 0.5 wt% and 0.25 wt%, that is to say, the mass ratio of Ca/Al should be 0.052 and 0.026, which were smaller than 0.4. Thus, this mass ratio calculation suggested that $(Al, Mg)_2Ca$ should be the only new phase present in the CaC_2 -treated

alloy, which would be mixed up with the remaining β -intermetallics. This is because there was insufficient amount of Ca to fully suppress the $Mg_{17}Al_{12}$ particles.

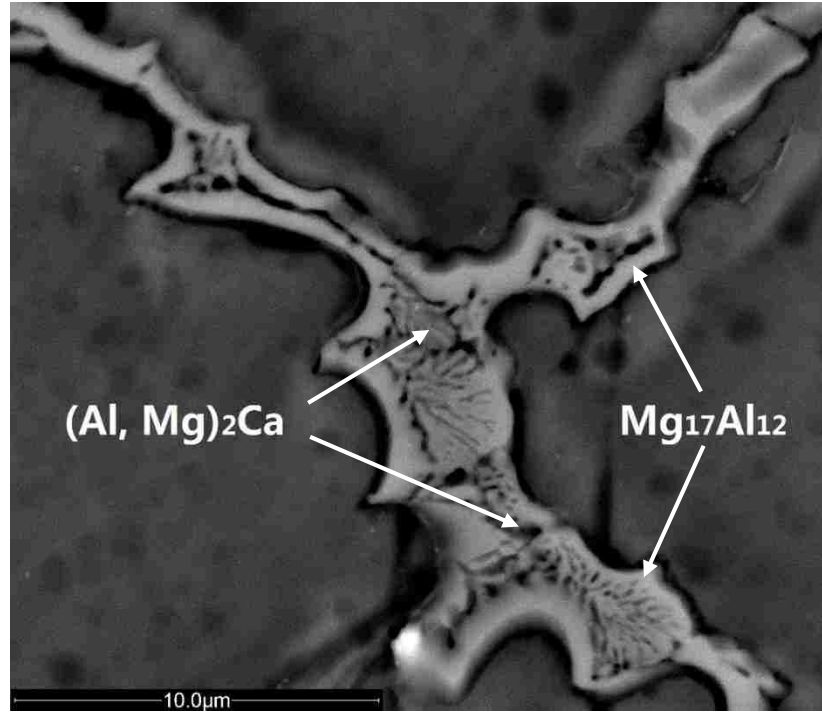
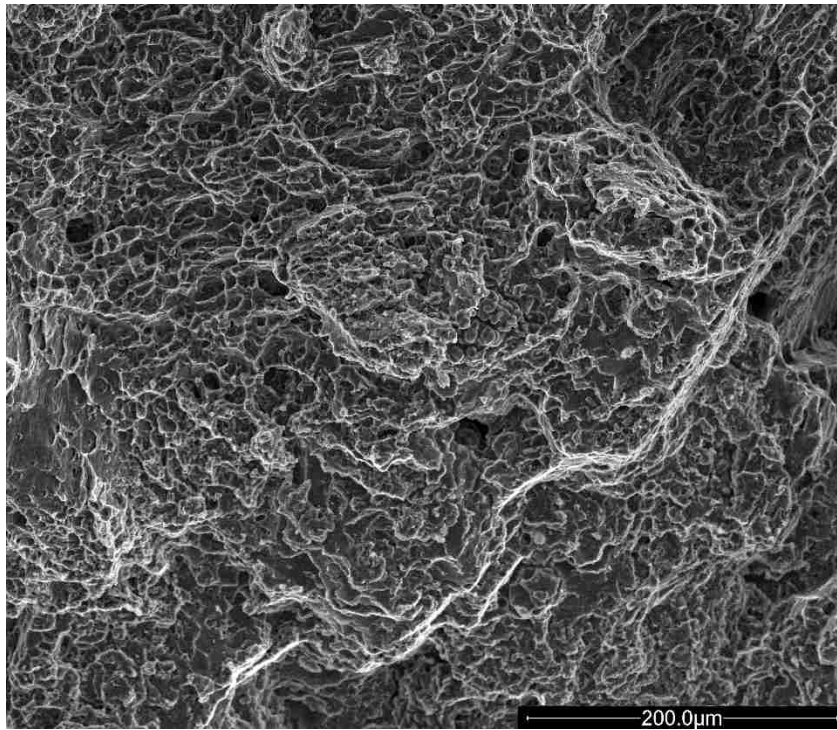


Figure 4- 29. High magnification SEM micrograph in SE mode showing the CaC_2 refined AM60 containing both $Mg_{17}Al_{12}$ and lamellar Al_2Ca phases.

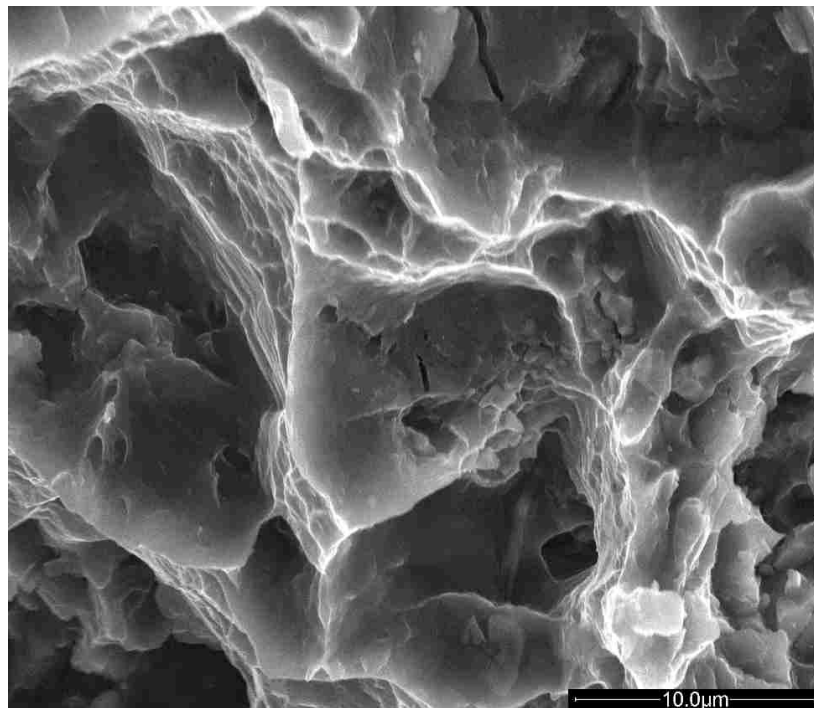
The SEM micrograph of $(Al, Mg)_2Ca$ and β -intermetallics phases in as-cast AM60 alloy with 0.25 wt% of CaC_2 addition is shown in Figure 4-29. The β -intermetallics were generally well distributed in the interdendritic areas. It can be seen that, with the addition of CaC_2 particles, the lamellar Al_2Ca was easily observed around the $Mg_{17}Al_{12}$ particles. The new formed Al_2Ca phase, with a melting temperature of 1079 $^{\circ}C$, which was much higher than the melting temperature of $Mg_{17}Al_{12}$ at only 437 $^{\circ}C$, was able to largely increase the high-temperature stability of the AM60 alloys. Meanwhile, when the alloy was subjected to T4 heat treatment, the thermal stable Al_2Ca would not be dissolved like $Mg_{17}Al_{12}$ particles, thus restrict the grain growth of the material.

4.5 Fracture surface analysis

Fracture surfaces of the untreated AM60 alloy and the C_2Cl_6/CaC_2 grain refined tensile specimens from 10 mm sections were examined by SEM. The fracture surfaces of all three specimens with low and high magnifications are illustrated in Figures 4-30 to 4-32, respectively. It can be found out from the fractographies that, the grain refiners had certain effect on the fracture behavior of the squeeze cast AM60 alloys. When comparing the three low magnification fracture figures, there were not much noticeable differences. The characteristics of cleavage fracture, flat facets covered with river markings and dimples were easily observed on all fracture surfaces. The river marking was the result of the crack moving through the grain along a number of parallel planes, which formed a series of plateaus and connecting ledges. The dimples were caused by the localized microvoid coalescence. The river marking combining with dimples indicated the energy absorption with local deformation prior to fracture. A close examination of the fracture surfaces by high magnifications of all three specimens in Figures 4-30 (b), 4-31 (b) and 4-32 (b) showed that, the dimple sizes of C_2Cl_6/CaC_2 refined specimen were smaller than those in the untreated specimen. Meanwhile, in the fractured surface of the grain refined specimens, a great deal of sub-sized dimples were well distributed within each primary dimple as shown in Figure 4-31 (b) and 4-32 (b). This could be considered to be an enhancement of fracture behaviour since high energy absorption was present to considerably extend local deformations which underwent large external loads before fracture.

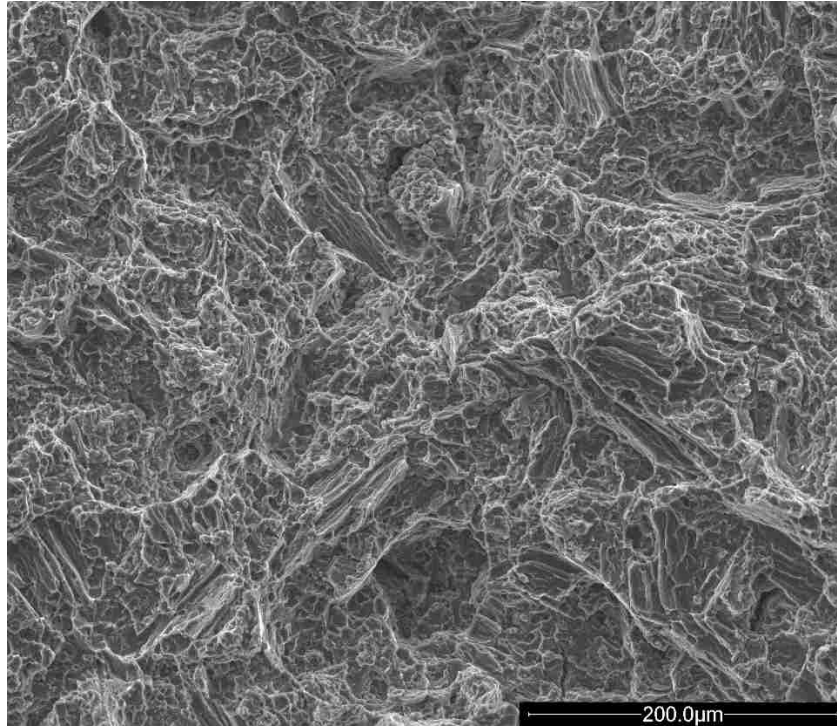


(a)

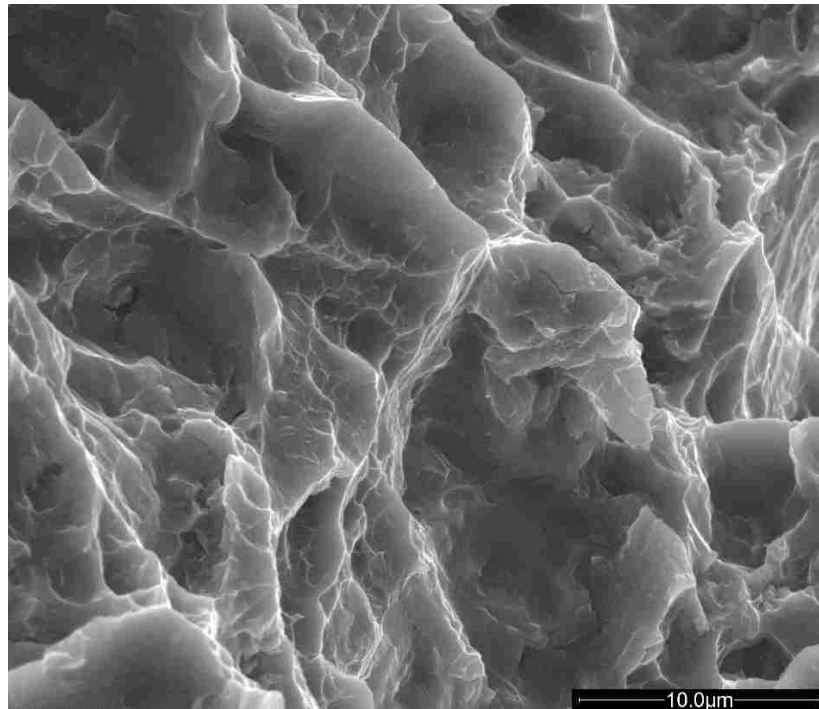


(b)

Figure 4- 30. SEM fractographs in SE mode of the untreated squeeze cast AM60, (a) low and (b) high magnification from 10 mm section thickness.

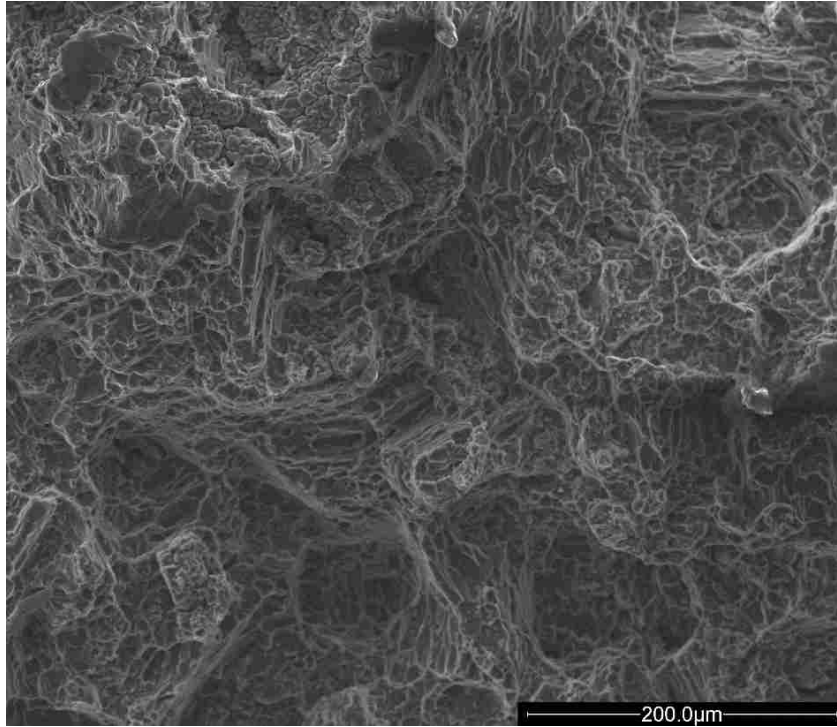


(a)

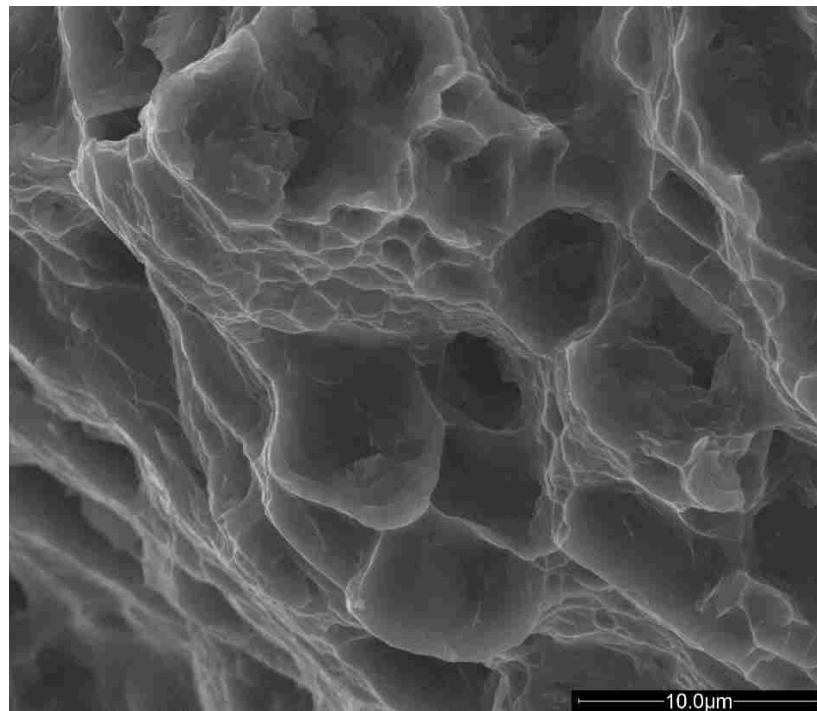


(b)

Figure 4- 31. SEM fractographs in SE mode of C_2Cl_6 -treated squeeze cast AM60, (a) low and (b) high magnification from 10 mm section thickness.



(a)



(b)

Figure 4- 32. SEM fractographs in SE mode of CaC_2 -treated squeeze cast AM60, (a) low and (b) high magnification from 10 mm section thickness.

As a result, the SEM fracture surface analysis results agree with the tensile data listed in Tables 4-4 and 4-5, where the elongation of grain refined specimens were higher than the untreated AM60 alloy. In other words, the ductility of the alloy was improved by the grain refiner addition.

4.6 Inclusion analysis

It has been reported by Hu [4, 8] that, calcium decreased the fluidity of casting magnesium alloys which led to poor die castability. As a result, the formation of casting defects such as cracks and die sticking are easily found in the casting products. Similar problems happened in this study as shown in Figure 4-33. The addition of CaC_2 immediately increase the viscosity of the molten alloy, thus, during the stirring process, gas entrapment and more importantly oxidation of the alloy occurred. The present defects can easily cause stress concentration during tensile testing which largely deteriorate the mechanical properties of casting products.

To figure out the composition of the entrapped inclusion, the SEM and EDS analysis were applied. As shown in SEM image (Figure 4-34), the bright area labeled A is the un-contaminated alloy which is confirmed by EDS analysis in Figure 4-35 (a). The dark area labeled B, however, has relatively higher content of Al, Ca and O, which indicated that, the inclusion was probably consisting of Al_2O_3 , MgO and CaO . Since the defect failed the engineering functionality of components such as pressure tightness, which hindered the commercialization of the CaC_2 refined magnesium alloys. Further studies on development of techniques to effectively add Ca into magnesium alloys are needed.

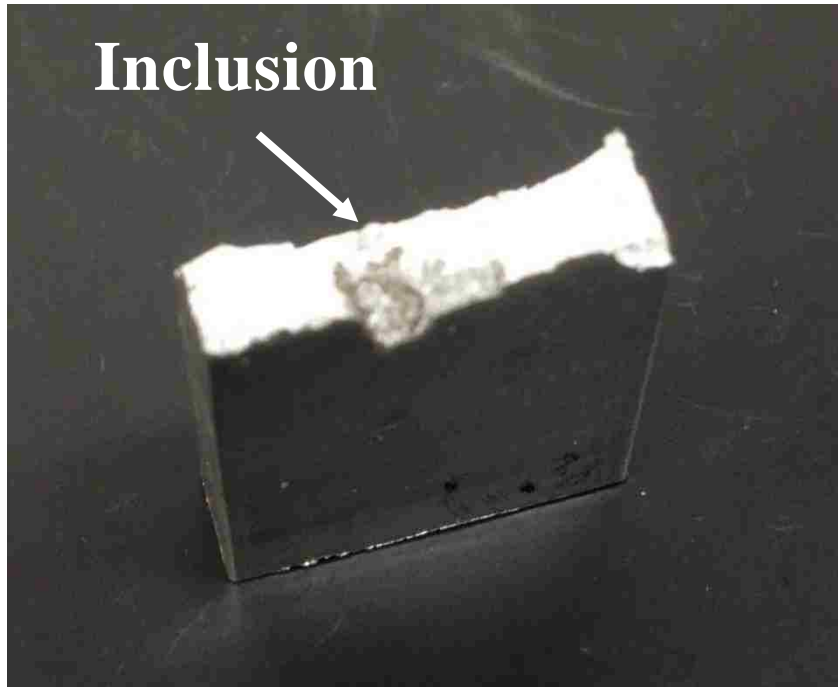


Figure 4- 33. Oxidation inclusion found in CaC_2 treated AM60 specimen.

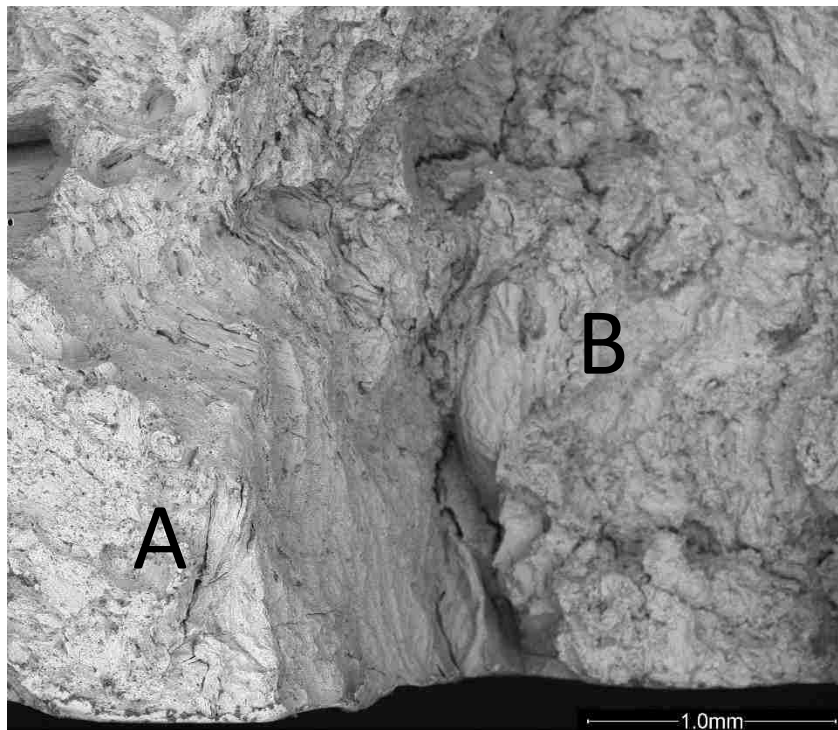
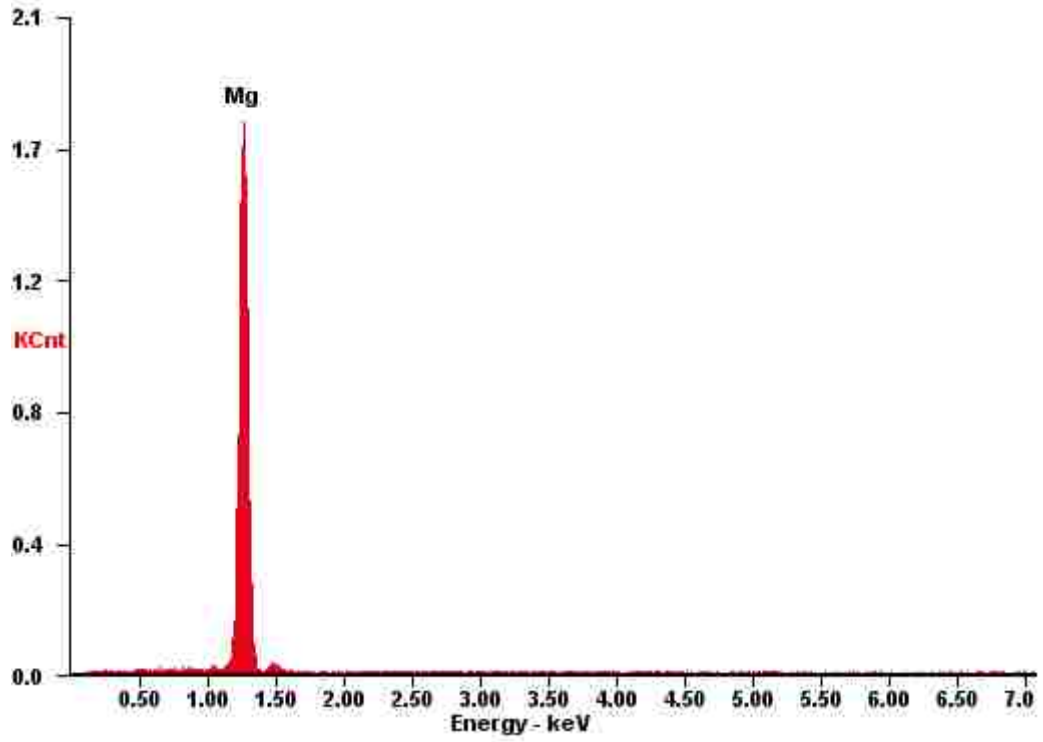
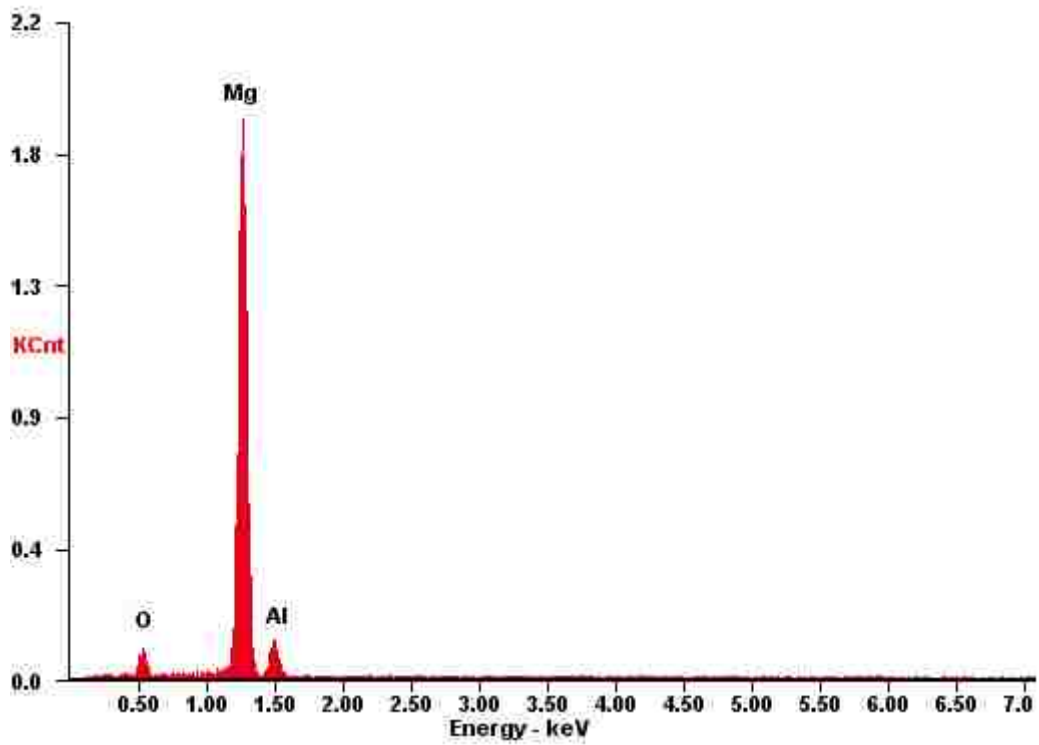


Figure 4- 34. SEM micrograph in BSE mode of inclusion area of CaC_2 treated AM60 specimen.



(a)



(b)

Figure 4- 35. EDS analysis of (a) un-contaminated alloy, and (b) oxidation inclusions.

4.7 Corrosion test

The corrosion behaviour is always a big issue that limits the applications of casting magnesium alloys, since magnesium has the lowest corrosion potential of 2.37 V compared to other structural metals with reference to the standard hydrogen electrode (SHE). Appearing at the bottom of the galvanic series, it is the most anodic of all metals and readily gives up Mg^{2+} ions. Magnesium is a passive metal which is usually protected by a thin film, $Mg(OH)_2$. Unfortunately, such protection films usually cannot be achieved since it is only stable in high pH, while most industrial environments are acidic or neutral. Once the passive film is damaged, it cannot protect the bare metal beneath, as a consequence, lead to severe corrosion damages of the material. The microstructure variation between the untreated and C_2Cl_6/CaC_2 treated AM60 alloys are shown in Figure 4-36. The difference in coarseness of the microstructure between the specimens can be easily observed, and the untreated specimen evidently shows coarser structure than the grain refined alloys.

It has been pointed out by Song and Atreus [80] that, the key to corrosion resistance of Mg-Al alloys is related to fine microstructure coupled with improved intermetallic continuity as shown in Figure 4-37. With the presence of the continuous β -phase as “ β barrier”, the corrosion only happens on the surface of the material and the depth of corrosion penetration is largely reduced. Thus, the observation by the SEM analysis indicates enhanced corrosion resistance behaviour for the grain-refined specimens over the untreated alloys due mainly to the finer microstructure and higher area percentage of the continuous β barriers. This was supported statistically by the

experimental measurements of the potentiodynamic polarization testing as shown in Figure 4-38 and Table 4-6. Both C_2Cl_6 and CaC_2 treated specimens showed low current density at $1.51 \mu A/cm^2$ and $1.79 \mu A/cm^2$ compared to the untreated alloy at $3.16 \mu A/cm^2$. The polarization resistance (R_p) were obtained by Tafel equation as shown in Equation 3-1. As shown in Table 4-7 that, the R_p of C_2Cl_6 treated specimen ($11.46 k\Omega cm^2$) increased by 282%, and the R_p of CaC_2 treated specimen ($9.35 k\Omega cm^2$) also increased by 187% in comparison with the untreated alloy ($5.89 k\Omega cm^2$). This observation evidently indicated the corrosion resistance of squeeze cast magnesium alloy AM60 was significantly improved by the addition of C_2Cl_6 and CaC_2 grain refiners.

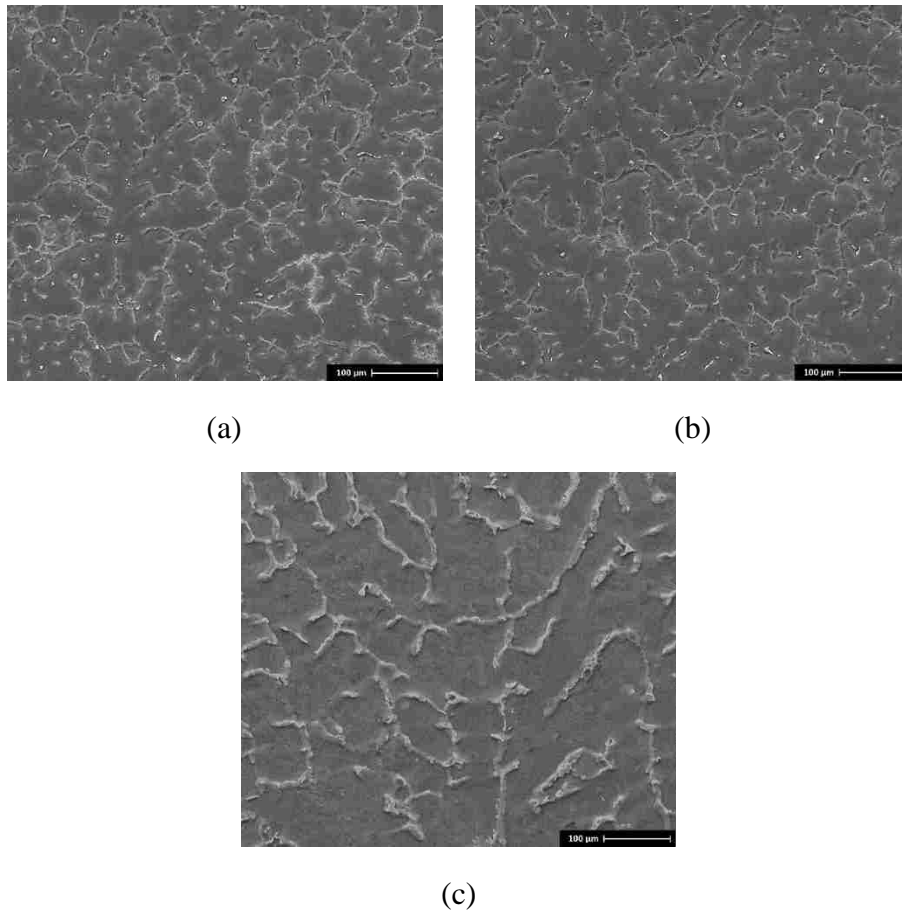


Figure 4- 36. SEM micrographs in SE mode showing the microstructures of (a) C_2Cl_6 refined specimen, (b) CaC_2 refined specimen, and (c) untreated AM60.

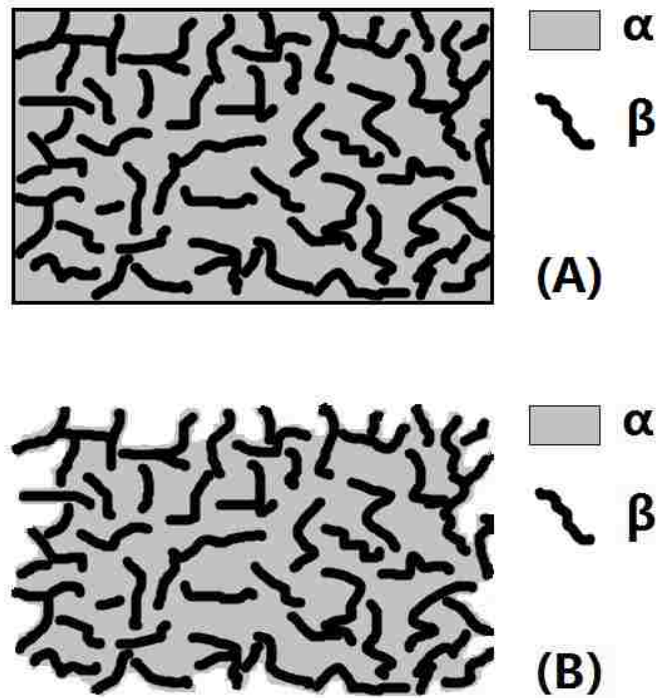


Figure 4- 37. The β -barrier concept showing the microstructure of (a) before and (b) after corrosion attack.

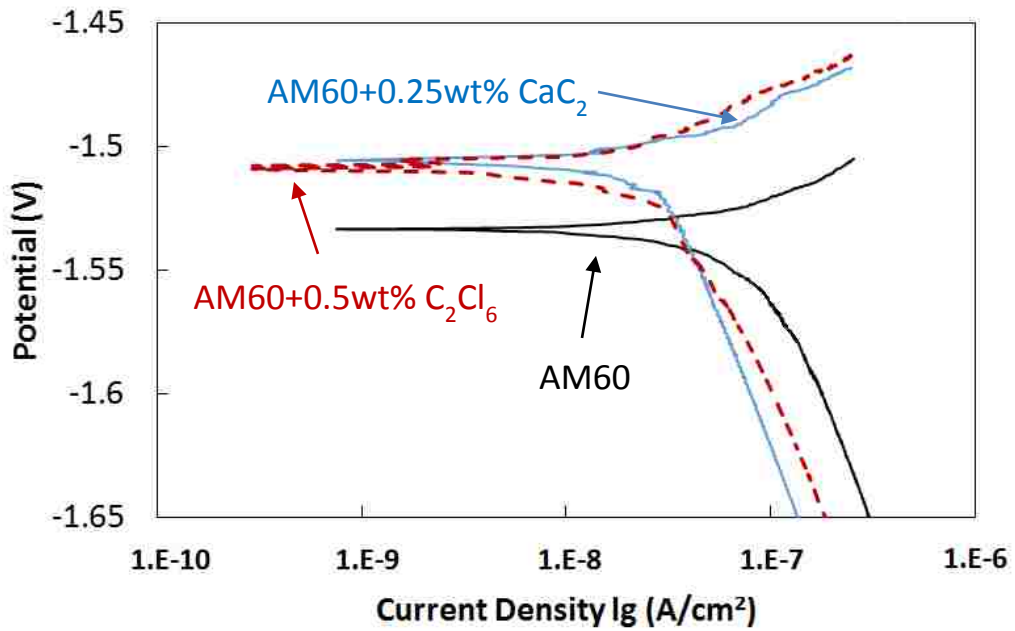


Figure 4- 38. Polarization curves for squeeze cast AM60 specimens in 3.5 wt% NaCl solution.

$$R = \frac{\beta_a \beta_c}{2.303 i_{corr} (\beta_a + \beta_c)} \quad (3-1)$$

Table 4-7 Characteristic values for the polarization curves in Figure 4-37

	β_A (mV/dec)	β_C (mV/dec)	I_{corr} ($\mu\text{A}/\text{cm}^2$)	R_p ($\text{k}\Omega \text{ cm}^2$)
AM60+C ₂ Cl ₆	51.8	172.6	1.51	11.46
AM60+CaC ₂	50.5	162.5	1.79	9.35
AM60	58.6	160.1	3.16	5.89

4.8 Summary

The observation of no apparent supercooling on the cooling curves of the C₂Cl₆/CaC₂-treated AM60 alloys imply a significant refinement of the grain structure. This implication is evidenced by both optical microstructural study and the grain size measurement. The average grain sizes of AM60 alloy were reduced from 70 μm to 35 μm and 38 μm by the addition of C₂Cl₆ and CaC₂ in the cylindrical coupon, respectively. In the case of 5-step-shaped specimens, the grain refiner trended to unify the grain sizes in different section thicknesses caused by different cooling rates. The grain sizes differences of the grain-refined specimens were significantly reduced compared with the un-refined alloy AM60. As a result, the mechanical properties of the thicker sections were largely improved. Meanwhile, the restricted grain sizes increase the corrosion resistance of the alloy, due to the well-distributed β -phases, which formed the β barrier to block the corrosion attack.

CHAPTER 5: CONCLUSIONS

1. The microstructure of squeeze casting magnesium AM60 was studied using both optical and SEM analysis. A porosity-free squeeze casting product was confirmed by optical micrograph and typical α -Mg, β -Mg₁₇Al₁₂ and Al-Mn phases were observed by SEM/EDS.
2. Section thicknesses had great influence on the microstructures of untreated squeeze casting AM60 alloy. The grain size increased with the increase in section thickness.
3. Tensile properties including UTS, YS and Elongation were also significantly influenced by different section thicknesses. The tensile properties decreased largely with the increase in section thicknesses.
4. The observation of no apparent supercooling on the cooling curves of both C₂Cl₆ and CaC₂ refined AM60 alloys indicated a significant refinement of the grain structure.
5. C₂Cl₆ had a remarkable capability of refining the grain structure of squeeze cast magnesium alloy AM60, which was evidently indicated by the grain size measurement in the center of a cylindrical AM60 coupon with the addition of the C₂Cl₆ powder.
6. C₂Cl₆ was able to unify the average grain sizes of squeeze cast magnesium alloy AM60 among different section thicknesses. The grain size of the 20 mm section thickness was reduced from 88 μm to an average of 28 μm .

7. CaC_2 had a great grain refining capability similar to C_2Cl_6 for squeeze cast magnesium alloy AM60.
8. The CaC_2 addition tended to decrease the fluidity of alloy AM60, which led to the entrapment of inclusions in the casting coupon.
9. Tensile properties in the thick sections (10 mm and 20 mm) of C_2Cl_6 and CaC_2 refined specimens were largely increased compared to those of the un-refined AM60 specimens.
10. Examination of fracture surfaces with SEM revealed that the thick section of grain refined specimens fractured in more ductile mode than the un-refined specimens. This observation agreed with the tensile results of which the UTS, YS and elongation of the refined specimens were higher than the un-refined AM60 alloy.
11. The corrosion resistance of squeeze casting AM60 specimens increased with the addition of the grain refiners. The improved corrosion resistance should be attributed to the well-distributed β -phase which could act as a corrosion barrier to block the corrosion attack to the α -Mg matrix.

CHAPTER 6: FUTURE WORK

The future work of this study can be classified into two primary research areas:

I. C_2Cl_6 as the grain refiner for the squeeze casting Magnesium alloy AM60:

Even though C_2Cl_6 exhibited excellent grain refining capability on squeeze cast magnesium alloy AM60, especially for the relatively thicker casting sections, the usage of this grain refiner in the automotive industry was limited from the environmental and health point of view due to the release of toxic dioxins gases when introduced to the molten alloys. Therefore, development of new carbon-containing grain refiners to replace C_2Cl_6 is essential. Candidates including carbon powder, C_6H_6 and $MgCO_3$ are mostly likely to fulfill this objective and deserve more attention.

II. CaC_2 as the grain refiner for the squeeze casting Magnesium alloy AM60:

Compare to C_2Cl_6 , CaC_2 is considered to be an environmental friendly grain refiner for squeeze casting magnesium alloy AM60. The ability of improving the thermal stability of magnesium alloys by suppress β -phase made it competitive among all Mg grain refiners. However, further research is still needed to solve the high tendency of inclusion in the CaC_2 -refined magnesium castings. The optimal amount of CaC_2 addition, at which, not only suppresses the unstable β -phase, yet limited the introduction of inclusions is the subject that should to be studied.

REFERENCES

- [1] G. Davies, Magnesium Materials for automotive bodies, Oxford, Butterworth-Heinemann, vol. 91 (2003) 158-159.
- [2] H. Hu, Squeeze casting of magnesium alloys and their composites, Journal of materials science, vol. 33, no. 6 (1998) 1579-1589.
- [3] J. F. Wallace, D. Schwam, and Y. Zhu, The Influence of Potential Grain Refiners on Magnesium Foundry Alloys, Transactions of the American Foundry Society and the One Hundred Seventh Annual Castings Congress, 03-141 (06), (2003) 1061-1075.
- [4] H. Hu and R. Shang. "Effect of Ca Addition of Grain Microstructure Development of Mg Alloy AM60" Transactions of the American Foundry Society, 2003.
- [5] Z. Brown et al. "Squeeze Cast Automotive Applications and Design Considerations" La Metallurgia Italiana, 2009.
- [6] M. K. Kulekci, Magnesium and its alloys applications in automotive industry, The International Journal of Advanced Manufacturing Technology, vol. 39, no. 9-10 (2008) 851-865.
- [7] Technical report, Magnesium Die Casting Handbook, NADCA, 1998.

- [8] H. Hu, A. Yu, N. Li, and J. E. Allison, Potential magnesium alloys for high temperature die cast automotive applications: a review, *Materials and Manufacturing Processes*, vol. 18, no. 5 (2003) 687-717.
- [9] I. J. Polmear, Magnesium alloys and applications, *Materials science and technology* vol. 10, no. 1 (1994) 1-16.
- [10] R. B. Ross, *Metallic Materials Specification Handbook*, 3rd edition, E and FN Spon Ltd, London, vol. 13, (1997) 76-79.
- [11] J. G. Barlock, and F. M. Lucio, Structure of Some Aluminum-Iron-Magnesium-Manganese-Silicon Alloys, *Zeitschrift fur Metallkunde*, vol. 66, no. 10 (1975) 605-611.
- [12] M. Mohsen, and H. Hu, Influence of applied pressure on microstructure and tensile properties of squeeze cast magnesium Mg–Al–Ca alloy, *Materials Science and Engineering, A* 528, no. 10 (2011) 3589-3593.
- [13] M. M. Avedesian, and H. Baker, *Magnesium and magnesium alloys*, ASM International, Materials Park, OH (1999) 15-18.
- [14] B. L. Mordike, and Tü Ebert, Magnesium: Properties applications potential, *Materials Science and Engineering, A* 302, no. 1 (2001) 37-45.
- [15] Technical report, *Introduction to Die Casting*, NADCA, 2006.

- [16] Internet article: Die casting 101, introduction to die casting; http://www.paceind.com/die-casting-101/introduction_what1s, retrieved on 2013-10-15.
- [17] Technical report, Die casting industry report – 2008, NADCA, 2008.
- [18] Internet article: Advantages of die casting; <http://www.deeco.net/for/advandie.htm>, retrieved on 2013-10-16.
- [19] A. Gordon, G. Meszaros, J. Naizer, C. Mobley, Equations for predicting the percent porosity in die castings, paper No T93-024, Transaction of NADCA International Die Casting Congress and Exposition, Cleveland, (1993) 106-110.
- [20] Internet article: Disadvantages of die casting process; <http://casting.forum-lunjian.com/t15-disadvantages-of-die-casting-process>, retrieved on 2013-10-18.
- [21] M. R. Ghomashchi, and A. Vikhrov, Squeeze casting: an overview, *Journal of Materials Processing Technology*, vol. 101, no. 1 (2000) 1-9.
- [22] M. Zhou, An experiment study of die and squeeze cast magnesium alloy AM50, Master thesis, Department of Material Science and Engineering, University of Windsor, 2004.
- [23] T. M. Yue, and G. A. Chadwick, Squeeze casting of light alloys and their composites, *Journal of materials processing technology*, vol. 58, no. 2 (1996) 302-307.

- [24] A. Yu, S. Wang, N. Li, and H. Hu, Pressurized solidification of magnesium alloy AM50A, *Journal of materials processing technology* vol. 191, no. 1 (2007) 247-250.
- [25] A. Luo, and M. O. Pekguleryuz, Cast magnesium alloys for elevated temperature applications, *Journal of Materials Science*, vol. 29, no. 20 (1994) 5259-5271.
- [26] M. S. Yong, and A. J. Clegg, Process optimisation for a squeeze cast magnesium alloy, *Journal of materials processing technology*, vol. 145, no. 1 (2004) 134-141.
- [27] G. A. Chadwick and T. M. Yue, Squeeze casting of light alloys and their composites, *Journal of Materials processing technology*, vol. 5, no. 1 (1991) 6.
- [28] M. Zhou H. Hu, N. Li, and J. Lo, Microstructure and tensile properties of squeeze cast magnesium alloy AM50, *Journal of materials engineering and performance*, vol. 14, no. 4 (2005) 539-545.
- [29] S. Li, K. Mine, S. Sanakanishi, and K. Anzai, Quantitative Prediction Method for Shrinkage Porosity Considering Molten Metal Supply by Pressure in Squeeze Casting, *Chuzo Kogaku (Journal of Japan Foundry Engineering)*, vol. 78, no. 12 (2006) 641-647.
- [30] S. Kleiner, O. Beffort, A. Wahlen, and P. J. Uggowitzer, Microstructure and mechanical properties of squeeze cast and semi-solid cast Mg–Al alloys, *Journal of Light Metals*, vol. 2, no. 4 (2002) 277-280.

- [31] N. Li, H. Hu, and M. Zhou, Effect of section thicknesses on tensile behavior and microstructure of high pressure die cast magnesium alloy AM50, *Materials Science Forum*, vol. 475, (2005) 463-468.
- [32] H. Hu, M. Zhou, Z. Sun, and N. Li, Tensile behaviour and fracture characteristics of die cast magnesium alloy AM50, *Journal of Materials Processing Technology*, vol. 201, no. 1 (2008) 364-368.
- [33] X. Zhang, M. Wang, Z. Sun, and H. Hu, Section thickness-dependent tensile properties of squeeze cast magnesium alloy AM60, *China Foundry*, vol. 9, no. 2 (2012) 178-183.
- [34] Z. Sun, X. Zhang, H. Hu, and X. Niu, Section thickness-dependant interfacial heat transfer in squeeze casting of aluminum alloy A443, *IOP Conference Series: Materials Science and Engineering*, vol. 27, no. 1 (2012) 012073.
- [35] D. St John, Q. Ma, M. A. Easton, P. Cao, and Z. Hildebrand, Grain refinement of magnesium alloys, *Metallurgical and Materials Transactions, A* 36, no. 7 (2005) 1669-1679.
- [36] E. F. Emley, *Principles of magnesium technology*, Pergamon Press, Oxford, UK (1966) 259.
- [37] Q. Ma, D. St John, and M. Frost, A new zirconium-rich master alloy for the grain refinement of magnesium alloys, *K. U. Kainer 6th international conference Magnesium alloys and their applications*, (2003) 706-712.

- [38] D. St John, Solidification of cast magnesium alloys, The minerals, metals and materials society Magnesium technology 2003, (2003) 193-198.
- [39] Q. Ma, D. St John, M. Frost, Zirconium alloying and grain refinement of magnesium alloys, The minerals, metals and materials society Magnesium technology 2003, (2003) 209.
- [40] H. Okamoto. Phase diagrams of dilute binary alloys, 1st edition, ASM international, Material Park, OH, (2002) 170.
- [41] Y. Lee, A. Dahle, D. St John, The role of solute in grain refinement of magnesium, Metallurgical and materials transactions A, vol. 31, issue 11 (2000) 2895-2906.
- [42] Y. Tamura, N. Kono, T. Motegi, and E. Sato, Grain refining mechanism and casting structure of Mg-Zr alloy, Journal of Japan institute of light metals, vol. 48, no. 4 (1998) 185-89.
- [43] Q. Ma, and A. Das, Grain refinement of magnesium alloys by zirconium: Formation of equiaxed grains, Scripta materialia, vol. 54, no. 5 (2006) 881-886.
- [44] Y. Lee, A. K. Dahle, and D. St John, The role of solute in grain refinement of magnesium, Metallurgical and Materials Transactions, A 31, no. 11 (2000) 2895-2906.
- [45] I.G. Farbenindustrie, Apparatus for producing carbon disulphide, United States patent office, GB359, (1931) 425.

- [46] D. St John, P. Cao and Q. Ma, A brief history of the development of grain refinement technology for cast magnesium alloys, *Magnesium technology 2013*, (2013) 3-8.
- [47] N. Tiner, Superheating of magnesium alloys, *Transactions of the American institute of mining, metallurgical and petroleum engineers*, vol. 12, no. 7 (1945) 1-19.
- [48] T. Motegi, Grain-refining mechanisms of superheat-treatment of and carbon addition to Mg–Al–Zn alloys, *Materials Science and Engineering, A* 413 (2005) 408-411.
- [49] P. Cao, Q. Ma, and D. St John, Mechanism for grain refinement of magnesium alloys by superheating, *Scripta materialia*, vol. 56, no. 7 (2007) 633-636.
- [50] T. Chang, J. Wang, and S. Lee Grain refining of magnesium alloy AZ31 by rolling, *Journal of Materials Processing Technology*, vol. 140, no. 1 (2003) 588-591.
- [51] Pérez-Prado, M. Teresa, and O. A. Ruano, Grain refinement of Mg–Al–Zn alloys via accumulative roll bonding, *Scripta materialia*, vol. 51, no. 11 (2004) 1093-1097.
- [52] P. Cao, Q. Ma, and D. St John, Native grain refinement of magnesium alloys, *Scripta Materialia*, vol. 53, no. 7 (2005) 841-844.
- [53] T. Motegi, E. Yano, Y. Tamura, and E. Sato, Effect of minor elements on grain size of Mg-9%Al alloy, *Materials Science Forum*, vol. 350-351, (2000) 199-204.

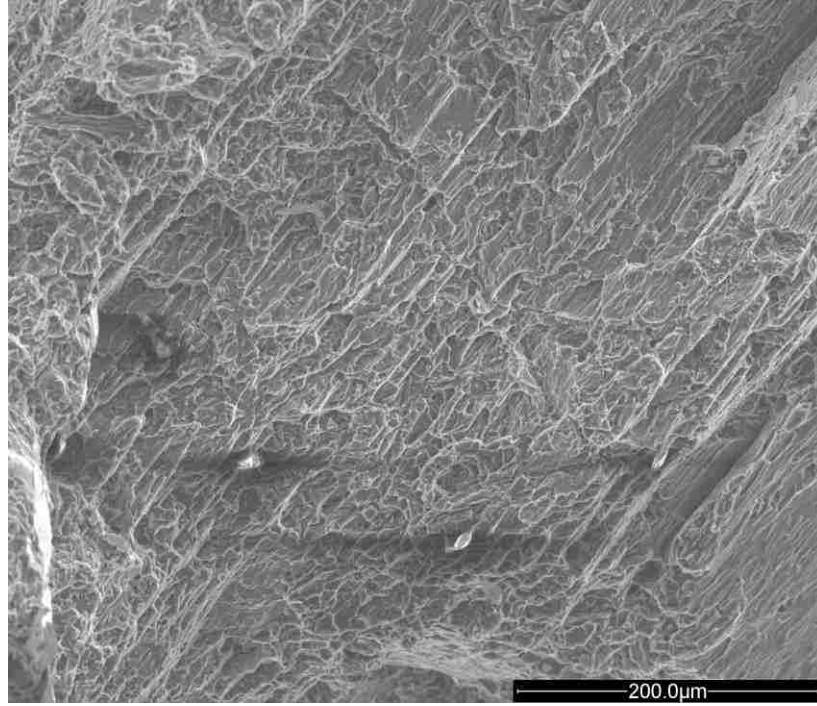
- [54] R. Hultgren and D. W. Mitchell, Magnesium alloys – grain refinement of magnesium alloys without superheating, Transactions of the American institute of mining, metallurgical and petroleum engineers, vol. 161, no. 471 (1945) 323-27.
- [55] Q. Jin, J. Eom, S. Lim, W. Park, and B. You, Grain refining mechanism of a carbon addition method in Mg–Al magnesium alloy, Scripta Materialia, vol. 49, no. 11 (2003) 1129-1132.
- [56] A. K. Dahle, Y. Lee, M. Nave, P. Schaffer, D. St John., Development of the as-cast microstructure in magnesium-aluminum alloys, Journal of Light Metals, vol. 1, issue 1 (2001) 61-72.
- [57] E. Yano, Y. Tamura, T. Motegi, E. Sato, Effect of carbon powder on grain refinement of AZ91 magnesium alloy, Journal of Japan Institute of Light Metals, vol. 51, no. 7 (2001) 395.
- [58] E. Yano, T. Yousuke, M. Tetsuichi, and S. Eiichiro, Effect of carbon powder on grain refinement of AZ91E magnesium alloy, Materials Transactions (Japan), vol. 44, no. 1 (2003) 107-110.
- [59] Q. Wang, W. Chen, X. Zeng, Y. Lu, W. Ding, Y. Zhu, X. Xu and M. Mabuchi, Effect of Ca addition on the microstructure and mechanical properties of AZ91 magnesium alloy, Journal of Materials Science, vol. 36(12), (2001) 3035-3040.
- [60] S. Y. Chang, H. Tezuka, A. Kamio, Mechanical properties and structure of Ignition-proof Mg-Ca-Zr alloys produced by squeeze casting, Materials Transactions, vol. 38, no. 6 (1997) 526-535.

- [61] R. Ninomiya, T. Ojio, K. Kubota, Improved heat resistance of Mg-Al alloys by the Ca addition, *Acta Metallurgica et Materialia*, vol. 43, no. 2 (1995) 669-674.
- [62] B. Kondori, and R. Mahmudi, Effect of Ca additions on the microstructure, thermal stability and mechanical properties of a cast AM60 magnesium alloy, *Materials Science and Engineering, A* 527, no. 7 (2010) 2014-2021.
- [63] D. O. Karlsen, Development of grain refiners for Al-containing Mg-alloys, Canada institute of mining, metallurgy and petroleum conference, Quebec, Canada, 1993.
- [64] P. Cao, D. St John and Q. Ma, The effect of manganese on the grain size of commercial AZ31 alloy, *Materials science forum*, vol. 488-489, (2005) 139-142.
- [65] Y. Ma, X. Zhang and H. Hao, Effect of CaC_2 particles concentration on microstructure and tensile properties of elemental magnesium, *Transactions of nonferrous metals society of China*, vol. 18, (2008) 283-287.
- [66] P. Cao, Q. Ma, and D. St John, Effect of iron on grain refinement of high-purity Mg-Al alloys, *Scripta Materialia*, vol. 51, (2004) 125-129.
- [67] N. V. Kumar, J. J. Blandin, C. Desrayaud, F. Montheilet and M. Suery, Grain refinement in AZ91 magnesium alloy during thermomechanical processing, *Materials science and engineering, A*359, (2003) 150-157.
- [68] W. Kasprzak, J. H. Sokolowski, M. Sahoo and L. A. Dobrzanski, Thermal characteristics of the AM50 magnesium alloy, *Journal of achievements in materials and manufacturing engineering*, vol. 29, issue 2 (2008) 179-182.

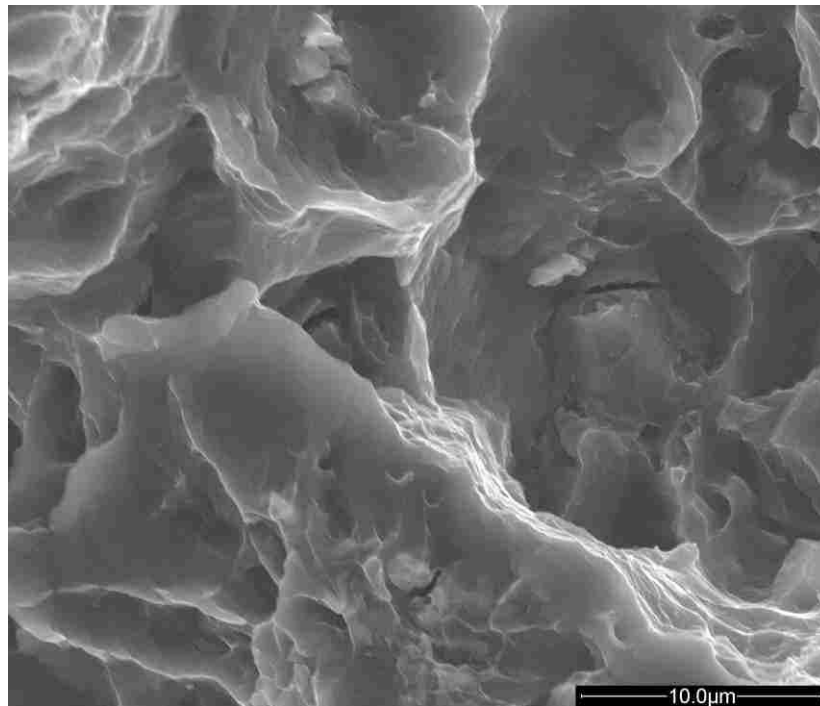
- [69] Z. Wang, Y. Kang, H. Zhao and Y. Xu, Grain refinement of Mg-Al magnesium alloys by carbon inoculation, Transactions of nonferrous metals society of China, vol. 16, (2006) 1851-1854.
- [70] W. Dong, Effect of T61 heat treatment and superheat on microstructure and mechanical properties of AM60 magnesium alloy, Automotive technology and material, vol. 7, (2004).
- [71] Q. Ma, Grain refinement of magnesium alloys by zirconium formation of equiaxed grains, Scripta materialia, vol. 54, (2006) 881-886.
- [72] Q. Ma, Creation of fine and spherical magnesium crystals via control of nucleation and growth instabilities, 7th international conference on magnesium alloys and their applications, Dresden Germany, (2006) 1-6.
- [73] J. F. King, Development of practical high temperature magnesium casting alloy, Magnesium alloys and their applications, (2000) 14-28.
- [74] N. Balasubramani, Studies on grain refinement and alloying additions on the microstructure and mechanical properties of Mg-8Zn-4Al alloy, Ph.D thesis from Cochin University of science and technology, (2012).
- [75] V. B. Kurfman, Method of grain refinement of magnesium base alloys, United Stated patent office, vol. 4, (1957) 1-6.
- [76] W. D. Callister, Fundamentals of materials science and engineering, 5th edition, Strengthening by grain size reduction, (2001) 256.

- [77] Y. Guo, M. Zhang and Y. Jin, Refinement mechanism of in-situ Al_4C_3 particles on AZ91 magnesium alloys, Journal of Wuhan University of Technology materials science, vol. 29, no. 1 (2014) 154-158.
- [78] Grain refinement of AZ31 magnesium alloy by new Al-Ti-C alloys, Transactions of nonferrous metals society of China, vol. 19, (2009) 1057-1064.
- [79] L. Han, H. Hu, D. O. Northwood and N. Li, Microstructure and nano-scale mechanical behavior of Mg-Al and Mg-Al-Ca alloys, Materials science and engineering, vol. 473, (2008) 16-27.
- [80] G. Song and A. Atrens, Understanding magnesium corrosion a frame work for improved alloy performance, Advanced engineering materials, vol. 5, no. 12 (2003) 837-858.

APPENDICES: ADDITIONAL FIGURES

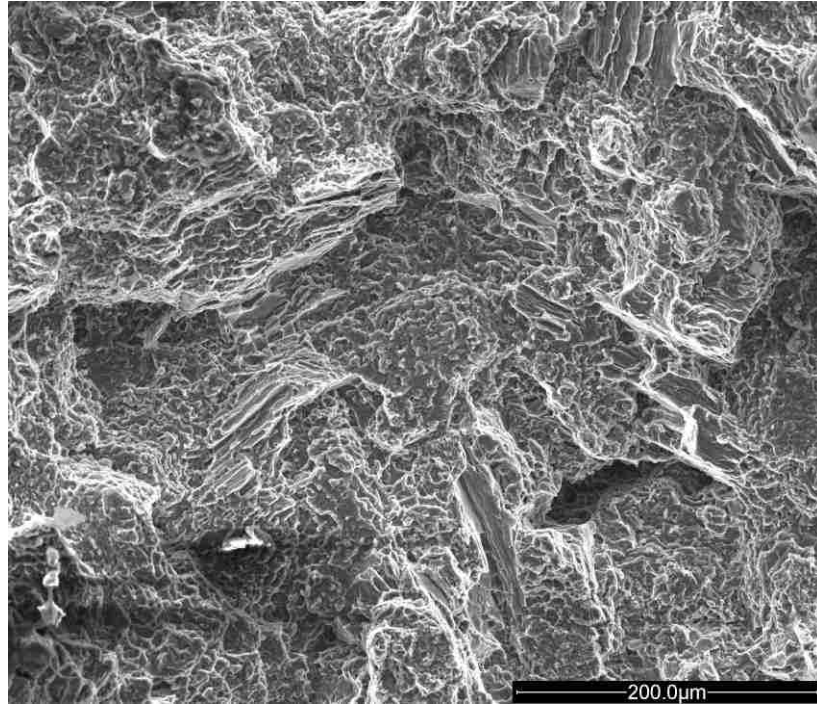


(a)

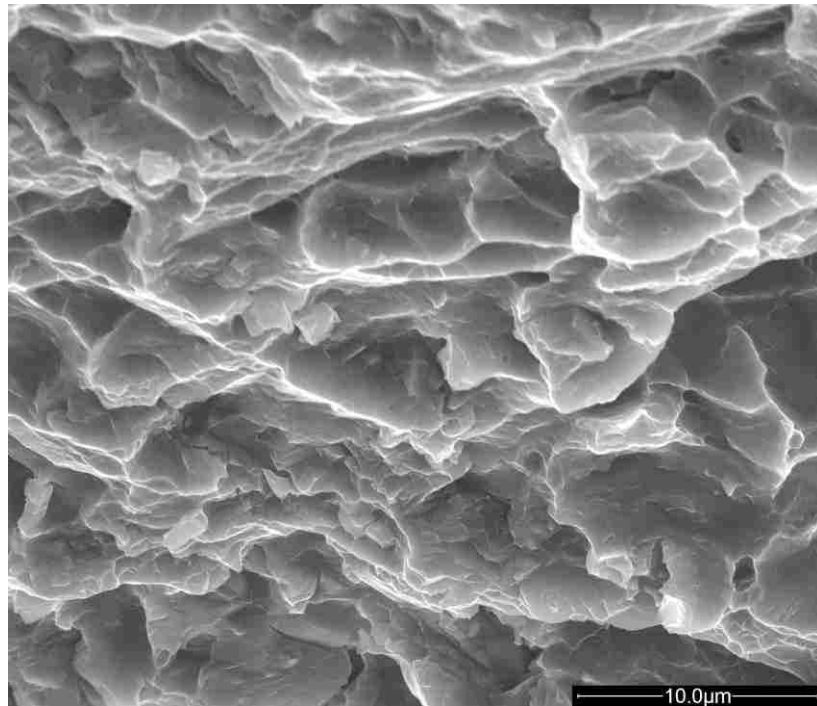


(b)

Figure Ap- 1. SEM fractographs in SE mode of the untreated squeeze cast AM60, (a) low and (b) high magnification from cylindrical coupon.

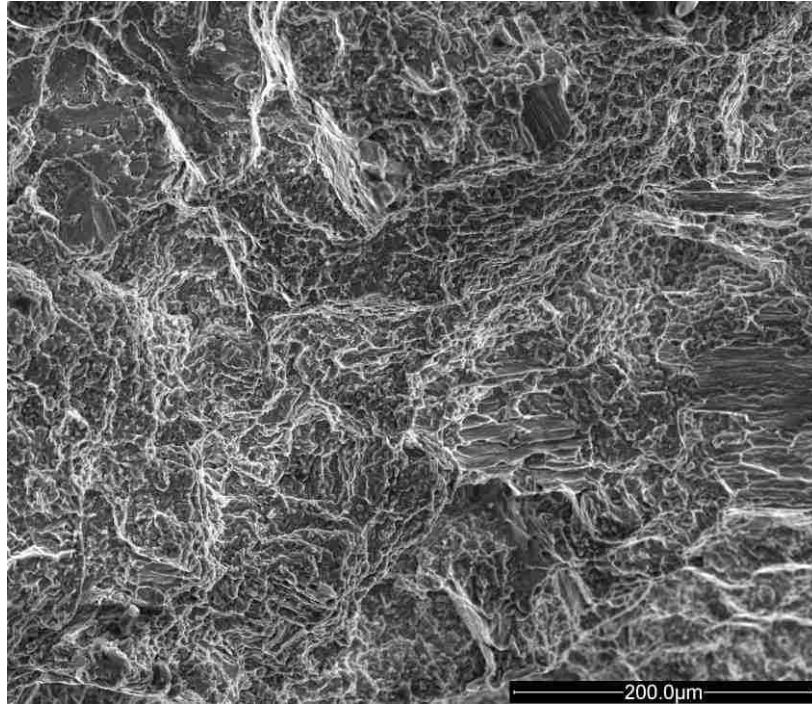


(a)



(b)

Figure Ap- 2. SEM fractographs in SE mode of the C_2Cl_6 -refined squeeze cast AM60, (a) low and (b) high magnification from cylindrical coupon.



(a)

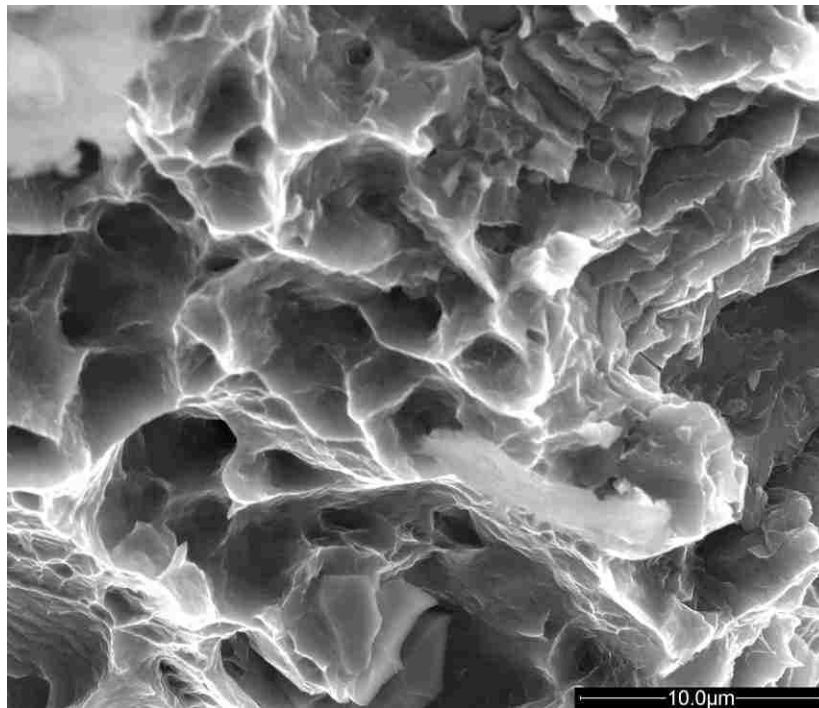
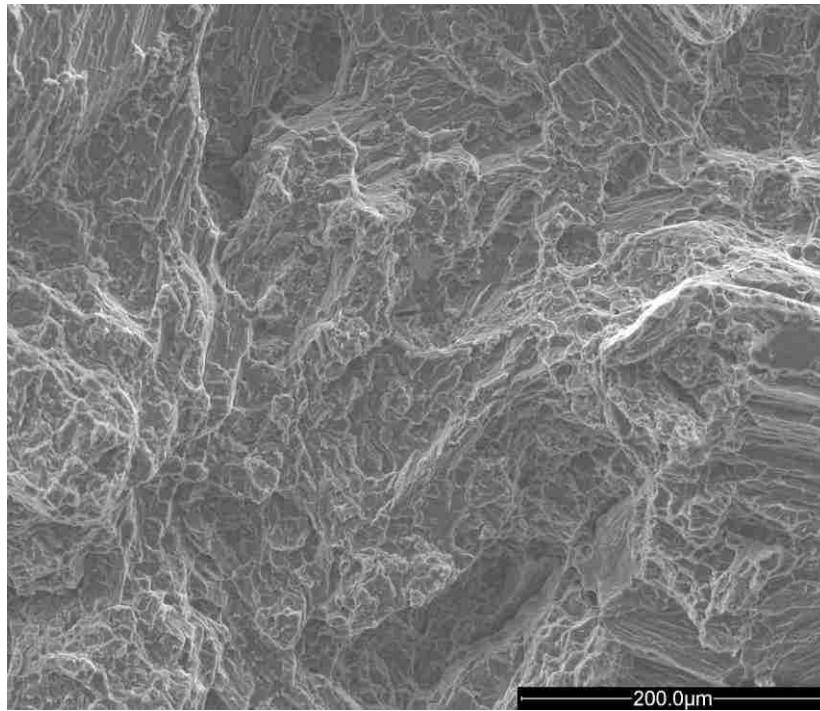
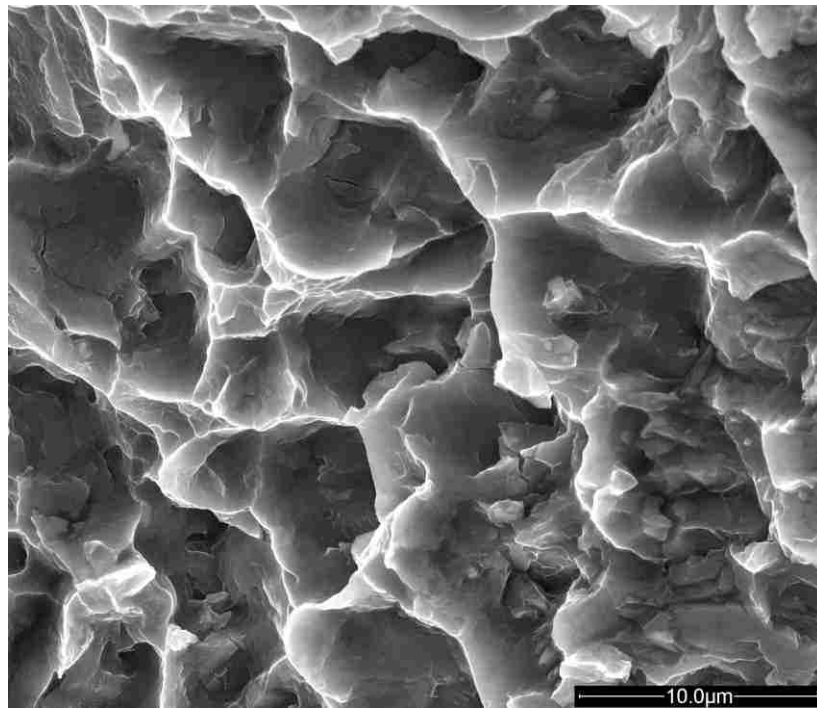


Figure Ap- 3. SEM fractographs in SE mode of the CaC_2 -refined squeeze cast AM60, (a) low and (b) high magnification from cylindrical coupon.

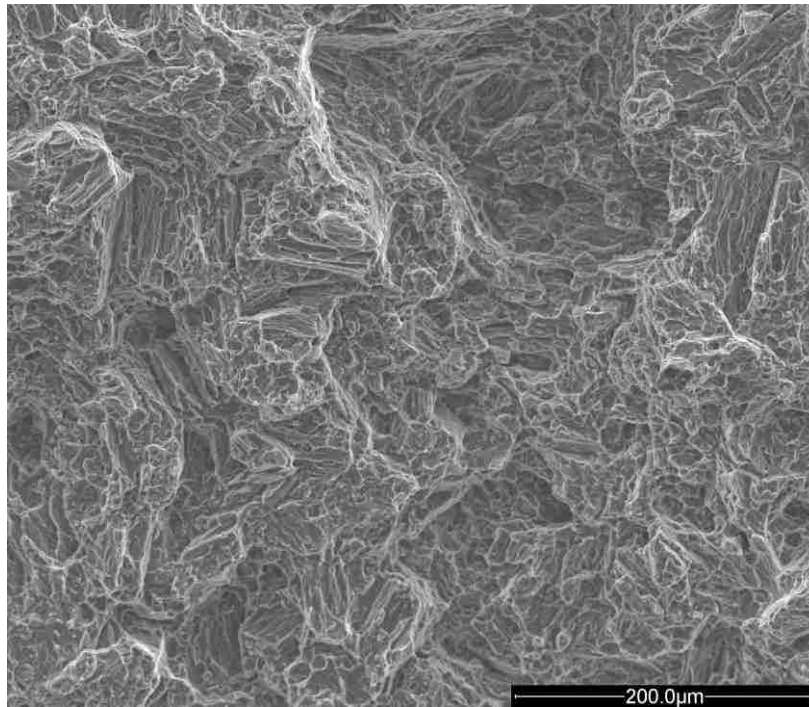


(a)

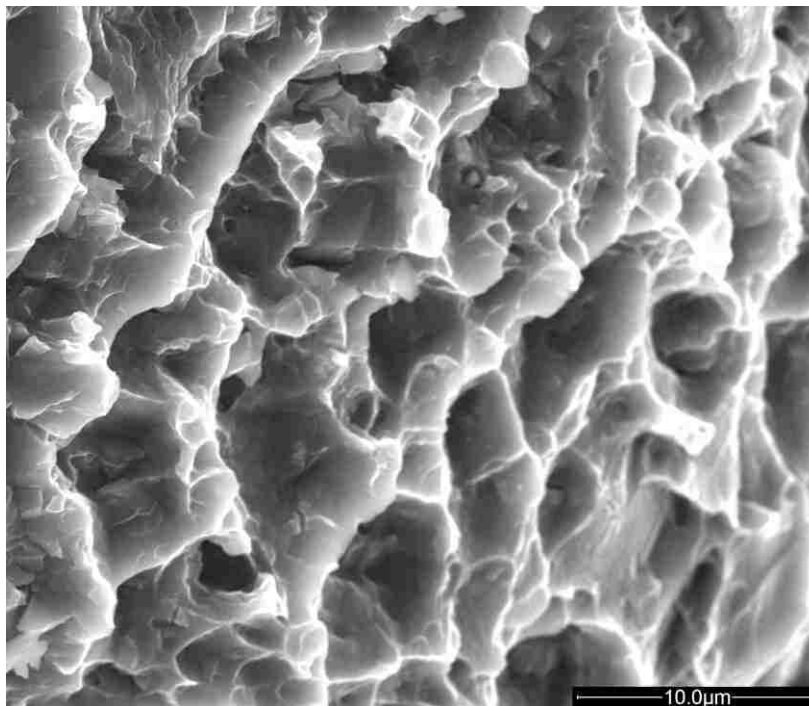


(b)

Figure Ap- 4. SEM fractographs in SE mode of the untreated squeeze cast AM60, (a) low and (b) high magnification form 6 mm section thickness.

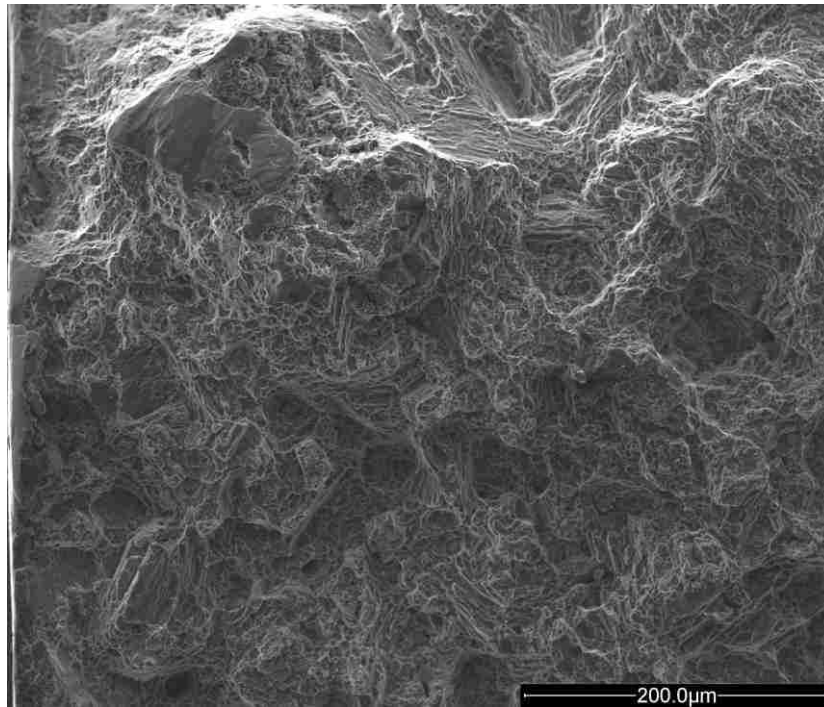


(a)

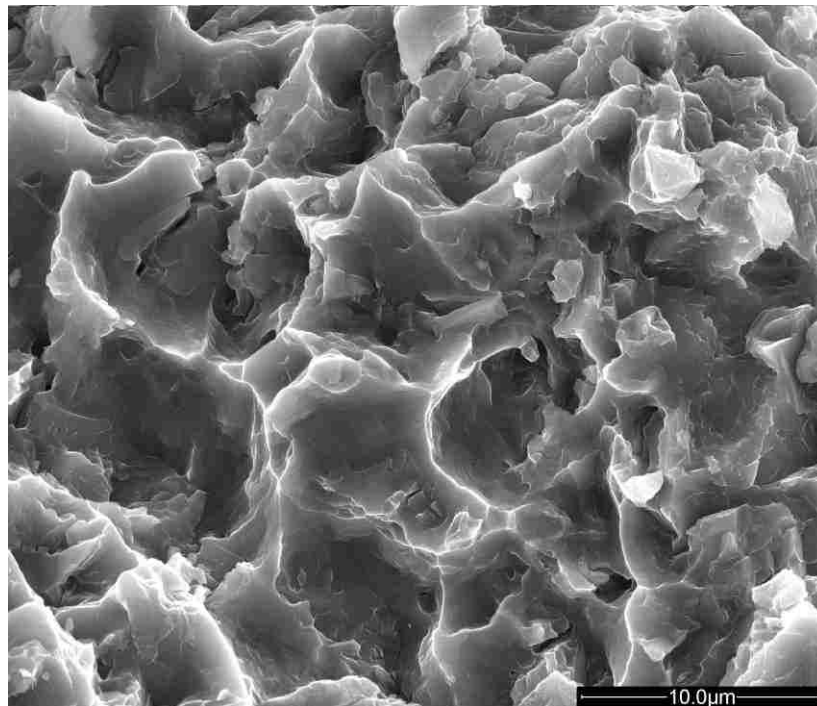


(b)

Figure Ap- 5. SEM fractographs in SE mode of the C_2Cl_6 -refined squeeze cast AM60, (a) low and (b) high magnification from 6 mm section thickness.

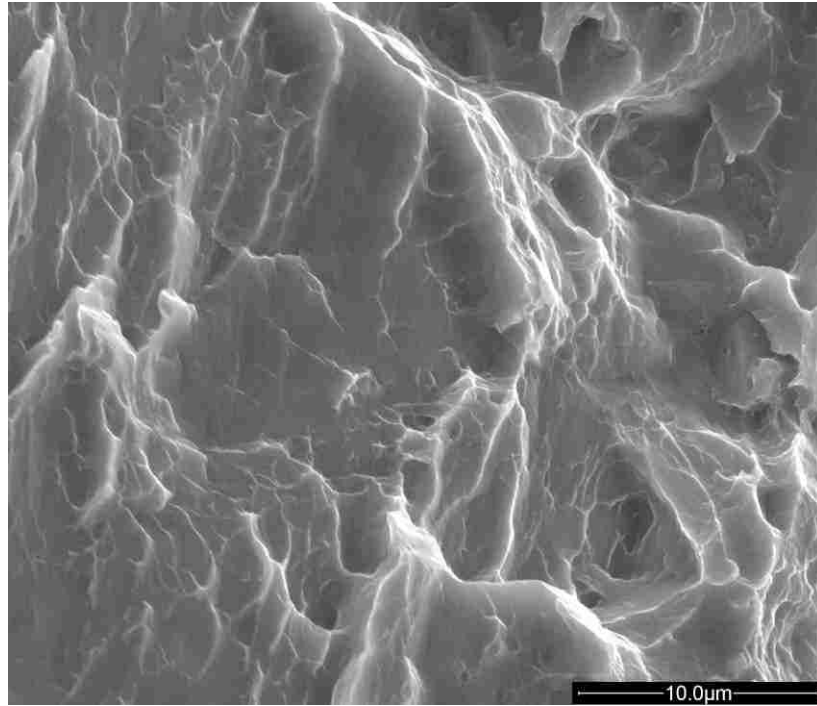


(a)

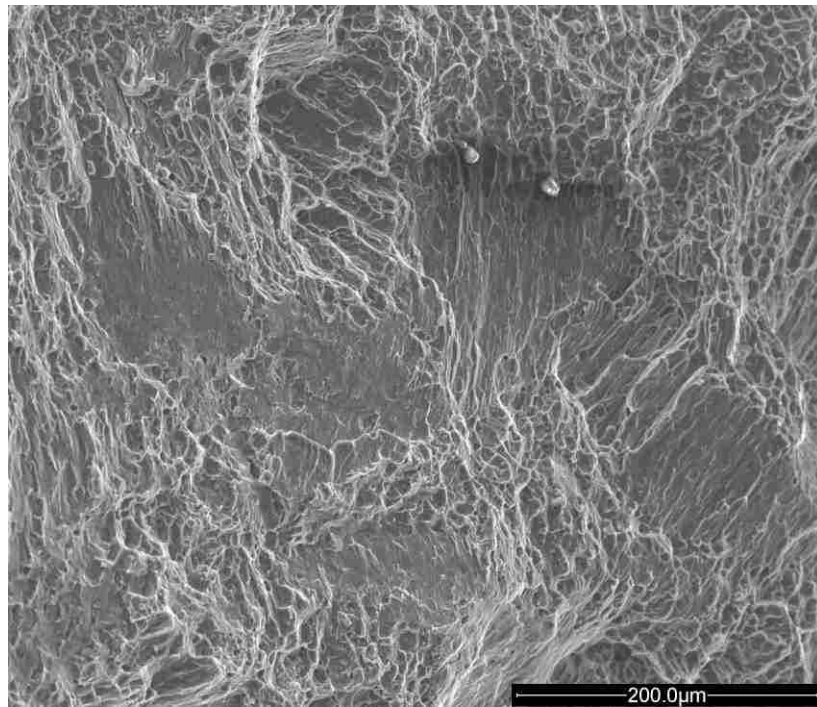


(b)

Figure Ap- 6. SEM fractographs in SE mode of the CaC_2 -refined squeeze cast AM60, (a) low and (b) high magnification from 6 mm section thickness.

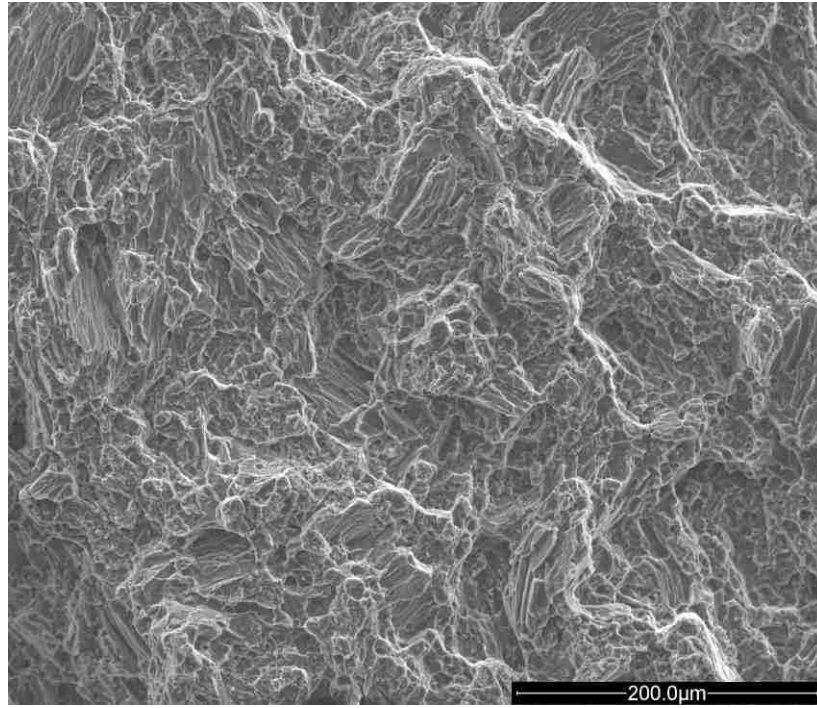


(a)

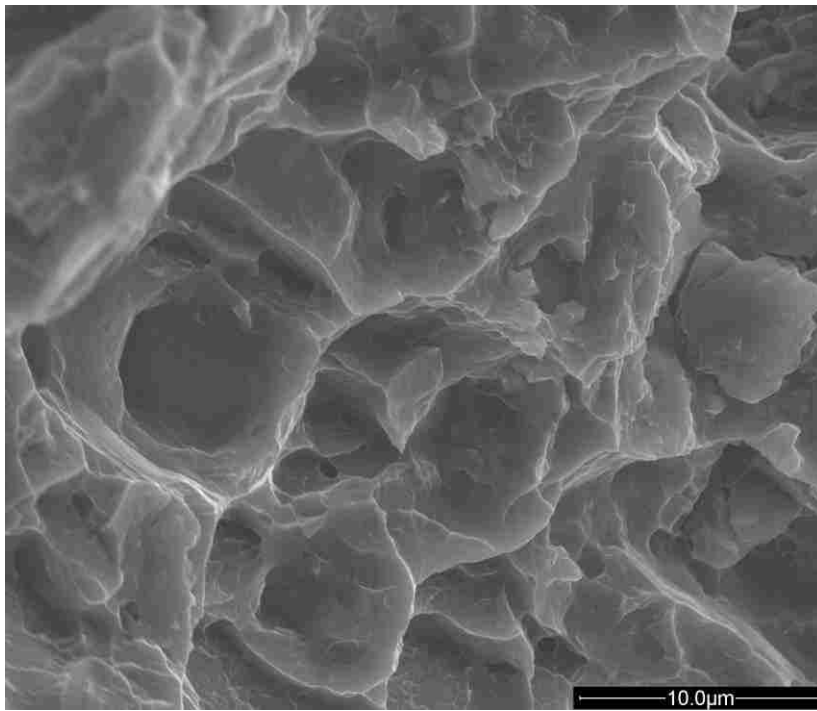


(b)

Figure Ap- 7. SEM fractographs in SE mode of the untreated squeeze cast AM60, (a) low and (b) high magnification form 20 mm section thickness.

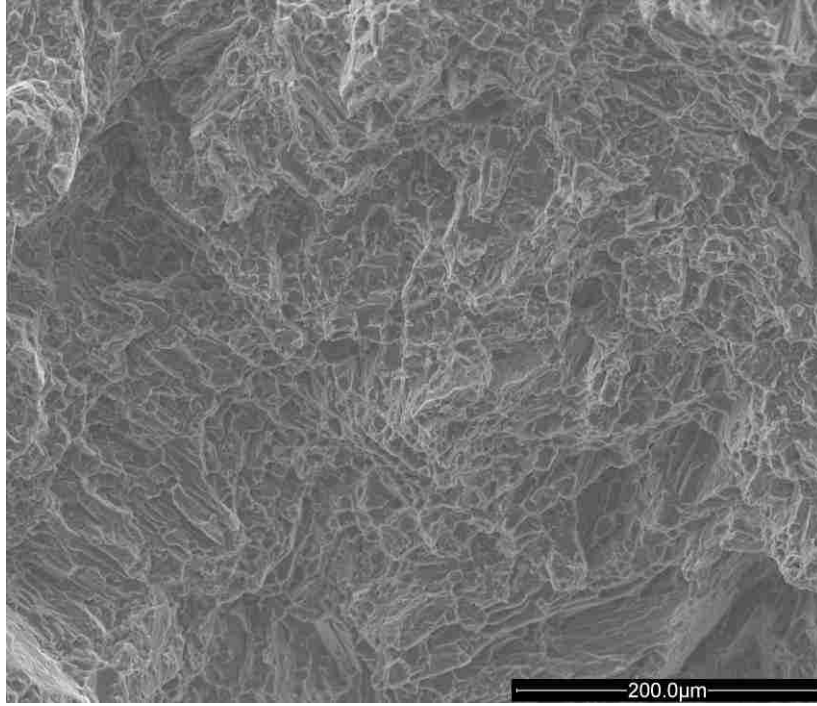


(a)



(b)

Figure Ap- 8. SEM fractographs in SE mode of the C_2Cl_6 -refined squeeze cast AM60, (a) low and (b) high magnification from 20 mm section thickness.



(a)

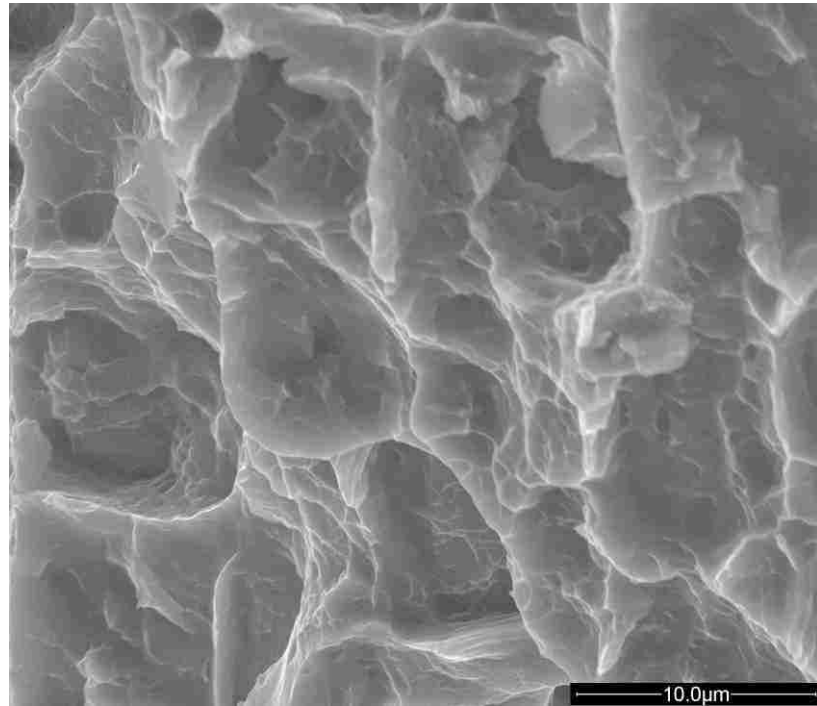


Figure Ap- 9. SEM fractographs in SE mode of the CaC₂-refined squeeze cast AM60, (a) low and (b) high magnification from 20 mm section thickness.

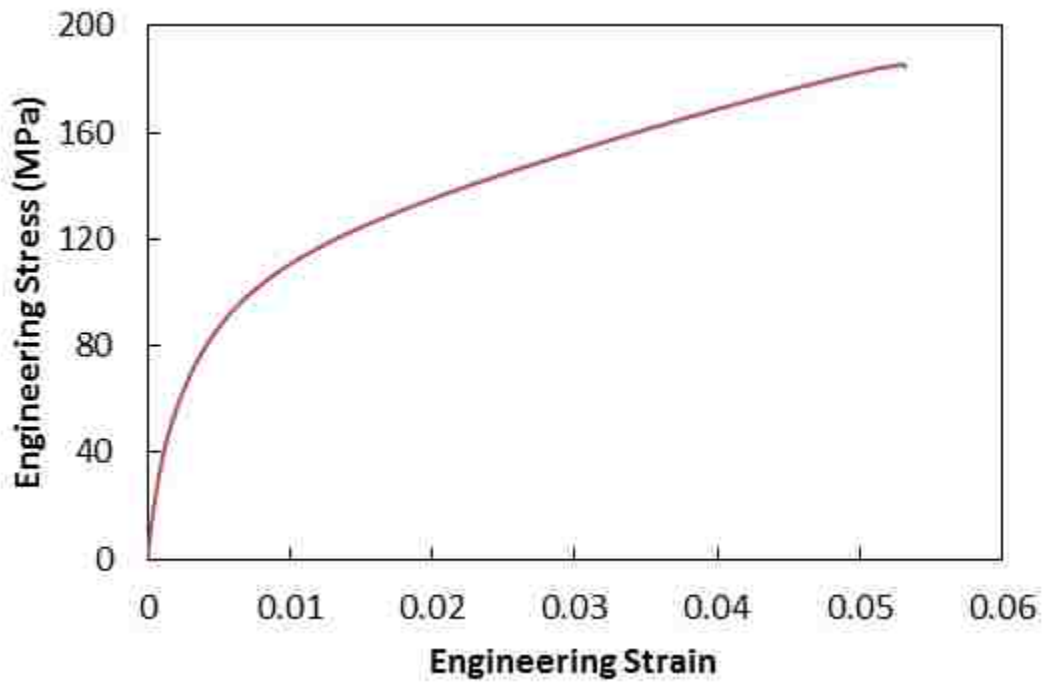
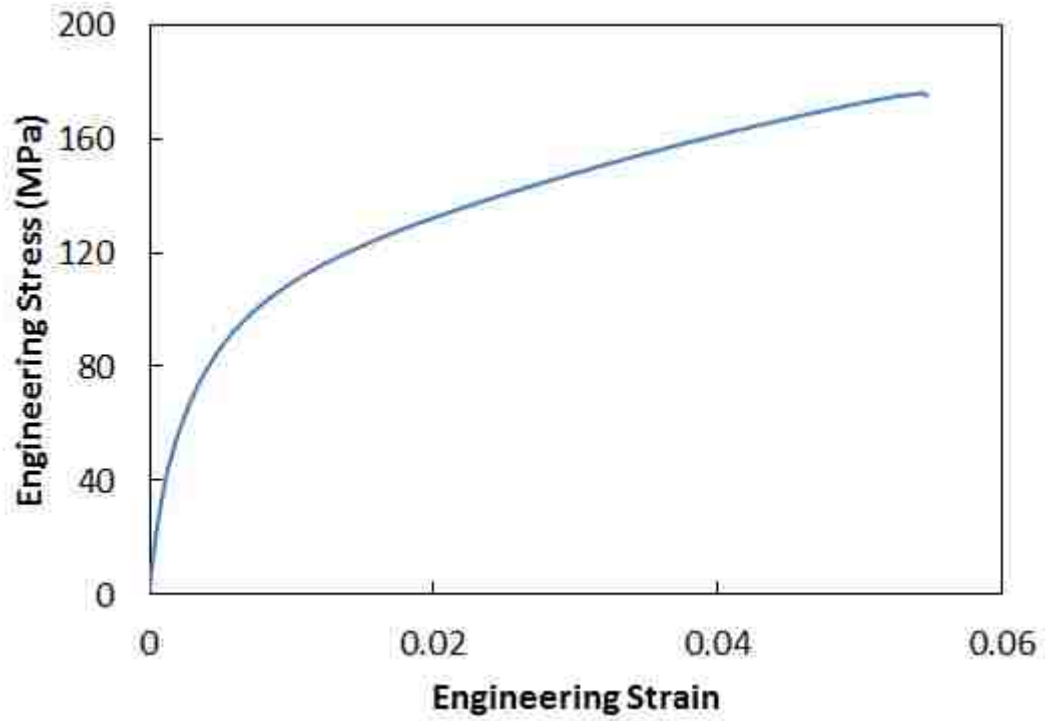


Figure Ap- 10. Engineering Stress-strain curves for AM60 from cylindrical coupon.

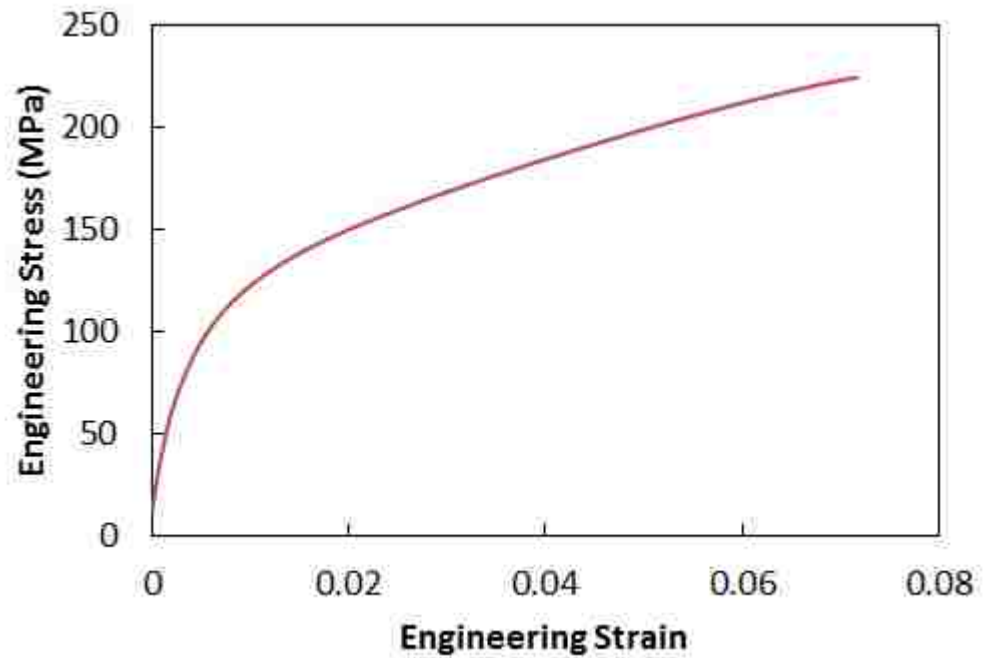
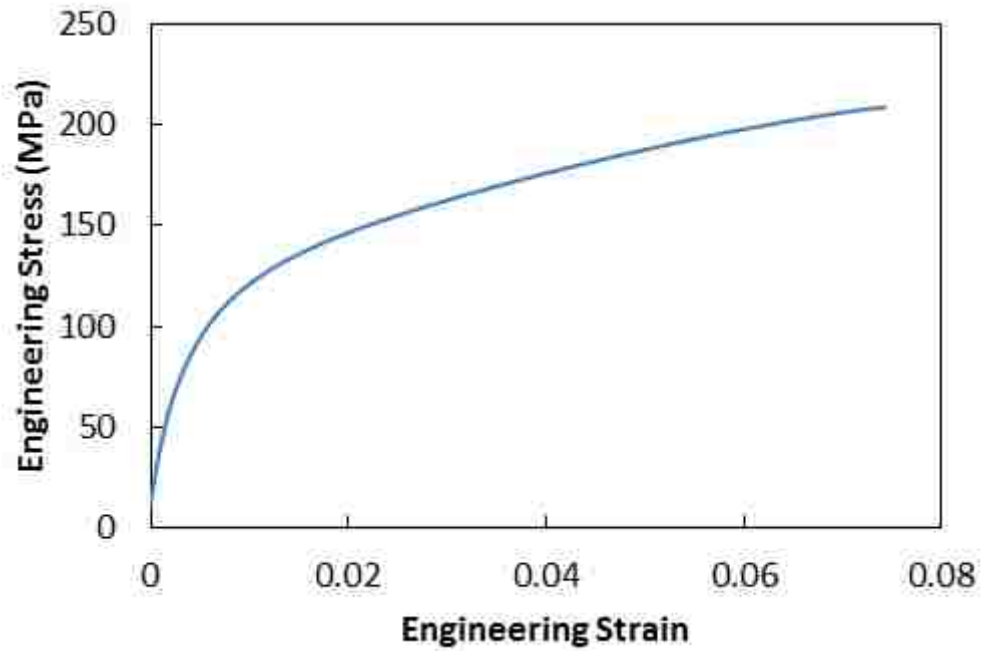


Figure Ap- 11. Engineering Stress-strain curves for C₂Cl₆-refined AM60 from cylindrical coupon.

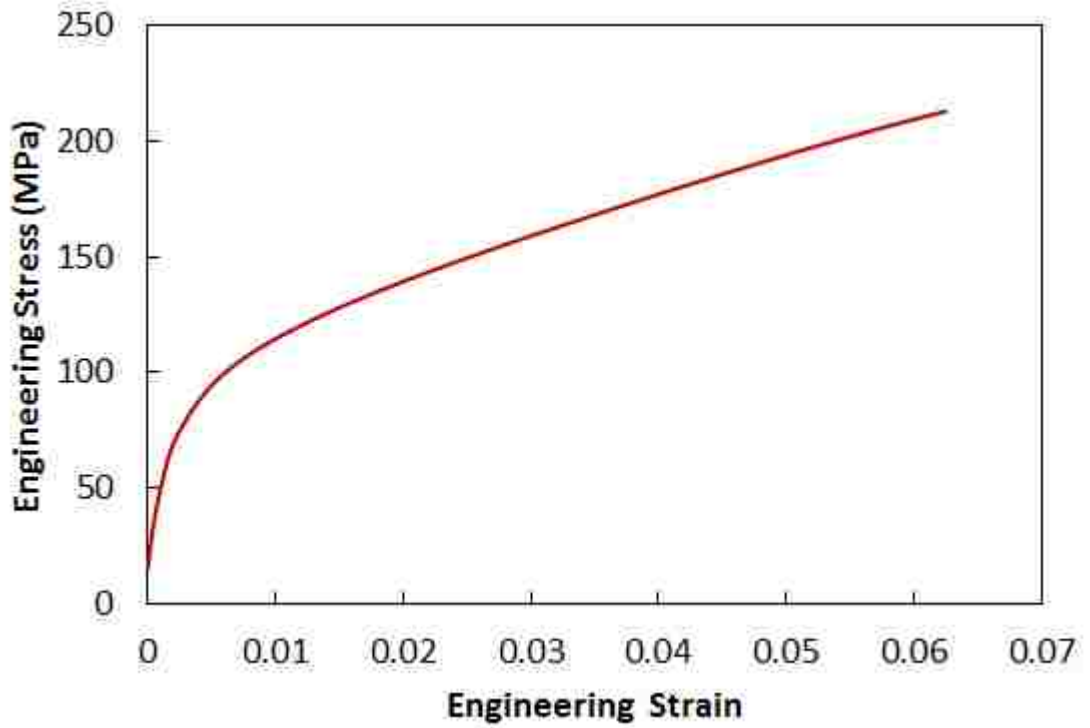
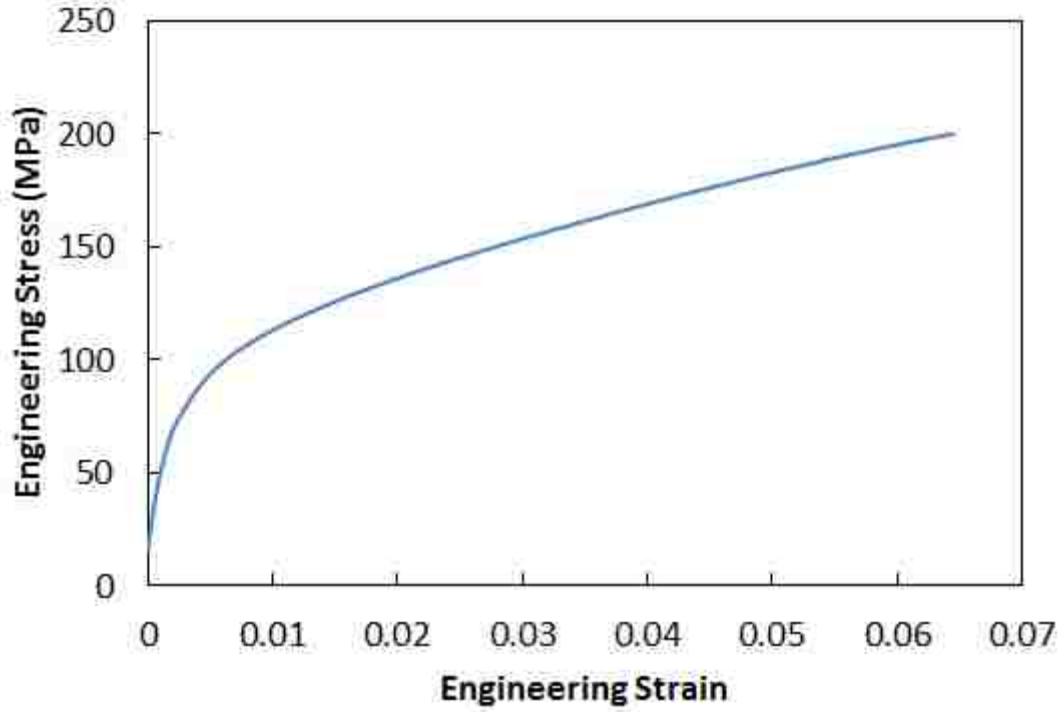
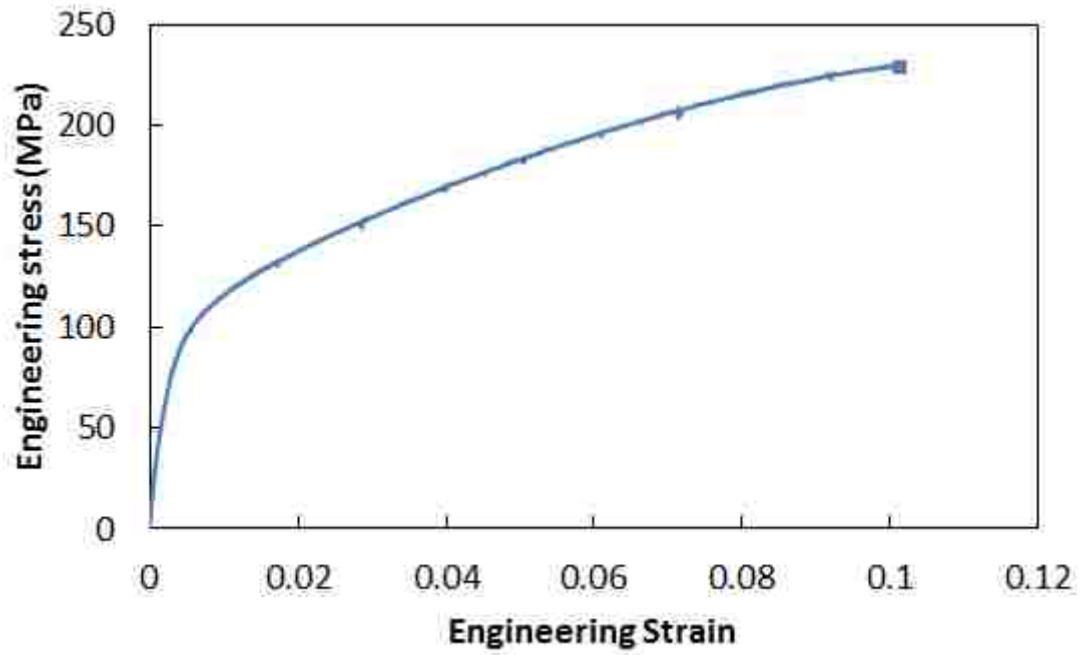
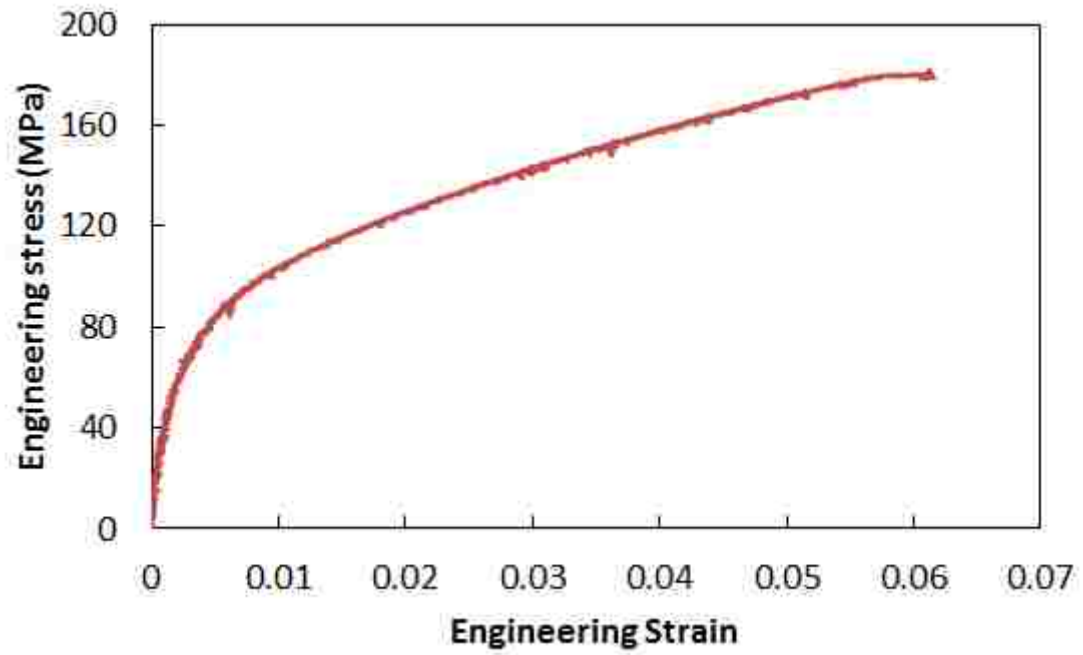


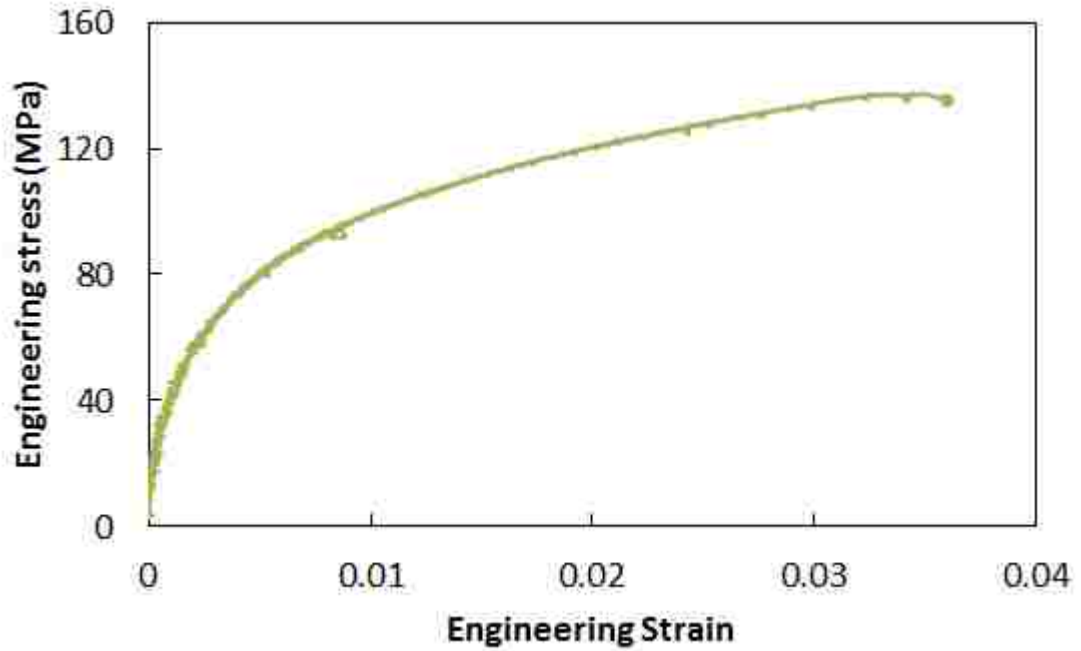
Figure Ap- 12. Engineering Stress-strain curves for CaC₂-refined AM60 from cylindrical coupon.



(a)

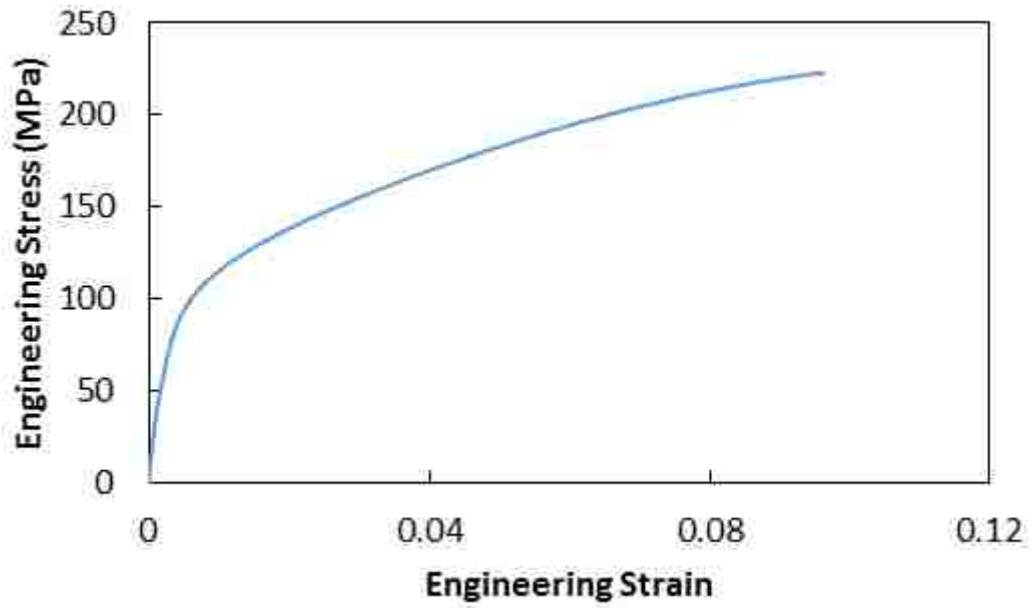


(b)

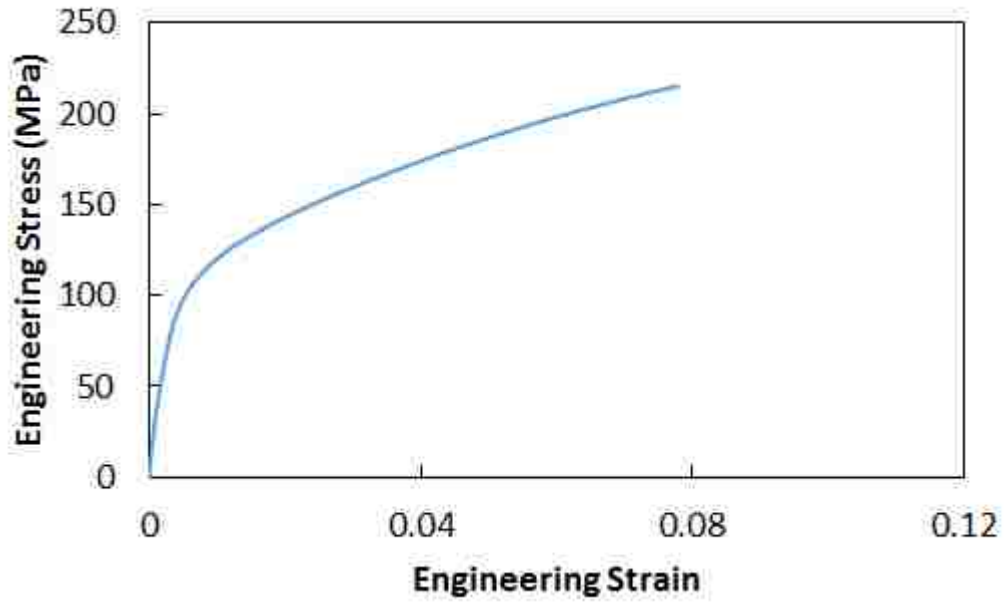


(c)

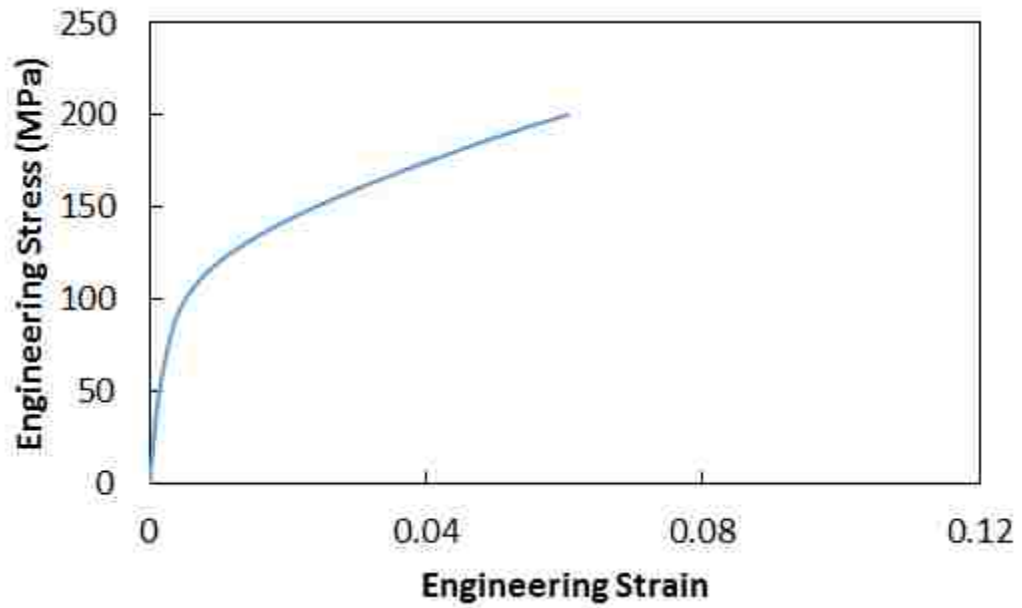
Figure Ap- 13. Engineering Stress-strain curves for squeeze cast AM60 in (a) 6 mm thickness, (b) 10 mm thickness, and (c) 20 mm thickness.



(a)

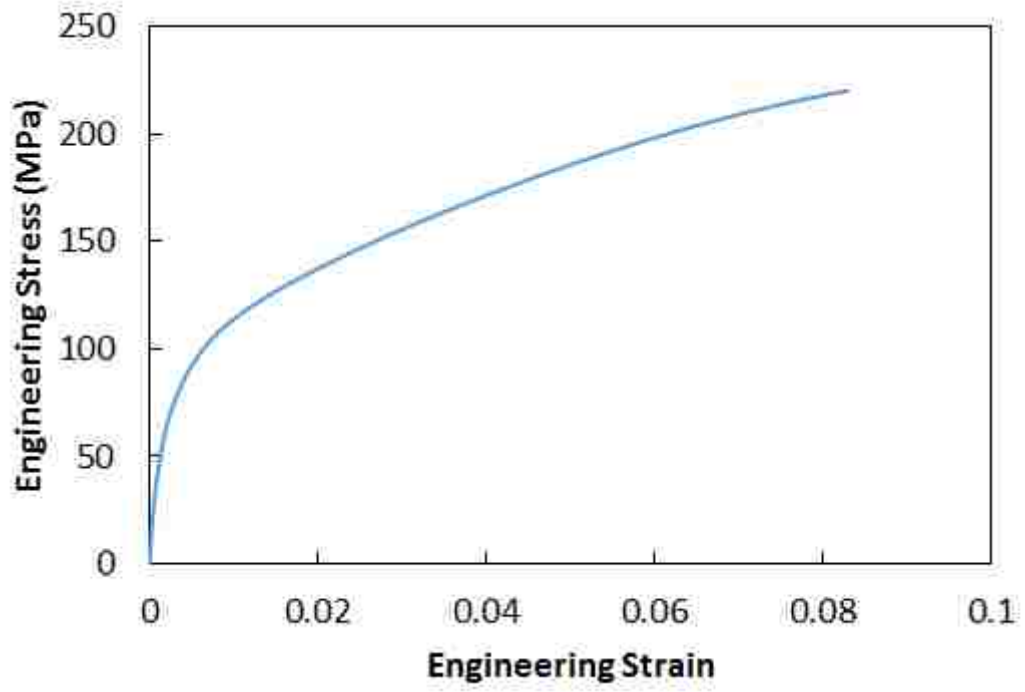


(b)

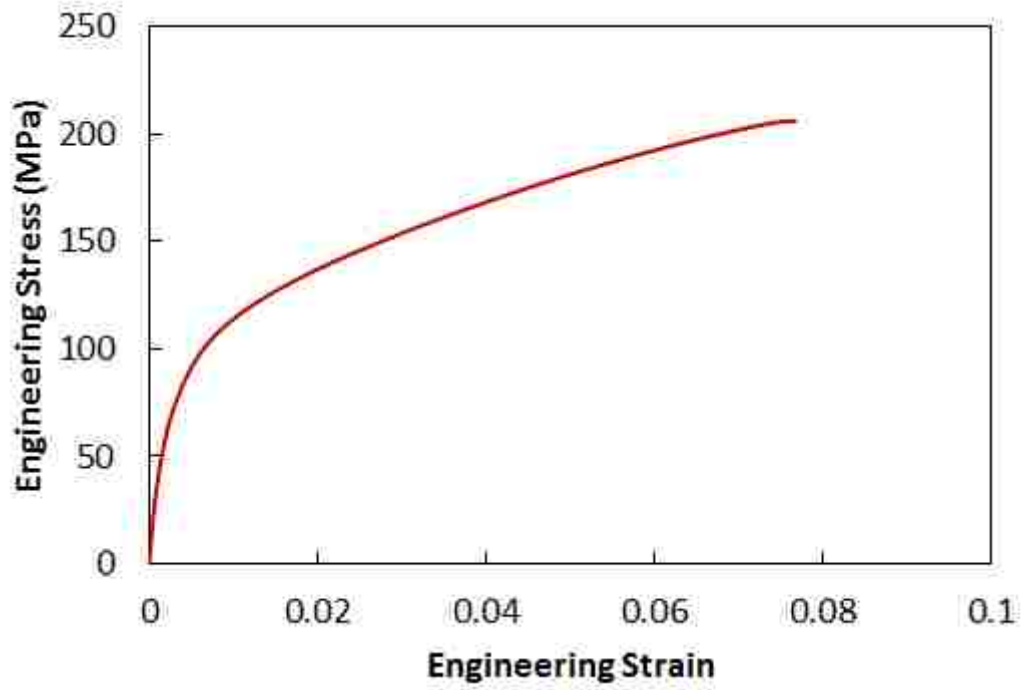


(c)

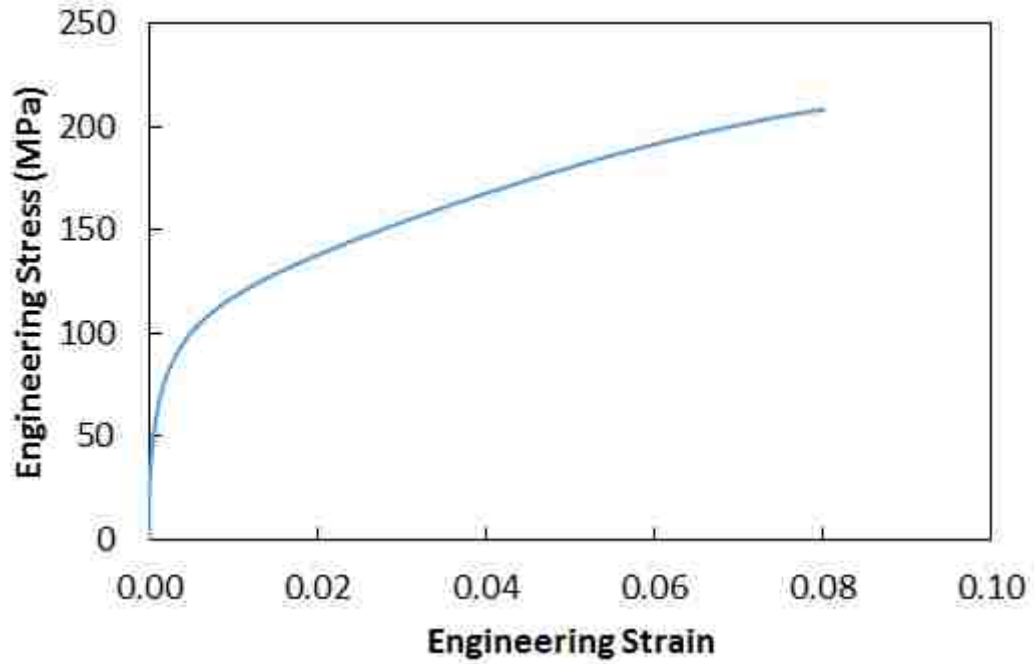
Figure Ap- 14. Engineering Stress-strain curves for C_2Cl_6 -refined squeeze cast AM60 in (a) 6 mm thickness, (b) 10 mm thickness, and (c) 20 mm thickness.



(a)



(b)



(c)

Figure Ap- 15. Engineering Stress-strain curves for CaC_2 -refined squeeze cast AM60 in (a) 6 mm thickness, (b) 10 mm thickness, and (c) 20 mm thickness.

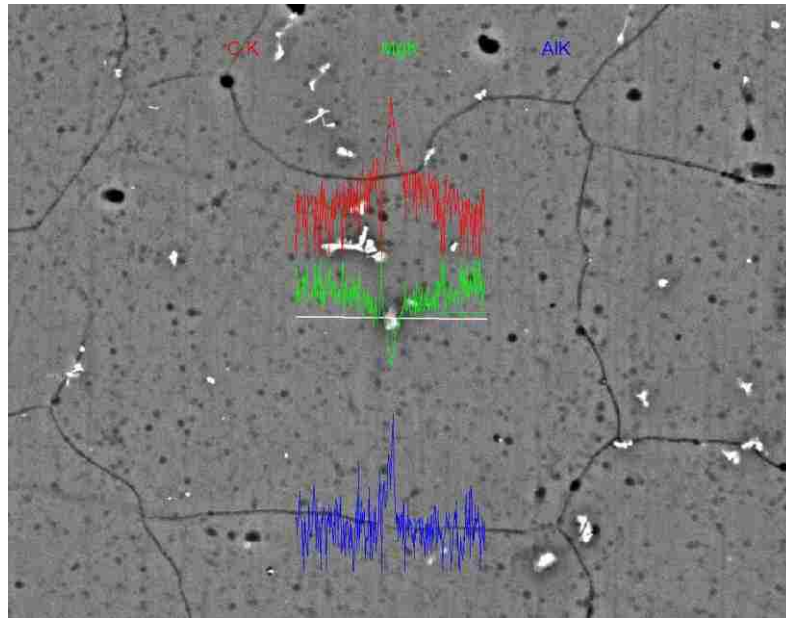
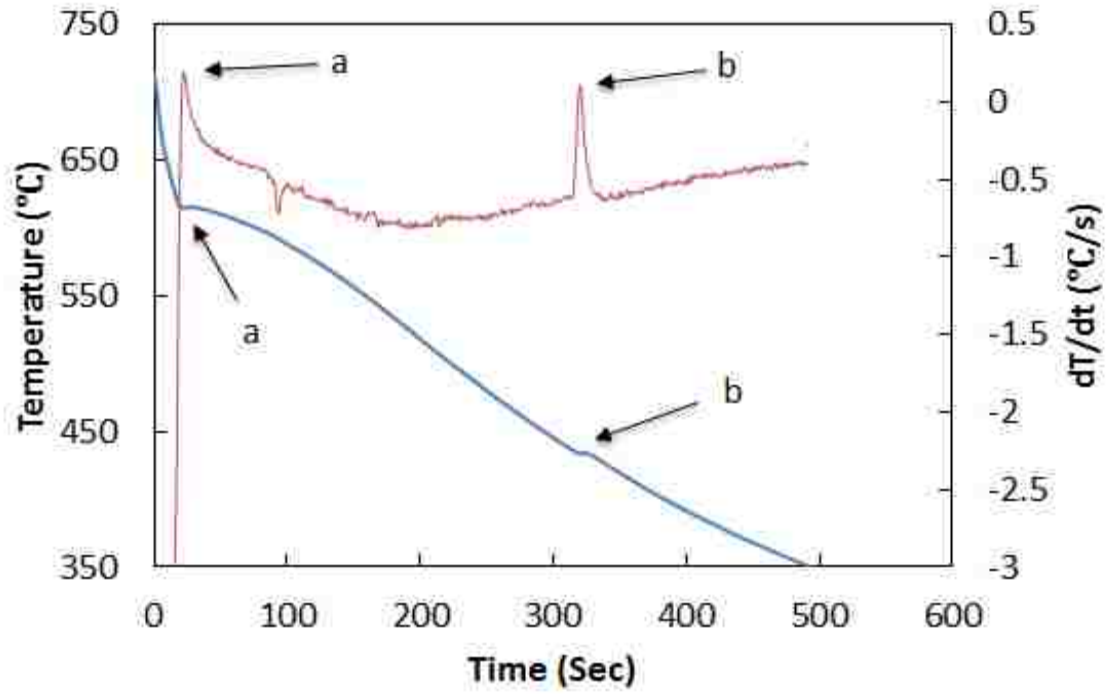
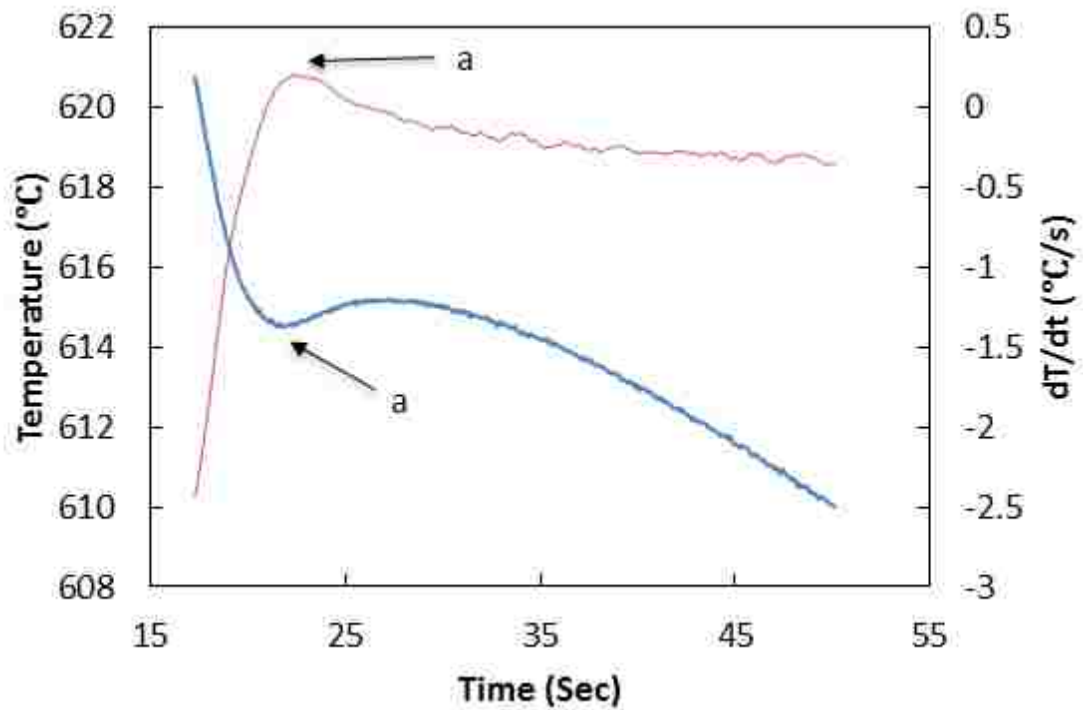


Figure Ap- 16. SEM micrograph in BSE mode showing Al_4C_3 as the heterogeneous nucleation site for C_2Cl_6 refined squeeze cast alloy AM60.

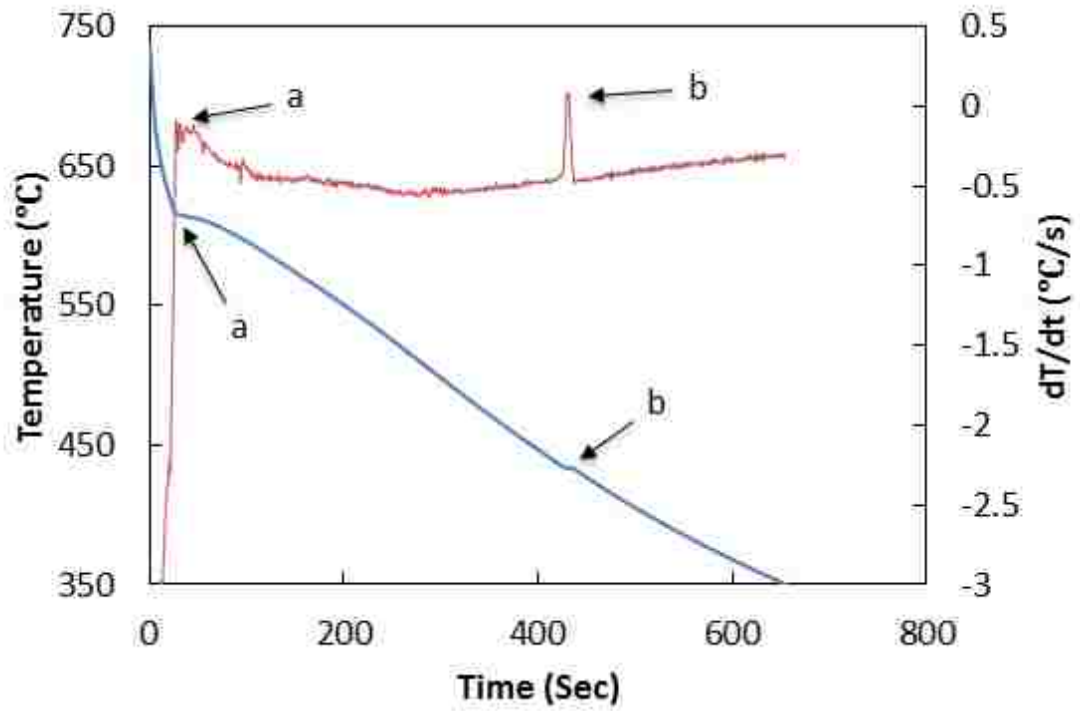


(a)

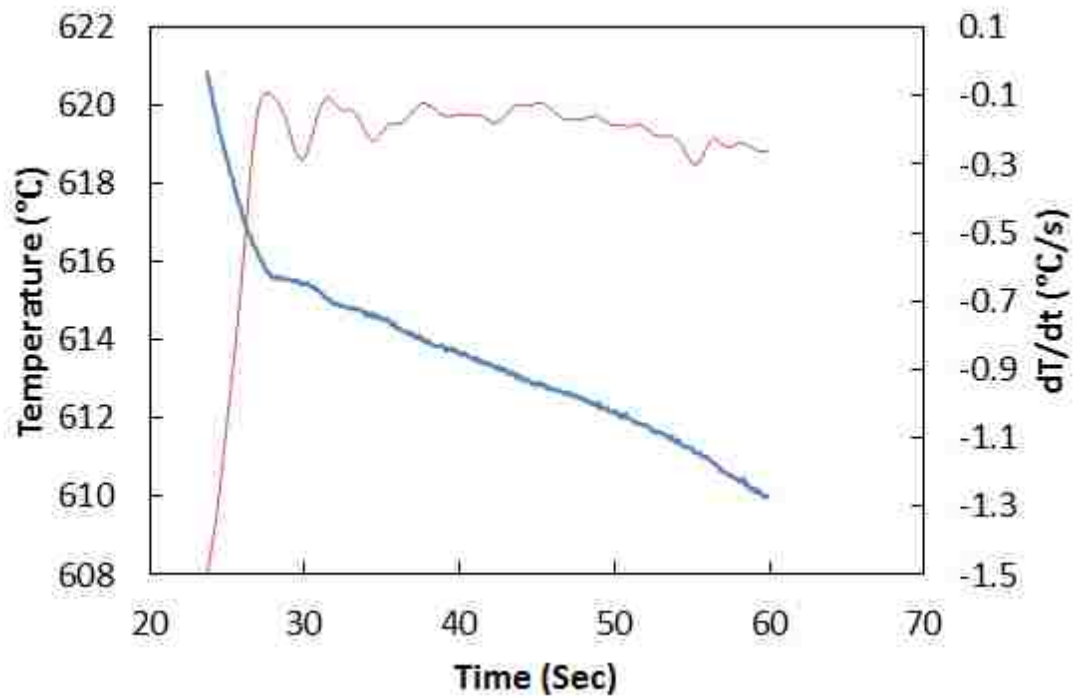


(b)

Figure Ap- 17. (a) Typical cooling curve, and (b) enlarge liquidus temperature region of AM60.

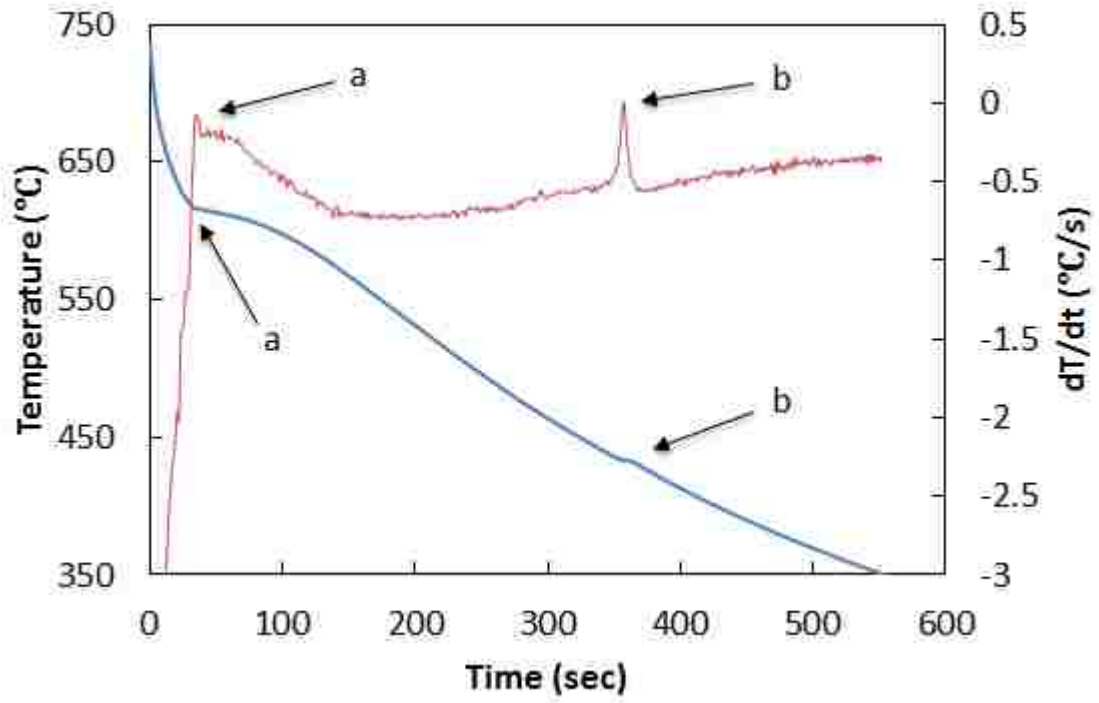


(a)

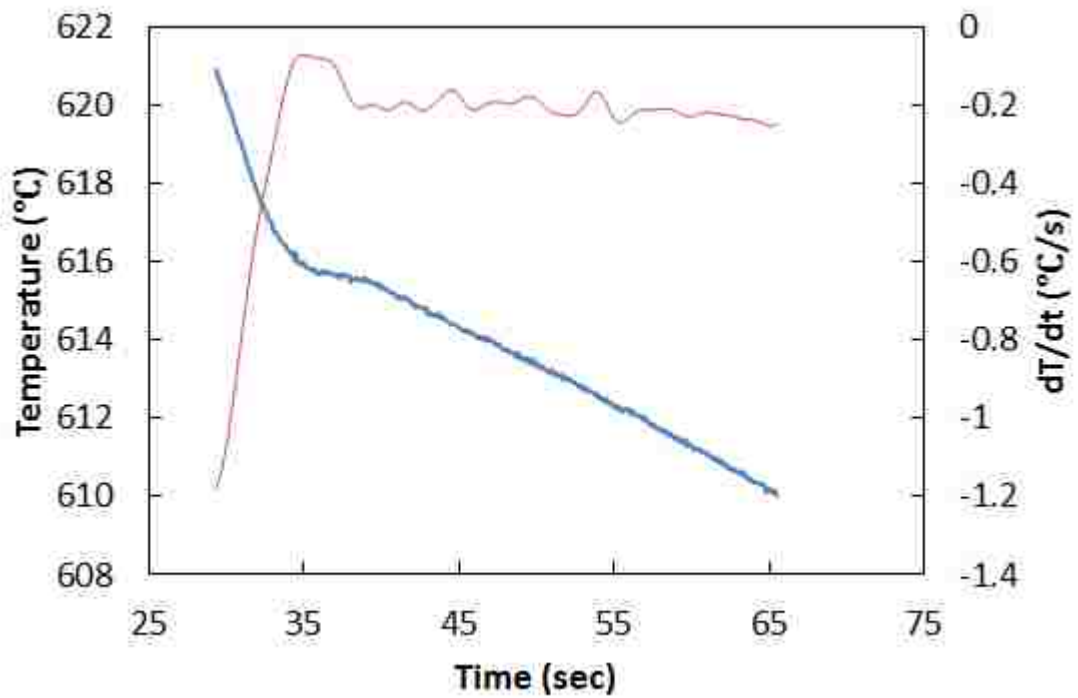


(b)

Figure Ap- 18. (a) Typical cooling curve, and (b) enlarge liquidus temperature region of C₂Cl₆-refined AM60.



(a)



(b)

Figure Ap- 19. (a) Typical cooling curve, and (b) enlarge liquidus temperature region of CaC₂-refined AM60.

VITA AUCTORIS

NAME: Yanda Zou

PLACE OF BIRTH: Dalian, China

YEAR OF BIRTH: 1989

EDUCATION: Yuming High School, Dalian, China, 2007

Beijing University of Chemical Technology, B.Sc.,
Beijing, China, 2011

University of Windsor, M.Sc., Windsor, ON, 2014